
AGENDA

10th Annual Space Radiation Health Investigators' Workshop

June 13-16, 1999 – Upton, New York



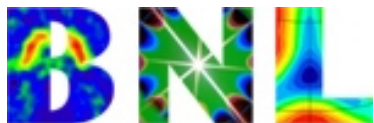
Sponsored by:

Brookhaven National Laboratory (BNL)

NASA Headquarters

NASA Johnson Space Center

Universities Space Research Association (USRA)



ABSTRACT TABLE OF CONTENTS

Physical and Biological Dosimetry in Space.....	1
Space Radiation Absorbed Dose Distribution in a Human Phantom <i>Gautam D. Badhwar, Tracy Yang, William Atwell, Neal Zapp, T. Cleghorn.....</i>	<i>2</i>
Effective Dose Equivalent Evaluated Using A Human Phantom Torso in the 9 th Shuttle/MIR Mission (STS-91) <i>H. Yasuda, T. Komiyama, G.D. Badhwar, K. Fujitaka.....</i>	<i>3</i>
Measurements of Energy Deposition in 1µm Diameter Volumes of Tissue By ⁵⁶ Fe at 400, 600, 700, 800 AND 1000 MEV Per Nucleon <i>B. Gersey, T. Borak, C. Zeitlin, J. Miller, L. Heilbronn</i>	<i>6</i>
Spaceflight Validation of HZETRN Code <i>J. W. Wilson, J. L. Shinn, R. C. Singleterry, F. F. Badavi, G. D. Badhwar, G. Reitz, R. Beaujean, F. A. Cucinotta.....</i>	<i>7</i>
Detection of DNA Damage Induced by Space Radiation in The MIR-Space Station and Space Shuttle by Post-Labeling of DNA <i>T. Nakano, K. Ohnishi, A. Takahashi, Y. Taniguchi, M. Sato, M. Fukui, S. Nagaoka, T. Ohnishi.....</i>	<i>10</i>
Posters I.....	12
Radiation Measurements on the Russian <i>Mir</i> Orbital Station <i>Gautam D. Badhwar</i>	<i>13</i>
Investigation of Proton-induced Target Fragmentation in Low Earth Orbit <i>Eric Benton, E. V. Benton</i>	<i>14</i>
Analysis of the Calibration Results Obtained with the Flight Model of the Mobile Radiation Exposure Control System Liulin for the “Dosimetric Mapping” Experiment to be Flown Onboard US Laboratory Module of ISS <i>Ts. Dachev, B. Tomov, Yu. Matviichuk, Pl. Dimitrov, J. Lemaire, Gh. Gregoire, G. Reitz, R. Beaujean</i>	<i>15</i>
Measurements of LET Distribution and Dose Equivalent with Realtime Monitoring Device (RRMD) Onboard a Series of Shuttle MIR Missions <i>T. Hayashi, T. Doke, N. Hasebe, T. Kashiwagi, J. Kikuchi, M. Kobayashi, S. Kono, A. Kyan, S. Nagaoka, T. Nakano, K. Ogura, T. Sakaguchi, K. Takahashi, S. Takahashi, T. Takagi, T. Takashima, K. Terasawa, E. Yoshihira, G. D. Badhwar.....</i>	<i>17</i>
High-LET Measurements in Low-Earth Orbits <i>E.G. Stassinopoulos, C.A. Stauffer.....</i>	<i>18</i>

DNA/Chromatin/Chromosomes – Damage and Repair	19
HPRT Mutation Induction in Human Cells by Heavy-Ion Irradiation <i>F. Yatagai, A. Gordon, S. Morimoto, N. Fukunishi, M. Honma, T. Sofuni, F. Hanaoka..</i>	20
Influence of HZE ⁵⁹ Fe Particles on Chromosome Aberrations in Rat Bone Marrow and Respiratory Tract Cells <i>A.L. Brooks, S. Bao, K. Rithidech, L.A. Couch, L.A. Braby.....</i>	22
The Effects of Microgravity on Ligase Activity in DNA Repair for Double Strand Breaks <i>T. Ohnishi, K. Ohnishi, A. Takahashi, T. Nakano, and S. Nagaoka</i>	24
Biodosimetry Using a Chemical-Induced Premature Chromosome Condensation Technique <i>H. Wu, T. Kawata, Y. Furusawa, T. Yang, D. R. Morrison.....</i>	27
Mutation.....	28
Characterization of Heavy-Ion Induced LACZ Mutants in Transgenic Animals <i>P. Y. Chang, N. Kanazawa, L. Lutze-Mann, R. A. Winegar.....</i>	29
Analysis of Alpha Particle Induced Chromosomal Aberrations and <i>HPRT</i> Gene Mutations <i>Hatsumi Nagasawa, John B. Little.....</i>	30
Study of the Role of the Mismatch Base Repair and Gene Mutation in Human Tumoral Cell Lines Exposed to Low-Energy Light Ions <i>R. Cherubini, F. Cucinotta, J.F. Dicello, S. Favaretto, D. Saggioro, J.R. Williams</i>	31
Cellular and Molecular Effects for Mutation Induction by Charged Particles with Different LET <i>M.Suzuki, Y.Kase, T.Kanai, M.Watanabe, T.K.Hei, E.J.Hall</i>	32
Posters II	34
DNA Damage by LZE and HZE Ions: Model of Induction of DNA Breaks and Recombination Repair <i>Francis A. Cucinotta, Hooshang Nikjoo, Peter O'Neill, and Dudley T. Goodhead</i>	35
Indicators of Genomic Instability Following Proton or Iron Ion Exposure of Human TK6 Lymphoblasts <i>A.J. Grosovsky, C. R. Giver, H. Bethel, K. Parks, L. Ritter, S. Gauny, C. Wiese, W. Liu A. Kronenberg</i>	36
Chromosomal Aberrations in Human Lymphocytes Induced by 1 GEV Protons in Vitro <i>E.Krasavin, R.Govorun, M.Repin, G.Tymoshenko, M.Lukashova, and S.Kozubek</i>	38

Mechanisms of Mutagenesis in Syngeneic Human Lymphoid Cells Exposed to 55 MeV Protons: Dissecting Mutational Mechanisms at the TK1 Locus as a Function of TP53 Status <i>A. Kronenberg, S. Gauny, C. Cherbonnel-Lasserre, W. Liu, C. Wiese</i>	39
KU-Protein Visualization After Heavy Ion Exposure <i>N.F. Metting</i>	41
Differential Pattern of a Proton- or Cobalt- Induced Genetic Fingerprint: Application to Radiation-Induced Cancer Chemoprevention Strategies <i>AC Miller, J Xu, T Whittaker, EJ Ainsworth, TM Seed</i>	44
Misrejoining of DNA Double-Strand Breaks Induced by 900 MeV/u Iron Ions and X-rays in Human Fibroblasts: Iron Ions are More Efficient Than X-rays at Lower Doses <i>B. Rydberg, B. Fouladi, and P. K. Cooper</i>	46
Clustered DNA Damage in Human Cells Irradiated with 1 GeV Fe ^{+26*} <i>Betsy M. Sutherland, Paula V. Bennett, John C. Sutherland, John Trunk, Denise Monteleone, Olga Sidorkina, Jacques Laval</i>	48
Use of the Comet Assay to Detect Radiation Damage of Selected Radiation Sensitive Cell Populations <i>D. Wilkinson, R.C. Wilkins, J.R.N. McLean</i>	50
Induction of Symmetrical and Asymmetrical Chromosome Aberrations in Mammalian Cells by Fe-ions, Protons and Photons: A Subalpha-Alpha-Omega Analysis <i>Jerry R. Williams, Haoming Zhou, John F. Dicello, Frank Cucinotta, Yonggang Zhang</i>	51
Radiation Risk	53
New Perspectives on Low Dose Risk Estimation <i>S. B. Curtis</i>	54
Multistage Models as an Approach To Quantitative Cancer Risk Assessment: Comparison of Theory and Experiment <i>F. Burns, Z. Hiz, R. Shore, P. Zhao, S. Chen, A. Nadas, N. Roy</i>	55
Mutagenicity as an Indicator for Radiation Risk <i>J. Kiefer</i>	58
Measuring Mutation in Cosmonauts <i>in vivo</i> : Lack of evidence that the space environment is mutagenic. <i>Barry W. Glickman, David J. Walsh, John Curry, Magomed Khaidakov</i>	59

Estimates of Genetic Risk in Offspring of Astronaut and The Counseling for Astronaut <i>T. Suemitsu, T. Komiyama, T. Abe</i>	60
Genomic Instability	63
Radiation Induced Chromosomal Instability: Studies of Radiation Quality and Targeted Effects <i>M. Kadhim, D. Pocock, S. Lorimore, D. Stevens, M. Hill, E. Wright and D. Goodhead</i> .	64
Emergency of Progressive Neoplastic Changes of Breast Epithelial Cells Treated with Estrogen and High LET Radiation <i>G. Calaf, T. K. Hei, E. J. Hall</i>	66
Induction of Genomic Instability in WTK1 Human Fibroblasts <i>Helen Evans, Minf-Fen Horng, Marlene Ricanati, Rob Jordan, Jeffrey L. Schwartz</i>	67
The XRCC2 and XRCC3 DNA Repair Genes are Required for Chromosomal Stability <i>E. H. Goodwin, X. Cui, M. Brennenman, J. Meyne, M. Oshimura, D. J. Chen</i>	68
Posters III	69
Persistent FE-ion-Induced Suppression of Cellular Protein Biosynthesis in Surviving Cells <i>Elizabeth K. Balcer-Kubiczek, George H. Harrison</i>	70
Proton-Induced Apoptosis in Confluent but not Exponential HLE <i>E. A. Blakely, M. P. McNamara, P. Y. Chang, K. A. Bjornstad, E. Chang</i>	71
Quantitation and Statistical Analysis of Physiological Responses to 1 GeV/nuc Fe Particle Irradiation Using Digital Fluorescence Image Data <i>D.E. Callahan, K.D. Benson, S. Costes, H. Chong, S.A. Ravani, C. Wang, M.H. Barcellos-Hoff</i>	73
FRTL-5 Cells Exposed to Photons Have Increased Protein Kinase C Isoenzymes, Reduced Polarity and a Transient Change in Immuno-Detectable Cx32 Gap Junction Protein <i>Lora M. Green, Deborah K. Murray, Ankur Bant, Da Thao Tran, Daila S. Gridley, Gregory A. Nelson</i>	76
Proton Versus Gamma Radiation Effects on Immunological Status in an Animal Model <i>D.S. Gridley, E.H. Kajioka, C. Gheorghe, J. Li, M.L. Andres, L.M. Green, G.A. Nelson, J.M. Slater</i>	79
Induction and Rejoining of Chromatid Breaks Following High-LET Radiation Exposure	

<i>T. Kawata, E. Gotoh, M. Durante, Y. Furusawa, H. Wu, T. Yang, D. R. Morrison</i>	82
Involvement of Mitochondria to Change Radiation Sensitivity in Human Osteosarcoma Cells <i>H.J. Majima, M. Suzuki, C. Yamaguchi, S. Kakinuma, H. Fuji, J.-P. Cao, D.C.Wallace, H.-C. Yen, K. Ando, K. Fujitaka, T. Nagano, T. Ozawa.....</i>	83
Aminothiol Induced Modulation of P53 Protein Structure <i>R.L. Warters, D.K. Thai, J.C. Roberts, D.K. Gaffney, A.E. Cress</i>	85
Risk Mitigation.....	86
Conception of Cosmonauts' Radiation Safety in Flight as Optimization of Radiation Safety System on the Basis of ALARA Principle <i>V.M. Petrov</i>	87
Comparisons of Methods for Organ Dose Estimates: Applications to the International Space Station <i>Neal Zapp, Francis A. Cucinotta</i>	88
Space Environment and the International Space Station: Recommendations to Reduce Radiation Risk During Solar Maximum <i>Ron Turner</i>	89
Project Review.....	90
Atmospheric Ionizing Radiation (AIR) Project Review <i>R.C. Singleterry Jr, J.W. Wilson, A.H. Whitehead, P.E. Goldhagen</i>	91
The Atmospheric Ionizing Radiation (AIR) Project – Preliminary Results for Neutron Spectra and Ionization Rate <i>P. Goldhagen, R. C. Singleterry Jr, M. Reginatto, J. W. Wilson, H. Tai, W. Van Steveninck, I. W. Jones, J. L. Shinn</i>	95
Posters IV.....	98
An Improved Algorithm for Neutron Exposures <i>M. S. Cloudsley, J. H. Heinbockel, J. L. Shinn, R. C. Singleterry, R. K. Tripathi, J. W. Wilson.....</i>	99
Recent Neutron Production Measurements Relevant to GCR Transport <i>L. Heilbronn, L. W. Townsend, R. S. Cary, F. Deak, K. Frankel, A. Galonsky, K. Holabird, Horvath, A. Kiss, J. Kruse, R. M. Ronningen, H. Schelin, Z. Seres, C. E. Stronach, J. Wang, P. Zecher, C. J. Zeitlin.....</i>	102
Solar Particle Event Exposures and Local Tissue Environments in Free Space and On Martian Surface <i>M. Y. Kim, J. L. Shinn, R. C. Singleterry, W. Atwell, J. W. Wilson.....</i>	103

A Comparison of Depth Dependence of Dose and Linear Energy Transfer Spectra in Aluminum and Polyethylene <i>Gautam D. Badhwar, Francis A. Cucinotta</i>	106
Nuclear Fragmentation of Light Ions <i>J. Miller, A. Fukumura, L. Heilbronn, T. Murakami, C. J. Zeitlin</i>	107
Current Status and New Developments in the Use of Three-Dimensional Computer Optical Memories for Radiation Dosimetry <i>M. Moscovitch, G. W. Phillips, A. K. Readshaw, G. O. Brown, R. G. Weiss, N. A. Guardala, J. L. Price, S. C. Mueller, D. Emfietzoglou, J. Mobley, J.S.Bogard, T. Vo-Dinh</i>	108
Estimates of Crew Dose Rates for the August 1972 Solar Particle Event: A High Dose Rate Event <i>J. L. Parsons, L. W. Townsend</i>	109
Observing Solar Particle Events <i>Ron Turner</i>	111
Program Reviews	114
Progress in Heavy Ion Researches with HIMAC <i>Kazunobu Fujitaka</i>	115
Loma Linda University Radiobiology Program Status Report <i>G.A. Nelson, J.O. Archambeau, L.M. Green, D.S. Gridley, M.M. Moyers, J.M. Slater</i> .	116
CNS	119
GCR Transport in the Brain: Assessment of Self-Shielding, Columnar Damage, and Nuclear Reactions on Cell Inactivation Rates <i>M.R. Shavers, W. Atwell, F. A. Cucinotta</i>	120
Induction of Apoptosis in Retinal Explants Exposed to Low- and High-LET Radiation <i>M. E. Vazquez, M. Saito, K. Nojima, Y. Furusawa, A. Pelzer</i>	122
The Neurobehavioral and Neurochemical Consequences of 1 GeV/n Fe Particle Exposure <i>M. E. Vazquez, S.J. Gatley, M. A. Cosenza, B. E. Pyatt</i>	125
Gene Expression	127
Evidence for the Presence of Factors Modulating Radiation-Induced G2 Delays <i>Nge Cheong, Ya Wang, George Iliakis</i>	128
Confocal Image Analysis of Laminin in Basement Membranes Following Whole	

Body Iron Particle (1 GeV/nuc) Irradiation	
<i>S. Costes, M.H. Barcellos-Hoff</i>	129

Monday, June 14

Brookhaven National Laboratory

8:30 a.m. – 10:10 a.m.

**Physical and Biological Dosimetry
in Space**

Berkner Hall

SPACE RADIATION ABSORBED DOSE DISTRIBUTION IN A HUMAN PHANTOM

Gautam D. Badhwar, Tracy Yang⁺, William Atwell, Neal Zapp⁺, T. Cleghorn
NASA Johnson Space Center, Houston, Texas 77058-3696
Boeing Aerospace Corporation, Houston, Texas 77058⁺

The radiation risk to astronauts has always been based on the measurements made by passive thermoluminescent dosimeters (TLDs). These dosimeters provide the low linear energy transfer (LET) component of their skin absorbed dose. These doses are then converted in *dose equivalent* using an average radiation quality factor based on model calculations. The radiological risk is, however, based on organ and tissue doses. There has been no experimental measurement that relates the skin dose to organ doses. The radiological assessment, however, requires a tissue-and organ-weighted dose, the *effective absorbed dose*, and the *effective dose equivalent*. This paper describes results from the first ever spaceflight (STS-91, 51.65° inclination, and ~ 400 km altitude) of a fully instrumented phantom torso (with head) to relate the skin dose to organ doses. Spatial distribution of absorbed dose in thirty four (34) 1- inch thick sections are described. In many sections, there is greater than 30% change in dose as one goes from the front to the back of the phantom body. A small active dosimeter was specifically developed to provide time-resolved measurements of absorbed dose rate, and quality factor. Five such dosimeters were mounted at the five organ locations (brain, thyroid, heart/lung, stomach, and colon) inside the phantom. Using these dosimeters, it is possible to separate out the trapped component from the galactic cosmic radiation component of the doses. The high ($> 5 \text{ keV}/\mu\text{m}$) LET spectrum was measured in the central section of the brain and can be used for studies related to the central nervous system (CNS). A tissue equivalent proportional counter (TEPC) and a Charged Particle Directional Spectrometer (CPDS) were flown along side the phantom torso to provide the incident external environment. Accurate models of the shielding distributions at the site of TEPC, CPDS, and phantom were developed that took into account the single module Spacehab and the Anti Matter Spectrometer (AMS) in the payload bay of the Shuttle. A scaleable Computerized Anatomical Model (CAM) of the phantom torso, but with no arms, hands, legs, and foot, was developed. This model was used to develop shielding distributions at two skin locations and five organ locations of the active dosimeters. In addition, fifty-seven passive detector assemblies, containing different types of TLDs, thermoluminescent glass, and plastic nuclear track detectors, provided by the National Space Development Agency of Japan (NASDA) were mounted inside the torso body. These measurements have provided the most comprehensive data set to map the dose distribution inside a human phantom, and to assess the accuracy and validity of radiation transport models throughout the human body. These measurements have also provided the first experimental relationship between skin dose and organ dose measurements, thus allowing for a more accurate assessment of radiation risk to astronauts.

EFFECTIVE DOSE EQUIVALENT EVALUATED USING A HUMAN PHANTOM TORSO IN THE 9TH SHUTTLE/MIR MISSION (STS-91)

H. Yasuda¹, T. Komiyama², G.D. Badhwar³, K. Fujitaka¹

¹ National Institute of Radiological Sciences, Chiba 263-8555, Japan, ² National Space Development Agency of Japan, Ibaraki 305-0047, Japan, ³ NASA Lyndon B. Johnson Space Center, Houston, TX 77058

INTRODUCTION

Health risk of astronauts attributing to space radiation exposure should be quantified as precisely as possible. Index of radiological risk to humans is called “effective dose equivalent” (ICRP, 1977) or “effective dose” (ICRP, 1990), which is obtained by summing up the absorbed dose with weighting by radiation quality and organ/tissue sensitivity. However, organ/tissue doses of astronauts as well as their qualities have never been measured. Numerical prediction of them is still a problematic subject because of complexity of a human body structure, multi-directional measurement of all particle species, and fragmentation process of high-energy particles. As a first attempt to evaluate directly the effective dose equivalent, a torso of real-size human phantom containing selected small dosimeters was loaded on the Spaceshuttle in the 9th Shuttle/Mir Mission (STS-91).

MATERIALS AND METHODS

The dosimeters adopted were radiophoto-luminescent glass (RPLG) (Toshiba Glass, SC-1), thermo-luminescent dosimeters of magnesium silicate (TLMS) (Kasei Optonics, TLD-MSO), and plastic nuclear track detector (PNTD) (Fukuvi, HARZLAS TD-1). The size of RPLG, TLMS, and PNTD are 3.2•3.2•0.5 mm³, 3.2•16•1.5 mm³, and 3.2•16•1.5 mm³, respectively. In ground calibration, four TLMSs, four RPLGs, and two PNTDs were packed in a rectangle case of tissue-equivalent resin (Toughwater phantom, KYOTO KAGAKU) of 80×80 mm² with a cover plate of 2 mm thickness. Then the dosimeter package described above was exposed to 10, 50, and 100 mGy of 70MeV proton beam in Cyclotron of National Institute of Radiological Sciences (NIRS-Cyclotron), and 150 MeV/u He, 290 MeV/u C, 400 MeV/u Ne, and 500 MeV/u Ar beams in Heavy Ion Medical Accelerator in Chiba of National Institute of Radiological Sciences (NIRS-HIMAC), and 1.0 GeV/u Fe in AGS of Brookhaven National Laboratory (BNL-AGS). RPLG and TLMS were read by an exclusive reader designed for each dosimeter. The value obtained was standardized as a γ -equivalent dose by 100 mGy ¹³⁷Cs- γ ray; no dose dependency was found for both dosimeters in the range of 10-100 mGy of ¹³⁷Cs- γ ray. The glowcurve of each TLMS up to 400° C was also analyzed. PNTD was etched in 6N NaOH at 60° C for 12 hours and its surface was observed by an optical microscope (OLYMPUS BX50) and an image analysis program (NIH Image ver.1.57 on Macintosh). The sensitivity (S) of each etchpit was calculated as

$$S = V_T/V_B - 1 = (16D_A^2B^2/(4B^2 - D_B^2)^2 + 1)^{0.5} - 1 \quad (1)$$

Where V_T is the etching rate along the track axis; V_B the bulk-etching rate; D_A is the major axis length of the etchpit ellipse [mm]; and D_B is the minor one [mm]. The S derived is related to the beam LET. The fluence of each LET was calculated with the theoretically-derived critical angle (θ_c) (Fleishcer, et al., 1975), less than which an incident beam cannot be detected. The θ_c s for selected heavy ion beams were also experimentally examined for the PNTDs inclined at 5-degree interval from 0° to 90°

Flight experiment was done in the S/MM-9 (STS-91) at June 2-12, for about 9.8 days. A real-size torso of human phantom made of tissue equivalent resin (Alderson RANDO Phantom) worn by a spacesuit was fixed by a wire on the locker of electric devices in the Spacehab module of Spaceshuttle "Discovery". At the radiologically-important positions in and on the phantom were put the 57 cases made of tissue equivalent resin of 1 mm thickness with the size of $6.8 \times 7.2 \times 18 \text{ mm}^3$. In each case, two RPLGs, three TLMSs, and two PNTDs were inserted. All the cases including background ones were sent back to Japan and analyzed within two weeks after landing.

RESULTS AND DISCUSSION

The TLMS and the RPLG showed different characteristics of LET dependencies. Although it is known that the specific sensitivity of TLD decreases with LET, the response curve of TLMS can be separated into two regions. At low LET less than $10 \text{ keV } \mu\text{m}^{-1}$ the relative efficiency of TLMS did not change much and was almost equal to that for ^{137}Cs γ -ray. But it reduced drastically with LET at higher LET region. The main reason of such efficiency reduction is considered to be saturation of color centers with increasing ionization density; all the secondary electrons could not be trapped in such highly-densed area along the track. This was supported by the fact that their glowcurve shapes did not change among various LET particles, which means the energy balance of trapped electrons is maintained.

While the relative efficiencies of RPLG decreased more gradually from low LET region. No plateau was seen at more than $0.5 \text{ keV } \mu\text{m}^{-1}$, the LET of ^{137}Cs γ -ray. Because RPLG has a large dynamic range up to several tens gray for γ or β -ray, it is considered that thermal effect (local annealing) along a particle track is working as a cause of the efficiency reduction.

Although slight fluctuation is found in the relationship between etchpits sensitivity (S) and LET in water, it is judged that LET of these ions can be estimated directly from S. The theoretically derived θ_c agrees well with the experimental results. It was found, however, the S values for low LET and highly-incident particles need to be corrected. This correction process was added to the following analysis of LET spectra of space radiation.

As results of the flight experiment, clear difference (20-30 %) between TLMS and RPLG was seen in the same position and the degree of this difference changed at each organ/tissue. This suggests presence of considerable fraction of high-LET particles. As to dosimeter location, relatively large variation up to a factor of 1.6 was found for both dosimeters. Then it should be noted that the dose measured by using this kind of dosimeter needs be corrected according to space radiation quality.

Differential fluence of charged particles versus LET for more than $13 \text{ keV } \mu\text{m}^{-1}$ was obtained by PNTD analysis. Absorbed doses of high LET particles were calculated from those data and this distribution was extrapolated to low LET region, which can correspond to the TLMS and RPLG values. Considering the shape of dose distribution previously measured in Spaceshuttle (Badhwar, 1996), the curve of accumulated absorbed dose was assumed to be approximated by a sum of positive and negative amplitude functions as the following double exponential equation (a gamma function); $D(\text{LET}) = D_{\text{max}} \times ((z+b-1)/(b-1))^{b-1} \times e^{-z}$, $z = (\log\text{LET} - \log L_0)/c$. Where D_{max} , b , c , and L_0 are constants obtained by fitting. The D takes the maximum value at $\text{LET} = L_0$. Fitting process was repeated until the most appropriate data set was obtained to

explain the the values of TLMS, and RPLG.

Based on those absorbed dose-LET plots, the dose equivalent and the effective quality factor (Q) were also calculated for each organ/tissue. The absorbed dose in or on the phantom torso for 9.8 days in this STS-91 mission ranged from 1.6 mGy at colon to 2.7 mGy at shoulder bone surface with a variation factor of 1.6. Quality factor (Q) was from 1.6 to 2.7 (factor 1.7) with little difference between two ICRP recommendations. The dose equivalent ranged from 3.2 mSv at colon to 5.2 mSv at gonad (factor 1.8). As a general tendency, both the absorbed dose and dose equivalent were smaller in deeper organs. Q values, however, showed a tendency to be higher in selected internal organs such as lung, bone marrow, and colon. By summing up these organ/tissue doses with tissue weighting factors (ICRP, 1977; ICRP, 1990), the effective dose equivalent during this mission was evaluated as 4 mSv.

CONCLUSION

The first phantom torso experiment was successfully done in STS-91. The data reported here indicate that radiation doses and qualities inside and surrounding an astronaut's body would change to large extent. It should be noted that the dose measured on the skin surface is not necessarily higher than some of internal organs/tissues. Although the doses of space radiation has been measured in atmosphere, it is hoped to discuss how their individual dose be measured for more appropriate quantification of radiological risk.

In this experiment, the highest value of dose equivalent was obtained in gonad. Many astronauts are, however, older than the maternity age. Then the existing tissue equivalent factors might be unsuitable to astronauts. It is also needed to consider the effect of microgravity and other peculiar stresses in space. The Q-L relationship in high-LET region, in other words, cancer risk induced by heavy ions is still unclear and should be investigated in ground research. It also should be recognized that this experiment was done in the Spacehab module of Spaceshuttle which is different from where astronauts usually stay. Concerning these uncertainties, it is expected that this kind of experiment to quantify the chronic health risk caused by space radiation exposure will be continued along with expanding manned space mission such as International Space Station and Mars mission.

AKNOWLEDGEMENTS

Sincere appreciation is expressed to Jack Miller (LBNL), Sayaka Sato, Ayuchi Nakamura, Masashi Takada, and Yukio Uchihori (NIRS) for their cooperation in the experiments of ground calibration. The parts of heavy ion beam experiments were carried out in chain of NIRS-HIMAC Collaborative Research. The spaceflight experiment in S/MM-8 was done with help of NASDA and NASA.

REFERENCES

- Badhwar, G.D. et al., Radiat. Meas., 26, 17-34 (1996).
- Doke, T. et al. Radiat. Meas., 24, 75-82 (1995).
- Fleishcer, R.L. et al. "Nuclear Tracks in Solid", Univ. California Press (1975).
- ICRP, ICRP Publ.26 (1977).
- ICRP, ICRP Publ.60 (1990).

MEASUREMENTS OF ENERGY DEPOSITION IN 1 μ m DIAMETER VOLUMES OF TISSUE BY ^{56}Fe AT 400, 600, 700, 800 AND 1000 MEV PER NUCLEON

B. Gersey ⁽¹⁾, T. Borak ⁽¹⁾, C. Zeitlin ⁽²⁾, J. Miller ⁽²⁾, L. Heilbronn ⁽²⁾.

(1) Colorado State University; (2) Lawrence Berkeley National Laboratory.

tborak@cvmbs.colostate.edu / (FAX) 970 491-0623

INTRODUCTION

Tissue-equivalent proportional counters (TEPC) are used during manned space missions to measure energy deposition in simulated volumes of tissue that are approximately 1 μ m diameter. There has been some concern that the wall used to define the volume of interest could influence energy deposition within the sensitive volume because the wall has a density significantly greater than the cavity gas.

METHODS

Measurements were made with ^{56}Fe particles at 600, 700, 800 and 1000 MeV/nucleon at the AGS in Brookhaven National Laboratory and 400 MeV/nucleon at the HIMAC in Japan. The TEPC was part of a particle spectrometer that tracks individual particles through the detector. This arrangement permits us to evaluate enhancements in energy deposition due to the wall as well as energy loss due the escape of high energy delta rays.

RESULTS

Energy deposition for ^{56}Fe particles that pass through the center the detector is about 75% of that expected by LET alone. This did not change significantly for incident energies between 400 and 1000 MeV/nucleon. Thus, any enhancement from electrons generated in the wall is overcome by high energy delta rays that escape the 1 μ m volume. However the enhancement of energy deposition from the wall increases for trajectories away from the center of the detector and is greatest for trajectories near the cavity/wall interface. An integration of the response indicates that charged particle equilibrium is essentially achieved for a wall thickness of 2.54 mm. However, estimates of the LET distribution for the incident particles are influenced by these wall effects.

CONCLUSIONS

A wall-less detector would be desirable for determining LET spectra using tissue equivalent proportional counters, but if the detector is also to be used for dosimetry, a wall is necessary to establish charged particle equilibrium.

SPACEFLIGHT VALIDATION OF HZETRN CODE

J. W. Wilson¹, J. L. Shinn¹, R. C. Singleterry¹, F. F. Badavi², G. D. Badhwar³, G. Reitz⁴,
Beaujean⁵, F. A. Cucinotta³

¹ Langley Research Center, Hampton, VA, ² Christopher Newport University, ³ Johnson Space
Center, Houston, TX, ⁴ Institut fur Flugmedizen, DLR, Koeln, DE, ⁵ Univ. of Kiel, Kiel, DE

INTRODUCTION

HZETRN is being developed as a fast deterministic radiation transport code applicable to neutrons, protons, and multiply charged ions in the space environment. It was recently applied to 50 hours of IMP8 data measured during the August 4, 1972 solar event to map the hourly exposures within the human body under several shield configurations. This calculation required only 18 hours on a VAX 4000 machine. A similar calculation using the Monte Carlo method would have required two years of dedicated computer time. The code has been benchmarked against well documented and tested Monte Carlo proton transport codes with good success. The code will allow important trade studies to be made with relative ease due to the computational speed and will be useful in assessing design alternatives in an integrated system software environment. Since there are no well tested Monte Carlo codes for HZE particles, we have been engaged in flight validation of the HZETRN results. To date we have made comparison with TEPC, CR-39, charge particle telescopes, and Bonner spheres. This broad range of detectors allows us to test a number of functions related to differing physical processes which add to the complicated radiation fields within a spacecraft or the human body, which functions can be calculated by the HZETRN code system. In the present report we will review these results.

METHOD

The estimation of the radiation within the tissues of an astronaut aboard a geometrically complicated spacecraft requires an adequate representation of the fragmentation of primary ions, the production of particles in collision with spacecraft structures and human tissues, and the correlated secondary electron distributions about the ion paths. Included in this representation must be the abundant neutrons and low energy target fragments which add to the high LET components of the radiation fields along with the HZE ions. To obtain accurate information from the above mentioned detectors one must pay close attention to the individual instrument response functions for the various components. The AP8 trapped environmental model, the Badhwar/O'Neill model for the galactic cosmic rays, the geomagnetic cutoffs of Smart and Shea, and estimates of the neutron albedo are used to represent the LEO environment. These are used with the Shuttle geometry, the HZETRN Code, and the instrument response functions to predict the outcome of the measurements within the Shuttle interior at the specific sites where the instruments are located.

RESULTS

The lineal energy distribution of the JSC TEPC during June 1993 resulting from the trapped protons in STS-57 in a 28.5° inclined 252 nmi orbit is shown in figure 1. Also shown are the HZETRN calculated distributions for comparison. There are slight differences near 10 and 100 keV/micron. Similar results are obtained for galactic cosmic ray contributions as shown in figure

2. There is a difference at the lowest lineal energies which may be due to meson production which is not yet in the HZETRN model or low LET events of passing HZE ions outside the active region of the detector. Generally, however, there is good agreement between the computational models and measurements. Another example is the CR-39 measurements of Heinrich et al. on the D1 mission shown in figure 3. The LET spectrum at the site of the measurement is shown as the dashed curve. Many of the high LET target fragmentation events were etched away in the processing of the foils. Our estimate of the etching losses are shown as the solid curve which agrees well with the measurements. But note, the CR-39 foils do not generally measure the full LET spectrum.

FINAL REMARKS

All detector types have certain limitations regarding their ability to detect radiation, their specificity for a particular radiation type(s), and their accuracy. For example, although the detectors used to obtain the data reported in figures 1-3 are largely driven by the charged particle environment, the TEPC device also responds to some extent to the neutron environment as well but there is no clear separation. Charged particle telescopes and Bonner spheres can separate charged particle and neutron contributions in the radiation fields. All of the detectors have their own unique performance characteristics, and these characteristics must properly be taken into account when interpreting their measurement results. The characteristics and limitations of the several types of detectors are discussed in further detail in this presentation along with the spaceflight data and comparisons with the HZETRN Code results.

Figure 1. Measured and calculated lineal energy spectra induced by trapped protons in a 252 nmi x 28.5° orbit in June 1993 aboard STS-57.

Figure 2. Measured and calculated lineal energy spectra induced by galactic cosmic rays in a 252 nmi x 28.5° orbit in June 1993 aboard STS-57.

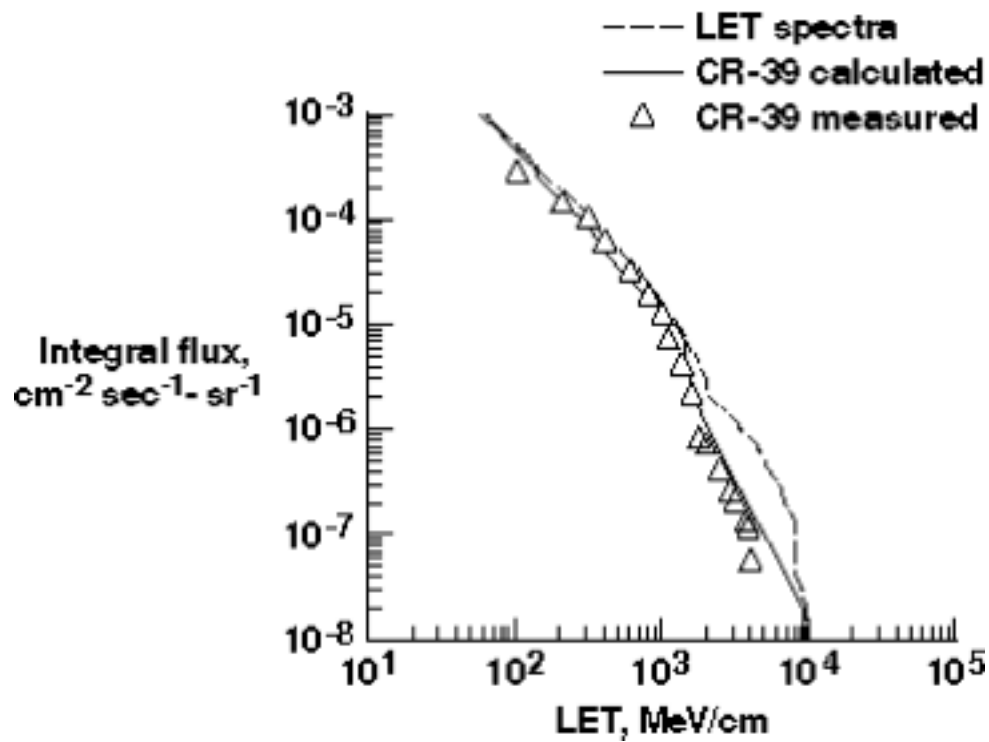


Figure 3. LET spectra measured and calculated using HZETRN Code.

DETECTION OF DNA DAMAGE INDUCED BY SPACE RADIATION IN THE MIR-SPACE STATION AND SPACE SHUTTLE BY POST-LABELLING OF DNA

T. Nakano¹, K. Ohnishi², A. Takahashi², Y. Taniguchi³, M. Sato¹, M. Fukui¹, S. Nagaoka¹ and T. Ohnishi²

¹Space Utilization Research Center, National Space Development Agency of Japan, Tsukuba, Ibaraki 305-0047,

²Department of Biology, Nara Medical University, Kashihara, Nara 634-8521,

³Toray Research Center Inc., Tebira Kamakura, Kanagawa 248-8555, Japan

INTRODUCTION

Space radiation found near the earth is mainly emitted from solar explosions, and contains many kinds of radiation, e.g., ultraviolet light, X-rays and heavy particles, such as Fe and so on. Large amounts of radiation penetrate into space crafts, where they have been measured physically. National Space Development Agency of Japan (NASDA) used the Russian space station Mir and Space Shuttle to carry out studies of the biological effects of space flight on a fixed human cells. Here we tried to directly measure the DNA damage by post-labeling of the 3'-ends of DNA molecules with strand breaks caused by space radiation in human melanoma (HMV1) cells.

METHODS

Human melanoma cells (HMV1 cells) were plated on CR-39 plates (17.5 mm x 35 mm; the plates were also used for other physical analyses of space radiation) which were placed in 10 cm cell culture dishes (about 5 x 10⁵ cells/dish). About 10 hr after the cell plating, the cells on the plates were washed with PBS (-) and fixed with methanol for 10 min. In the MIR experiment, the samples were carried from Nara, Japan, to Baikonur, Russia at room temperature in the dark, and there they were loaded on Progress M-35. The space samples were carried by "Progress" and exposed to space radiation on the Mir Space Station for 40 days (J/Mir mission (STS-89); July 5-August 14, 1997). For the 8th Shuttle/MIR Mission experiment (S/MM-8; January 23-February 1, 1998), the samples were similarly carried from Nara Medical University, Japan, to Kennedy Space Center, Florida, USA.

The space samples were exposed to space radiation on the Space Shuttle "Endeavor" for 9 days. During this period, the control samples were stored on earth at room temperature in the dark.

HMV1 cells of both space and ground samples were incubated with 30 ml of reaction mixture for end-labeling with [3H]-labeled thymidine triphosphate to damaged DNA molecules. The cells were dipped into autoradiographic emulsion, and exposed to the fixed emulsion at 4°C for 5-14 days. Finally, the samples were autoradiographed, stained with 2% Giemsa's solution and observed with a light microscope. The number of grains in 100 cells of samples (at least 3 plates in each scheduled group) was counted.

RESULTS

We detected most frequently HMV1 cells which had 11-20 grains (about 65% out of the total observed cells) in both of the ground samples and the samples after space flight for 9 days in S/MM8 experiment. In contrast to S/MM8, in J/Mir mission, cells having many grains (over 31 grains) were more frequently observed in the space samples (80%) than in the ground samples

(30%). These results confirm that space radiation indeed induces DNA damage of human cells. Further, our data based on the molecular level analysis support the previous reports that space crews had chromosomal aberrations in their lymphocytes after space flight. Another important finding of this study is that DNA damage was increased with length of space stay. DNA damage was more frequently induced with about 2-fold in the 40-days space stay than in the 9-day space stay on the basis of the numbers of cells having over 21 grains in space and ground samples. Since the dose rate of space radiation (about 1 mSv/day, personal communication from Dr. T. Doke, Waseda University) and the height of flight orbit (about 400 km) were almost the same in the two space experiments, the difference in results between the two flight experiments is surely due to the difference in length of space stay.

In J/Mir mission samples, we detected clusters of several cells containing many grains, but we detected no such clusters in ground samples. We presume that the clusters result from large tracks of heavy particles present in space radiation. Compared with low LET radiation, such as gamma-rays or X-rays, high LET heavy particles result in larger numbers of DNA strand breaks, and thus the clusters observed in J/Mir mission samples may be due to high LET heavy particles. Few tracks of heavy particles due to the short flight period might account for the lack of clusters in S/MM-8 samples.

Physical monitoring of space radiation has previously been performed. From the physical data, we can indirectly estimate the biological effects of space radiation. However, the direct effects of space radiation on organisms are unknown to date. Here, we provide direct evidence of the biological effects of space radiation. Clusters of cells having large amounts of DNA damage were observed in samples from the long-term space flight. The biological monitoring performed in the present study is available for determination of the maximum permissible period of exposure to space radiation and will provide guidelines for the physical protection from the serious effects of space radiation during long stays in space.

CONCLUSION

To detect DNA damage induced by space radiation, we placed the fixed human melanoma cultured cells (HVM1) in the Russian Mir-space station for 40 days and in an American space shuttle for 9 days. After launch, we post-labelled space-radiation-induced DNA strand breaks by enzymatic incorporation of [³H]dATP with terminal deoxyribonucleotidyl transferase (TdT). We detected DNA damages as many grains of fixed silver emulsion resulting from beta-rays emitted from ³H-atoms in the nuclei of the cells placed in the Mir-station (J/Mir mission), but detected hardly any in the ground control sample. In the space shuttle samples (S/MM-8), the number of cells having many grains was lower than in the J/Mir mission samples. These results suggest that DNA damage is induced by space radiation and that it is dependent on the length of the space flight. The present study provides information useful for the estimation of the maximum permissible period of stay in space for space crews.

ACKNOWLEDGMENTS

This study was funded in part by the "Ground Research for Space Utilization" promoted by NASDA and the Japan Space Forum. It was also supported by the Russian Space Agency (RSC) Energia, JGC Co.

Monday, June 14

Brookhaven National Laboratory

10:10 a.m. – 11:10 a.m.

Posters I

Berkner Rooms A & C

RADIATION MEASUREMENTS ON THE RUSSIAN *MIR* ORBITAL STATION

Gautam D. Badhwar

NASA Johnson Space Center, Houston, Texas 77058-3696

The Russian *Mir* orbital station was launched into an orbit with a 51.65° inclination in March 1986. It has operated continuously in the altitude range of 380 to 460 km. Almost immediately, cosmonauts began to carry out missions to the station. To date, there have been some 27 Russian missions. As part of the NASA Mir Program, a comprehensive set of radiation measurements were made to map the radiation in all of the Mir module.

Numerous radiation measurements have been made on the *Mir* station throughout its lifetime. However, the comparison of these measurements have been difficult because of different sensitivities of detectors, some active and some passive, differing self shielding and in most cases unknown location shielding. In spite of these complications, very significant progress in the knowledge of the radiation environment onboard the *Mir* station has been made. These results are directly applicable to expected radiation environment on the *International Space Station*.

In this paper, we describe the combined results from all seven NASA Mir missions. We show: (1) the absorbed dose rate from trapped particles is well correlated with the atmospheric density computed nearly 400 days earlier than the time of observation, (2) developed a relationship between the absorbed dose rate from galactic cosmic rays to the deceleration potential derived using the Climax neutron monitor rate, giving a tool to predict GCR dose rates to $\pm 15\%$ nearly 90 days prior to observations, (3) describe the drift of the South Atlantic Anomaly (SAA) with time, (4) compare the predictions of the dose rates as a function of time from the November 6-8, 1998 solar particle event with observations, (5) compare measurements made with NASA Tissue Equivalent Proportional Counter (TEPC) with the ESA DOSTEL device, the Hungarian Pille system, and the Russian R-16 dosimeter. Implications of these measurements for the *ISS* will be discussed.

INVESTIGATION OF PROTON-INDUCED TARGET FRAGMENTATION IN LOW EARTH ORBIT

Eric Benton and E. V. Benton

Eril Research, Inc. P. O. Box 150788, San Rafael, CA 9495-0788

The secondary radiation field produced by the passage of energetic protons through shielding is to a large extent determined by the composition and volume density of the shielding material. Investigation into the role played by proton-induced, high-LET target fragmentation in the overall radiation exposure encountered in low Earth orbit (LEO) is ongoing. Measurements made, both aboard the Russian Mir Space Station and at the Loma Linda University Proton Treatment Center (LLUPTC), using plastic nuclear track detectors (PNTD) demonstrate that high-LET target fragments are a significant source of the dose equivalent resulting from exposure to energetic protons. Measurements made in CR-39 PNTD exposed to proton beams at LLUPTC show that secondary particles of $LET > 10 \text{ keV}/\mu\text{m}$ contribute $\sim 4\%$ to total dose and $\sim 30\%$ to total dose equivalent. Current methods of detector analysis using PNTDs are not able to measure short-range, high-LET recoils from proton interactions with heavy nuclei such as Ca. A new method utilizing Atomic Force Microscopy is being developed to analyze these short range particle tracks in CR-39 PNTDs.

ANALYSIS OF THE CALIBRATION RESULTS OBTAINED WITH THE FLIGHT MODEL
OF THE MOBILE RADIATION EXPOSURE CONTROL SYSTEM LIULIN FOR THE
“DOSIMETRIC MAPPING” EXPERIMENT TO BE FLOWN ONBOARD US
LABORATORY MODULE OF ISS

Ts. Dachev¹, B. Tomov¹, Yu. Matviichuk¹, Pl. Dimitrov¹, J. Lemaire², Gh. Gregoire³
G. Reitz⁴, R. Beaujean⁵

¹ Solar-Terrestrial Influences Laboratory, 1113 Sofia, Bulgaria; stilrad@bgciict.acad.bg

² Institut d’Aeronomie spatiale de Belgique, 1180 BRUXELLES, Belgique

³ Institut de Physique, Universite Catholique de Louvain , Louvain-la-Neuve, Belgique

⁴ DLR, Institute fuer Luft-und Raumfahrtmedizin, Linder Hohe, 51140, Cologne, Germany

⁵ Institute fuer Kernphysik des Universitaet Kiel, d-24118 Kiel, Germany

INTRODUCTION

The Mobile Radiation Exposure Control System (Liulin) is a part of the experiment Dosimetric Mapping E094, which is developed to be placed in the US Laboratory Module as a part of the Human Research Facility (HRF). The German (University of Kiel) build two DOSimetric TELEscopes (DOSTEL) and Hungarian build 10 Thermoluminescent Dosimeters and reader (PILLE) are the other 2 instruments included in the experiment Dosimetric Mapping. The PI of the experiment is Dr. Guenther Reitz from DLR, Germany. All units of the experiment are connected trough the Power Box service unit, build by University of Kiel, with the HRF laptop PC and power line of the station. The dosimetry information from E094 experiment will be transmitted by RS-232 to the HRF PC hard disc drive. Part of it is passed to the Earth.

METHODS

The Mobile Radiation Exposure Control System’s (Liulin) main purpose is to monitor simultaneously the doses and fluxes at four independent places of the station or to be used as a personal dosimeter. The system consists of 4 battery operated Mobile Dosimetry Units (MDU) and one Control and Interface Unit (CIU). The Flight model of the system is already developed and builds. It is scheduled for intensive calibration procedures in the next few months. The first tests will be in the laboratories of STIL-BAS and will be directed mainly to the electronic schema performance tests of the MDUs by use of electronic pulser and standard ¹³⁷Cs source. Next will be tested the accuracy of the 12 bit ADC using ²⁴¹Am alpha particles source inside of vacuum chamber. The dosimetric characteristics of the system will be tested at the standard gamma test facility of Bulgaria. The last calibrations are scheduled at the University of Louvain, Belgium, Cyclotron facility at up to 90 MeV protons beam. First MDUs will be irradiated together with a standard monitor to be calibrated the flux accuracy measurements. Next the angular characteristics of MDUs will be studied and compared with preliminary Monte-Carlo model calculations. The last planed tests will occur during airplane flights in conditions close to the real. Cari-3 model intercomparisons are planed also.

RESULTS

All expected results of the tests and calibrations procedures will be analyzed and presented to the workshop.

CONCLUSIONS

The authors of this paper are looking with great interest on the opportunity to exchange ideas with other experimental groups on the proposed above calibration and intercalibration plan during the workshop.

**MEASUREMENTS OF LET DISTRIBUTION AND DOSE EQUIVALENT
WITH REALTIME RADIATION MONITORING DEVICE (RRMD)
ONBOARD A SERIES OF SHUTTLE MIR MISSIONS**

T. Hayashi¹, T. Doke¹, N. Hasebe¹, T. Kashiwagi², J. Kikuchi¹, M. Kobayashi¹, S. Kono¹, A. Kyan³, S. Nagaoka⁴, T. Nakano⁴, K. Ogura⁵, T. Sakaguchi¹, K. Takahashi¹, S. Takahashi⁴, T. Takagi¹, T. Takashima¹, K. Terasawa¹, E. Yoshihira¹, and G. D. Badhwar⁶

¹Advanced Research Institute for Science and Engineering, Waseda University, Okubo 3-4-1, Shinjuku-ku, Tokyo 169-8555, Japan

²Department of Industrial Engineering, Kanagawa University, Rokkakubashi 3-27-1, Kanagawa-ku, Yokohama 221-8686, Japan

³Faculty of Science, Ibaraki University, Bunkyo 2-1-1, Mito, Ibaraki 310-8512, Japan

⁴Tsukuba Space Center, NASDA, Sengen 2-1-1, Tsukuba, Ibaraki 305-8505, Japan

⁵College of Industrial Technology, Nihon University, Izumi-cho 1-2-1, Narashino, Chiba 275-8575, Japan

⁶NASA Johnson Space Center, Houston, TX 77058, USA

Space radiation dosimetry measurements have been made onboard a series of Shuttle Mir Missions (51.6 deg. x 400 km). In these measurements, Real time Radiation Monitoring Device III (RRMD-III) of an improved silicon detector which can detect minimum ionizing particles was used as well as a low sensitive silicon detector (RRMD-II) with a large area and conventional passive detectors of thermoluminescence dosimeters (TLDs) and CR-39 plastic track detectors. The data from RRMD-III were separated into two contributions from trapped particles and galactic cosmic rays (GCRs). A precise investigation on linear energy transfer (LET) distributions was made by comparing the results of passive detectors and of other groups using TEPC. The results of RRMD-II and CR-39 are in good agreement for LET of 15 - 200 keV/ μ m and difference below 15 keV/ μ m and above 200 keV/ μ m can be explained by the characteristics of CR-39 etched track formation. A discrepancy below 6 keV/ μ m was also found between results of RRMD-III and TEPC mainly due to the lower sensitivity of TEPC and the intrinsic limitation in the resolution of LET values by the TEPC detector shape. In this presentation, we will discuss about absorbed dose rate 4.80 μ Gy/m and effective quality factor 1.19 by ICRP-Pub.26 for trapped particles, and 0.120 μ Gy/m, 3.16 for GCRs in detail as well as comparison of observed LET distributions with the calculated ones of several models.

HIGH-LET MEASUREMENTS IN LOW-EARTH ORBITS

E.G. Stassinopoulos and C.A. Stauffer

A newly developed compact High-LET Radiation Spectrometer (HiLRS) was flown on the STS-95 DISCOVERY mission. The space-qualified instrument was designed on microelectronics principles and its primary objective was to measure the energy deposited by: a) galactic and solar cosmic rays and their progeny from interactions with spacecraft materials, and b) spallation, fractionation, or recoil products from energetic trapped protons. Results and conclusions from this flight will be presented.

Monday, June 14

Brookhaven National Laboratory

11:10 a.m. – 12:30 p.m.

**DNA/Chromatin/Chromosomes –
Damage and Repair**

Berkner Hall

HPRT MUTATION INDUCTION IN HUMAN CELLS BY HEAVY-ION IRRADIATION

F. Yatagai¹, A. Gordon¹, S. Morimoto¹, N. Fukunishi¹, M. Honma², T. Sofuni² and F. Hanaoka¹

¹The Institute of Physical and Chemical Research, Saitama 351-0198, JAPAN and ²National Institute of Health Sciences, Tokyo 158-8501, JAPAN.

INTRODUCTION

Our approach to understand the biological influence of space environments as well as the basic mechanisms of mutation induction is to elucidate the mutational specificity of heavy ions of various LET (Linear Energy Transfer). It is of interest to study the nature of mutations caused by high-LET radiation since it is suggested that such radiation produces DNA damage different from that produced by conventional ionizing radiation. Indeed, our analyses of hypoxanthine phosphoribosyltransferase (*hprt*) mutations in human cultured cells reveals heavy-ion energy dependent mutational spectra. For example, we observe a high frequency of recovery of point mutations at a high-level of LET, at that point when ions will lose most of their total energy and stop shortly after passing the cells. In this same energy region, we also observe mutational events that represent complex loss of multiple non-contiguous exon regions.

Recently, the tumor suppressor gene *p53* has come to be regarded as a guardian of cells against not only radiation but also various chemicals. In this report, we assess the influence of mutant *p53* gene on heavy-ion-induced mutagenesis in human lymphoblastoid cells.

METHODS

WI-L2-NS and TK6 are lymphoblastoid cell lines that are derived from the same human spleen. WI-L2-NS has a mutation in codon 237 of *p53* and contains only mutant *p53* protein due to hemizygoty at the *p53* locus. For irradiation on these cells, the energies of C-, Ne- and Fe-ions were adjusted so to irradiate the cells with three different LETs: one at the initial energy, one at the peak of Relative Biological Effectiveness (RBE) and at that point when ions will lose most of their total energy and stop shortly after passing the cells. The *hprt* mutant cells were selected by their resistance to 6-thioguanine (6-TG; 5 mg/ml) and the *hprt* mutations were mainly analyzed by multiplex PCR methodology using genomic DNA. Mutational events judged to be relatively large deletions were further analyzed by chromosome painting (FISH). The induction of *p53* and *p21* (*waf-1*) proteins after heavy-ion irradiation was also determined by Western blotting methodology.

RESULTS

Similar to the results for X-ray irradiation, WI-L2-NS cells were more radio-resistant and mutable than TK6 cells after C-, Ne-, Ar- and Fe-ion irradiation at particular levels of beam-energy (initial energy) (Table 1). The *p53* and *p21* protein induction patterns for the two cell lines after such heavy-ion irradiations were similar to that found after X-ray irradiation (in TK6, *p53* and *p21* were induced; in WI-L2-NS, *p53* was constitutively expressed and *p21* was not expressed). The *hprt* mutations obtained after radiation treatments were analyzed mainly by multiplex PCR methodology. We did not observe any striking difference in the pattern of exon deletion between the two cell lines (Fig. 1). However, a difference in the partial deletion pattern was observed after analysis of Ne-ion induced mutants (data not shown). Interestingly, chromosome painting analysis of partial deletion events demonstrated that the same C-terminal

deletion event isolated from different cell-lines may result in a different type of translocation (data not shown).

Table 1 *hprt* mutation induction after the exposure of heavy-ions.

Ion (LET: keV/ μ m)	TK6			WI-L2-NS (WTK1)		
	Dose (Gy)	SF	MF ($\times 10^{-4}$)	Dose (Gy)	SF	MF ($\times 10^{-4}$)
C (22)	2.0	0.058	7.2	2.4	0.068	9.8
Ne (67)	1.0	0.056	9.9	1.2	0.14	31
Fe (1000)	2.0	0.24	7.6	2.4	0.27	17

SF: Surviving fraction, MF: Mutation frequency

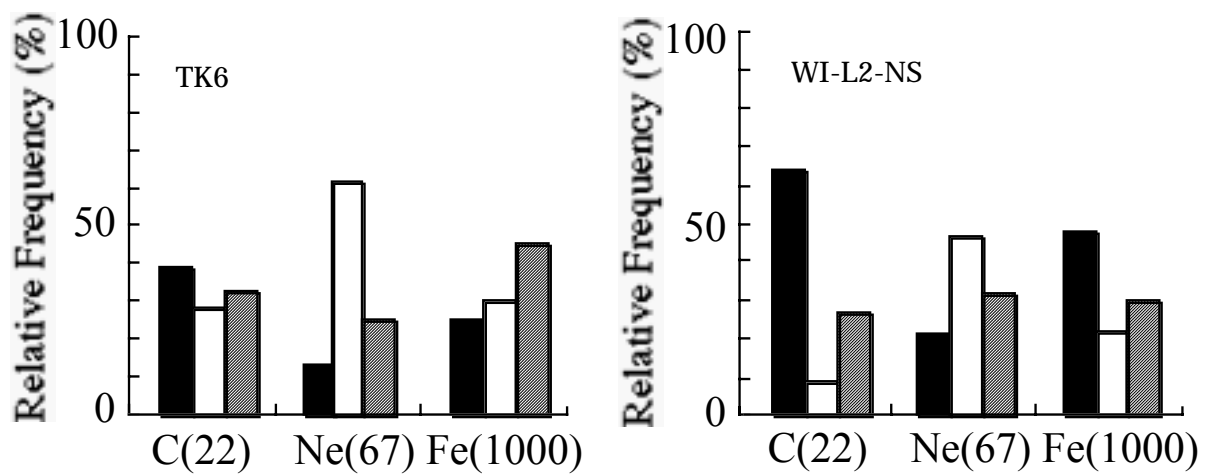


Fig.1 Classification of Mutational Events: Here, \blacksquare ; point mutation (normal amplification); \square ; partial deletion (some regions are amplified), \hatched complete deletion (no amplification).

CONCLUSION

We do not observe a strong influence of mutant p53 on the specificity of heavy-ion induced *hprt* mutations, however our analysis is not yet complete.

INFLUENCE OF HZE ^{59}Fe PARTICLES ON CHROMOSOME ABERRATIONS IN RAT BONE MARROW AND RESPIRATORY TRACT CELLS

A.L. Brooks¹, S. Bao², K. Rithidech³, L.A. Couch¹, L.A. Braby⁴ 1. Washington State University, Tricities, Richland WA 99352, 2. U.S. Transuranium and Uranium Registries Washington State University, Tricities, Richland WA 99352, 3. SUNY at Stony Brook, Stony Brook NY. 11795, 4. Texas A&M University, College Station TX 77843.

INTRODUCTION

During prolonged space flight there is a high probability that a significant exposure to cosmic rays will occur. It is important to understand how exposure to cosmic rays, which contain HZE particles like ^{56}Fe , impact the risk for development of cancer. As part of developing this understanding, the relationships that exists between initial chromosome damage, chromosome damage that persists for long periods of time, multiple-damaged sites on single chromosomes in single cells and the induction of genomic instability are being defined. Studies are being conducted in rapidly dividing bone marrow cells and in two epithelial cell types that have longer cell turnover times. The epithelial cells selected for study are the tracheal epithelial cells, which are very resistant to the induction of cancer from high LET radiation, and the deep lung epithelial cells, which are sensitive to radiation induced cancer.

METHODS

Ten Wistar rats were exposed to each of a series of graded doses of ^{56}Fe particles (1000 Mev/AMU) at 0.0, 0.2, 0.5, 1.0 and 2.0 Gy using a dose rate of 0.2 Gy/min. Cells from the bone marrow and respiratory tract were isolated and grown in short term culture. The frequency and distribution of chromosome damage was evaluated in the bone marrow. As a measure of genetic damage, the frequency of micronuclei per binucleated cell was scored in both fibroblasts and epithelial cells of the respiratory tract. Cells were also maintained in culture for multiple passage and chromosomes prepared for evaluation of genomic instability. Indicators of cell proliferation and chromosome damage were evaluated as a function of exposure, dose and time after exposure.

RESULTS

The data demonstrated that the exposure to HZE particles caused a mitotic delay in bone marrow cells, and also demonstrated that there was an increase in the mitotic index as a function of time after the end of the exposure. There was an increase in the frequency of chromosome aberrations as a linear function of dose, with the slope of 0.32 aberrations/cell/Gy. Fitting the data to a polynomial function did not significantly improve the fit. Most of the aberrations were of the chromatid type, since the bone marrow cells are rapidly dividing at the time of the radiation exposure. In the high exposure group (2.0 Gy), it was observed that some cells had multiple aberrations present on individual chromosomes, suggesting a "direct hit" of the HZE particle on the chromosome.

The frequency of micronuclei in both the fibroblasts and epithelial cells of the trachea and lung increased as a linear function of dose. The slopes of the dose-response relationships were 1.1×10^{-2} micronuclei/binucleated cell/Gy for both the fibroblasts and epithelial cells of the trachea.

For the deep lung, the slope of the dose-response relationship was 7.0×10^{-3} and 1.2×10^{-2} micronuclei/binucleated cell/Gy for the fibroblasts and epithelial cells respectively.

CONCLUSIONS

Initial damage has been characterized in three different tissues following exposure to HZE particles. Mitotic lag was induced in the bone marrow and chromatid aberrations were increased. The presence of multiple-damaged sites on individual chromosomes requires additional study with non-dividing tissue and is currently underway. There were no differences between the sensitivity of the epithelial cells from the two anatomical sites in the respiratory tract. In the deep lung, the fibroblasts were more resistant to the effects of HZE particles than were the epithelial cells. The response of the respiratory tract epithelial cells to HZE particles per Gy was compared that observed for gamma rays and alpha particles from radon inhalation. It was determined that HZE particles were 1.3 and 3.3 times more effective than ^{60}Co gamma rays for induction of micronuclei in deep lung and tracheal epithelial cells, respectively. The HZE ^{56}Fe particles were only 14% and 25% as effective as Radon alpha particles in producing micronuclei in the deep lung and tracheal epithelial cells, respectively. Such studies help place the HZE particles in proper perspective for the induction of initial chromosome damage. Studies are continuing to relate the repair of initial damage from induced by HZE particles to the repair of damage from other radiation types. Repair of the initial cytogenetic damage may play an important role in the induction of genomic instability. Research supported by a Grant # 2 RO1 CA74053-01 from NIH/NCI and NASA with Washington State University Tricities.

THE EFFECTS OF MICROGRAVITY ON LIGASE ACTIVITY IN DNA REPAIR FOR DOUBLE STRAND BREAKS

T. Ohnishi^{1*}, K. Ohnishi¹, A. Takahashi¹, T. Nakano², and S. Nagaoka²

¹Department of Biology, Nara Medical University, Kashihara, Nara 634-8521 and ²Space Experiment Department, National Space Development Agency (NASDA) of Japan, Tsukuba, Ibaraki 305-0047, Japan

INTRODUCTION

Exposures in space consist of low-level background components from space radiation, occasional intense-energetic solar-particle events, periodic passes through geomagnetic-trapped radiation, and exposure from possible onboard nuclear-propulsion engines. The low-level background exposures of space radiation, including heavy ions and other high linear energy transfer (LET) radiation, will be the ultimate limiting factor for astronaut career exposure. In recent years, physical monitoring of space radiation has detected about 1 mSv per day. This value is almost 30 times higher than that on the surface of the earth. However, the direct effects of space radiation on organisms is currently unknown. Therefore, it is important to measure biological dosimetry to calculate relative biological effectiveness (RBE) for human health during long-term flight. It is easily assumed that such space radiation might induce a serious amount of DNA damage compared with radiation exposure on the ground, because the earth is protected from such high exposure by the ozone layer, atmosphere chemicals and magnetic field of the earth. Diverse biological effects of space environment have been reported; for instance, microgravity enhanced radiation effects on abnormal development in *Carausius morosus* and induced mutation frequency in *Drosophila melanogaster*. These findings suggest that space radiation may depress recovery from DNA damage induced by space radiation. As one possibility, we proposed that DNA ligation in the final step of DNA repair is depressed by microgravity. Ligase reaction was performed during a space flight by the Space Shuttle Discovery (STS-91; on June 2, 1998, 10 days).

METHODS

Samples and experimental procedures. Double strand breaks (DSBs) of plasmid DNA pRC (2.2 kbp) was formed by enzymic digestion with a restriction enzyme (*Sma* I). The structure of the DNA end was blunt end. Two kinds of liquid of 200 μ l reaction buffer containing DSB DNA and 10 μ l enzyme dilution buffer containing T4 DNA ligase were separately sealed in a special short tube (2.2 cm x 6.0 cm) (Fig.1). The short tube was specially constructed from polypropylene sheet. To investigate the rate of enzymic reaction, T4 DNA ligase was enveloped by different concentrations (0-3 Weiss Unit/ μ g). As activation, the separating films were broken by manually pushing from one side of the separated compartment in each stripped bag. And then, the chemical reaction of ligation started with mixing of the two kinds of liquid reaction buffer containing DSB DNA and enzyme dilution buffer containing T4 DNA ligase. The reaction was incubated at room temperature (21.6-22.1 \circ C) for 10 h. The reaction was stopped with mixing 300 μ l of stop solution containing SDS and proteinase K. Finally, the short tubes were stored in a freezer (-20 \circ C). These steps from activation to deactivation were performed by two crews. Post-flight control experiments on earth were performed at the NASA Johnson Space Center (JSC), Houston, USA under almost the same condition after getting down-link information about space experimental condition from Space Shuttle.

Measurement of DNA ligase activity. The plasmid DNA was purified immediately after landing at SPACEHAB's Payload Processing Facility in Cape Canaveral with a single extraction of the supernatant with phenol:chloroform. The DNA bands of plasmid DNA was analyzed by 1% agarose gel electrophoresis.

RESULTS AND DISCUSSION

We analyzed the rejoining of DSBs of plasmid DNA after flight by electrophoresis through a 1% agarose gel (Fig. 2A). Purified plasmid DNA (pRC) was indicated to be mainly closed circular DNA (ccDNA) and slightly open circular DNA (ocDNA) (Fig. 2A, lane C). The plasmid DNA digested with a *Sma* I restriction endonuclease indicated linear DNA (2.2 kbp) (Fig. 2A, lane L). By raising the ligase concentration, the linear DNA was decreased and ligated products, ccDNA, ocDNA and multi-ligated products, were increased (Fig. 2A and 2B). The results indicate that there was almost no effect of microgravity on DNA rejoining of the damaged DNA in space (Fig. 2A and 2B). In addition, we found no significant differences in DNA rejoining between space and control ground samples at 4°C for 15 h (data not shown). We did not detect smear fragments which were probably produced by space radiation. The effects of space environment on survival, induced mutation and repair remain unclear. It has been also reported that the space environment did not have any effect on induction of mutation in *E. coli* (1) and *Dictyostelium discoideum* (2,3) or on repair activity in *E. coli* and human fibroblasts. Space radiation includes heavy ions and other high LET radiation exposures during space flight. Radiation with differing energy qualities may influence the extent and fidelity of rejoining. The slowing down of rejoining and the increase in residual DNA damage with increased residual DNA damage with increasing atomic number and LET has been reported. Moreover, inappropriate rejoining of DSB from two separate tracks was dominant at low LET and inappropriate rejoining of DSB from a single track was dominant at high LET. The yield of rejoined chromosome measured soon after exposure was higher for high-LET than low-LET radiation.

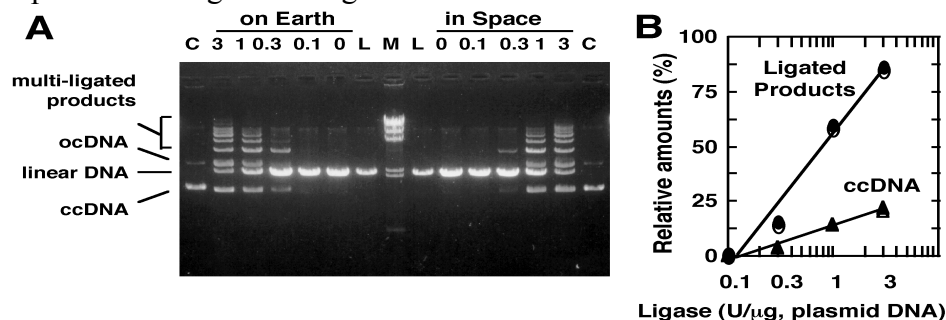


Fig. 1 Systems of enzymic reaction. a, blunt end of strand-break DNA and reaction buffer solution; b, blue bead and ligase; c, empty compartment; d, red bead and reaction stop solution containing detergent. e, f and g, special temporary sealing band. e, marking with red arrow; f, marking with blue arrow. A, before activation; B, after activation; C, after deactivation.

Fig. 2 Rejoining of DNA double strand breaks. A, typical pattern of gel-electrophoresis. Lane C, pRC; lane L, pRC digested by *Sma* I; lane M, molecular marker (IDNA-*Hind* III fragment). 0, 0.1, 0.3, 1 and 3, different concentrations of DNA ligase (U/μg, plasmid DNA). B, measurement of the density of DNA bands at room temperature (21.6-22.1°C) for 10 h. Closed symbols, on earth; open symbols, in space. Circle, ligated products (ccDNA, ocDNA and multi-ligated products); triangle, ccDNA.

CONCLUSION

Previous papers suggested that space radiation may depress recovery from DNA damage induced space radiation. When ionizing radiation strikes a cell, it induces DNA DSBs. We attempted to measure the effects of microgravity on rejoining of DNA DSBs. In recent years, some papers have reported synergism in the biological effects of space radiation and microgravity. As one possible mechanism, we investigated the effects of microgravity on repair activity of T4 DNA ligase for DSB prepared with digestion of a restriction enzyme to plasmid DNA. Investigations were performed during a US Space Shuttle mission (Discovery; STS-91). We detected almost no difference in DNA ligase activities between space and the control ground experiments. Therefore, we must accept other possible mechanisms to explain the synergism if it exists.

ACKNOWLEDGEMENTS

The data were obtained from the joint NASA and NASDA Real Time Radiation Monitoring Dosimetry (RRMD) program.

REFERENCES

1. K. Harada, Y. Obiya, T. Nakano, M. Kawashima, T. Miki, Y. Kobayashi, H. Watanabe, K. Okaichi, T. Ohnishi, C. Mukai and S. Nagaoka, Cancer risk in space due to radiation assessed by determining cell lethality and mutation frequencies of prokaryotes and a plasmid during the Second International Microgravity Laboratory (IML-2) Space Shuttle experiment. *Oncol. Rep.* **4**, 691-695 (1997).
2. T. Ohnishi, A. Takahashi, K. Okaichi, K. Ohnishi, H. Matsumoto, S. Takahashi, H. Yamanaka, T. Nakano and S. Nagaoka, Cell growth and morphology of *Dictyostelium discoideum*. in space environment. *Biol. Sci. Space* **11**, 29-34 (1997).
3. A. Takahashi, K. Ohnishi, M. Fukui, T. Nakano, K. Yamaguchi, S. Nagaoka and T. Ohnishi, Mutation frequency of *Dictyostelium discoideum* spores exposed to the space environment. *Biol. Sci. Space* **11**, 81-86 (1997).

BIODOSIMETRY USING A CHEMICAL-INDUCED PREMATURE CHROMOSOME CONDENSATION TECHNIQUE

H. Wu^{1,2}, T. Kawata^{2,3}, Y. Furusawa⁴, T. Yang² and D. R. Morrison²

¹Kelsey-Seybold Clinic, Houston, Texas; ²NASA Johnson Space Center, Houston, Texas;

³University of Keio, Tokyo, Japan; ⁴National Institute of Radiological Sciences, Chiba, Japan

INTRODUCTION

Analysis of chromosome aberrations in cells reaching mitosis is the current method for biodosimetry for space radiation exposures. Recently a chemical-induced premature chromosome condensation (PCC) technique that condenses both G2 and M phase cells has been developed. In this study, we compared chromosome aberration frequencies in human lymphocytes exposed to high-LET iron ions using both the metaphase and the PCC technique, and determined which method was more appropriate for assessing space radiation damages.

METHODS

Human lymphocyte cells were exposed to 0.3 Gy and 2 Gy of 200 MeV/u Fe ions and were stimulated to grow immediately after irradiation. The condensed cells were collected using both a chemical-induced PCC technique and the traditional metaphase technique after 48 and 72 hours of incubation. Chromosome aberrations were analyzed using a fluorescence *in situ* hybridization (FISH) technique with chromosome #1 and #2 probes. Chromosome aberrations were classified by the number of chromosome breaks in the painted chromosomes.

RESULTS

The frequency of aberrant cells using the PCC technique was found to be two to three times higher than that using the metaphase technique, suggesting that the damaged cells are less likely to reach mitosis than the undamaged ones. Compared to the cells collected after 48 hours of incubation with the PCC technique, the frequency of aberrant cells was observed to be twice in samples collected after 72 hours of incubation at high dose. A higher fraction of cells with multiple breaks was also found in 72 hour samples. Our results indicated that severely damaged cells grew slower than less damaged cells.

CONCLUSION

Compared to the traditional metaphase method, the PCC technique detects higher frequencies of chromosome aberrations induced by high-LET radiation and should be considered as the choice for biodosimetry for space radiation exposures.

Monday, June 14

Brookhaven National Laboratory

1:30 p.m. – 2:50 p.m.

Mutation

Berkner Hall

CHARACTERIZATION OF HEAVY-ION INDUCED LACZ MUTANTS IN TRANSGENIC ANIMALS

P. Y. Chang¹, N. Kanazawa¹, L. Lutze-Mann², and R. A. Winegar¹

¹SRI International, Menlo Park, CA 94025; ²University of New South Wales, Sydney, Australia

INTRODUCTION

Exposure to cosmic radiation poses significant risk to personnel who embark on long space missions. The objective of our research is to use a transgenic mouse model system to evaluate the risks of mutations associated with exposure to particle radiation. The plasmid-based transgenic mice, with an integrated lacZ target gene in every cell of the organism, provide a unique approach for measurement and characterization of gene mutations in essentially any tissue. Furthermore, to determine the effect of genetic background, we are using animals with the lacZ target gene integrated into their genomes that are either hemizygous or nullizygous for the p53 gene. At the previous meetings, we have reported an increase in the target transgene mutation frequencies in animals exposed to 1Gy of 1GeV/amu iron particle radiation in the brain and spleen tissues. We have extended our studies to examine and characterize the mutants harvested from these tissues.

METHODS

Transgenic lacZ mice with different p53 genotypes were exposed to 1 Gy of 1 GeV/amu iron ions at the AGS at Brookhaven National Laboratory. The mutation frequency in the lacZ target gene was analyzed based on the procedure of Gossen et al. (Biotechniques, 14: 624-629, 1993). Mutant colonies were harvested and grown in CircleGrow medium with ampicillin (75 µg/ml) and kanamycin (25 µg/ml). Plasmid DNA was extracted using the UltraClean Mini Plasmid Prep Kit from MoBio (CA) and restriction fragment length polymorphism (RFLP) analysis was performed. DNA was digested with a single enzyme, RsaI, or dual digested with PstI/SacI. The restriction patterns for the lacZ containing plasmid pUR288 were used as the control.

RESULTS

Based on the differences in the restriction patterns of mutant plasmid DNA derived from the same tissue, we were able to distinguish mutant clones that were either unique or those that could be derived from clonal expansions. A significant percentage of the mutations were large deletions greater than 1-kilobase. Some mutants appear to have deletions that appear to extend past the transgene into mouse genomic DNA. This is in contrast to the published data showing that more than 50% of spleen mutants selected from X-ray-irradiated p53+/+ animals are point mutations (Gossen et. al., Mutation. Res., 331: 89-971995).

CONCLUSION

Large deletions appear to be the predominant lesion in the lacZ target gene as a result of the exposure of transgenic mice to 1 Gy of 1 GeV iron particles.

ANALYSIS OF ALPHA PARTICLE INDUCED CHROMOSOMAL ABERRATIONS AND *HPRT* GENE MUTATIONS

Hatsumi Nagasawa and John B. Little
Harvard School of Public Health, Boston, MA 02115

An understanding of the effects of radiation at low total doses is important in the determination of radiation protection standards for occupational and environmental exposures to low levels of radiation. It has generally been reported that cell killing and the induction of chromosomal aberrations and HPRT gene mutations are linearly related with dose for α -particle irradiation, but show linear-quadratic relationship for gamma or X rays. Employing a specially constructed source that allows exposure to very low fluences of ^{238}Pu alpha particles, we have observed biphasic dose-response curves with a transition at approximately 10 cGy for chromosomal aberrations and HPRT gene mutations. There was a noticeable shoulder region on the survival curve after exposure of cells synchronized in G₁ to alpha particle doses of less than 10cGy. The rate of induction of chromosomal aberrations and HPRT gene mutations was nearly three times higher after low dose exposures (less than 10cGy) than following doses up to 300 cGy. There was no threshold observed for alpha particle induced chromosomal aberrations and HPRT gene mutations with doses below 10cGy. Alpha particle induced HPRT gene mutation frequencies were 2.25×10^{-5} per track for doses of 10-300 cGy. However, the mutation frequencies per track increased sharply with doses below 10cGy, reaching 16.0×10^{-5} per track at 0.83 cGy (0.031 track per nucleus). We are currently examining the DNA repair deficient mutant strain xrs 5 in order to determine the role of DNA repair in these endpoints.

STUDY OF THE ROLE OF THE MISMATCH BASE REPAIR AND GENE MUTATION IN HUMAN TUMORAL CELL LINES EXPOSED TO LOW-ENERGY LIGHT IONS.

R. Cherubini¹, F. Cucinotta², J.F. Dicello³, S. Favaretto¹, D. Saggioro⁴ and J.R. Williams³

¹INFN-Laboratori Nazionali di Legnaro-Padova, Italy; ²NASA Johnson Space Center, Houston,TX-USA; ³Johns Hopkins University, Oncology Center, Baltimore, MD-USA; ⁴I.S.T., Sezione di Biotecnologie-Dipartimento di Scienze Oncologiche e Chirurgiche, Universita' di Padova - Padova, Italy.

Low-energy protons and alpha particles are the most important high LET radiation experienced by humans in both ground environmental and therapeutic conditions. Moreover, low-energy protons and alphas are expected to be major contributors to cancer risk in the space behind spacecraft and body shielding.

In the recent years experimental evidence has shown an increased biological effectiveness of low-protons and alpha particles with respect to X-/gamma-rays for several cellular and molecular endpoints. The role of cell cycle control proteins in the radiation injuries as well as the biochemical mechanisms involved in the increased effectiveness of high LET radiation are still poorly understood.

As it is already known, cell death from radiation exposure is controlled by the activation/inhibition of important metabolic pathways mediated by several proteins including p53, Bax, Bcl-2 and p21CIP, involved in the cell cycle control.

Moreover, mutation in p53 and mismatch base repair (MMR) genes can have an important role in genetic instability and in the cell response to radiation. To contribute to understanding of the biochemical mechanisms involved in the cell response to the high LET, low-energy accelerated light ions, we have undertaken a systematic investigation of cell inactivation, gene mutation and protein expression induced by protons and alpha particles with different quality in human colorectal cell lines.

Irradiation experiments are performed at the radiobiological facility of the 7 MV CN Van de Graaff accelerator at the INFN-Laboratori Nazionali di Legnaro, Padova-Italy

In the present work we will report preliminary results on cell inactivation and early p53 expression (1 hr after exposure) in DLD-1 (p53 mut; MMR mut) and HCT116 (p53 wildtype; MMR mut) human tumor cell lines irradiated with 80 and 101 keV/um helium-4 ions. Irradiation with ⁶⁰Co gamma rays have been performed for comparison purpose.

CELLULAR AND MOLECULAR EFFECTS FOR MUTATION INDUCTION BY CHARGED PARTICLES WITH DIFFERENT LET

M.Suzuki¹, Y.Kase², T.Kanai², M.Watanabe³, T.K.Hei¹ and E.J.Hall¹

¹Center for Radiological Research, Columbia University, New York 10032,

²National Institute of Radiological Sciences, Chiba 263,

³ Nagasaki University, School of Pharmaceutical Sciences, Nagasaki 852.

INTRODUCTION

It is very important and necessary for risk estimation of cosmic rays in space to make clear biological effects, such as mutation and transformation, for charged particles with different kinds of ions and linear energy transfers (LETs). It has been well known the mutation induction by high-LET radiations is higher than by low-LET radiations for various gene markers on human and rodent cell system. Hei et al. (1988) reported the LET-dependent effect of hprt mutation in primary human fibroblast cells using charged particles defined LET ranged from 10keV/ μ m proton to 150keV/ μ m 4He ions generated by the Radiological Research Accelerator Facility (RARAF) at Nevis Laboratories of Columbia University (1). The limited data for LET dependence of the mutation induction by using various kinds of heavy-ion beams show that the most effective range of LET in producing mutation is 100 to 200keV/ μ m. In molecular studies, very limited information is available for detecting the mutation spectra of high-LET-induced mutants by using the southern blot hybridization method and the PCR method. Zhu et al. (1996) reported that the deletion of hprt gene in mutants induced by 150keV/ μ m 4He ions is higher frequent than those by 137Cs gamma rays (2). On the other hand, the results indicated that there was no evidence that qualitatively different types of radiation might cause different mutation spectra (3,4). In this study we investigated the LET dependence of different kinds of ion beams for the dose-response curves of mutation induction on the HPRT locus cells and analyzed the molecular characterization for the deletion spectra on the exons using the multiplex PCR method in normal human.

METHODS

Human fibroblast cells were used in this study. The cells were irradiated with different kinds of ion beams ranging in LET from 10keV/ μ m to 335keV/ μ m. Carbon- and neon-ion beams generated by the Riken Ring Cyclotron (RRC) at the Institute of Physical and Chemical Research in Japan and the cyclotron at the National Institute of Radiological Sciences (NIRS) in Japan. Protons and helium-ion beams were generated by the Radiological Research Accelerator Facility (RARAF) at Nevis Laboratories of Columbia University. The energy of both the carbon- and neon-ion beams were 135 MeV/n. Lucite absorbers with different thickness were used to change energies of the beams in order to make various LET-beams. At the sample position, we estimated the LET^o values to be 22, 39, 68, 75, 110, 124, 148 and 230 keV/ μ m for carbon-ion beams and to be 63, 105, 131, 191, 234, 285 and 335 keV/ μ m for neon-ion beams. The LET^o values of protons and 4He ions were 10keV/ μ m and 150keV/ μ m, respectively. The frequency of mutation induction was determined as the number of 6TG-resistant colonies per 10⁶ survivors. The molecular characterization for deletion patterns of the exons in the hprt locus was analyzed by the multiplex polymerase chain reaction (PCR).

RESULTS

The results showed that the dose-response curves for mutation induction by C-ion beams were steeply increased up to 2.0Gy and the frequency of mutation induction by C-ion beams was 2.7 to 7.3 times higher than by ¹³⁷Cs gamma rays. On the other hand, the dose-response curves by Ne-ion beams were steeply increased up to 0.5Gy and were plateau or gradually decreased over the dose range of 1Gy compared to the response by C-ion beams. The maximum frequency of mutation induction, therefore, by Ne-ion beams was 10 to 100 times smaller than by C-ion beams. The deletion pattern of the exons in the *hprt* locus was LET-specific for C-ion beams. Almost all the mutants induced by 124 keV/μm carbon-ion beams showed deletion of the entire gene, while all mutants induced by 230keV/μm carbon-ion beams showed no deletion. In the case of Ne-ion beams, the deletion pattern was non-specific with LETs. About 80 to 95% of the mutants induced by Ne-ion beams with LETs of 63 to 335keV/μm showed all or partial deletion of exons and there were no difference of the deletion pattern with various LETs tested.

CONCLUSION

Our results suggest that the qualitatively different types of damage led to mutation following irradiation by qualitatively different types of radiation, such as C- and Ne-ion beams.

REFERENCES

- (1) T.K.Hei, D.J.Chen, D.J.Brenner and E.J.Hall, Mutation induction by charged particles of defined linear energy transfer. *Carcinogenesis*, 9, 1233-1236 (1988).
- (2) L.X.Zhu, C.A.Waldern, D.Vannais and T.K.Hei, Cellular and molecular analysis of mutagenesis induced by charged particles of defined linear energy transfer. *Radiat. Res.*, 145, 251-259 (1996).
- (3) J.Thacker, The nature of mutants induced by ionising radiation in cultured hamster cells. III. Molecular characterization of HPRT-deficient mutants induced by g-rays or α-particles showing that the majority have deletions of all or part of the *hprt* gene. *Mutation Research*, 160, 267-275 (1986).
- (4) S.Z.Aghamohammadi, T. Morris, D.L. Stevens and J.Thacker, Rapid screening for deletion mutations in the *hprt* gene using the polymerase chain reaction: X-ray and α-particle mutant spectra. *Mutation Research*, 269, 1-7 (1992).

Monday, June 14

Brookhaven National Laboratory

2:50 p.m. – 3:50 p.m.

Posters II

Berkner Rooms A & C

DNA DAMAGE BY LZE AND HZE IONS: MODEL OF INDUCTION OF DNA BREAKS AND RECOMBINATION REPAIR

Francis A. Cucinotta¹, Hooshang Nikjoo², Peter O'Neill², and Dudley T. Goodhead²

¹NASA Johnson Space Center, Houston TX 77058, USA

²MRC, Radiation and Genome Stability Unit, Harwell Didcot, OX11 0RD, U.K.

The induction and processing of double strand breaks (DSB's) is an important issue in understanding high linear energy transfer (LET) radiation. For galactic cosmic rays (GCR) exposures, high LET components are divided nearly equally between high-energy and charge (HZE) ions and light-energy and charge (LZE) produced in nuclear reactions. We discuss calculations of yields of DNA breaks for ions including single strand breaks (SSB), double strand breaks (DSB), and complex breaks within a 50 bp segment. Response functions that relate energy deposition to break types have been derived by Nikjoo et al. using Monte-Carlo simulations of DNA structure which consider direct, indirect, and hybrid (mixed direct and indirect) modes of action. In order to estimate yields of initial damage from LZE and HZE ions, response functions are folded with frequency distributions evaluated using an analytic track structure model for LZE and HZE ions. Calculations for energy deposition in DNA are compared to results from Monte-Carlo simulation codes for low-energy protons and alpha particles. Calculations of yields for SSB's and DSB's compared to measurements in the literature, and predictions for yields of complex breaks for LZE and HZE ions discussed.

Several processes are available for the repair of DSB's including homologous recombination and non-homologous end joining (NHEJ). We study a mathematical description of DSB repair and chromosome exchange aberration formation using a biochemical kinetics approach where damage processing is mediated by the formation of an enzyme-DSB complex. We show that fast and slow components of DSB repair, often modeled assuming biphasic kinetics, arise naturally in a model involving an enzyme-DSB complex. We discuss the roles of competition and saturation in damage processing pathways as a mechanism leading to non-linear dose responses. Our calculations indicate that the kinetics and dose response observed experimentally for DSB repair and exchange aberrations are consistent with a model of recombination repair of isolated DSB's without involving a pairwise interaction model. Implications of the model for understanding the processing of simple and complex DNA damage from LZE or HZE ions are discussed.

INDICATORS OF GENOMIC INSTABILITY FOLLOWING PROTON OR IRON ION EXPOSURE OF HUMAN TK6 LYMPHOBLASTS

A.J. Grosovsky¹, C. R. Giver¹, H. Bethel¹, K. Parks¹, L. Ritter¹, S. Gauny², C. Wiese², W. Liu² and A. Kronenberg²,

¹ Biomedical Sciences and Environmental Toxicology Graduate Programs, University of California, Riverside, 92521, and ² Life Sciences Division, Lawrence Berkeley National Laboratory, Berkeley, CA 94720

INTRODUCTION

One of the important questions for risk assessment for spaceflight radiations is their ability to induce a persistent state of genomic instability in the progeny of cells that may be exposed. We have previously shown that sparsely ionizing radiations such as x-rays or gamma-rays can produce karyotypic instability in the descendants of human TK6 lymphoblasts that that persists 80-100 generations after the original exposure (Grosovsky, et al., *Mol. Cell. Biol.* 16:6252-6262, 1996). A subset of the cells that had karyotypic instability also showed complex chromosomal rearrangements and increased mutation rates as established by Luria-Delbruck fluctuation analyses. The purpose of our ongoing study is to determine whether or not 55 MeV protons or 1 GeV Fe ions elicit any or all of the following indicators of instability in the clonal progeny of irradiated TK6 cells: 1) karyotypic instability as determined by G-banding, 2) increased mutation rate at the *TK1* locus, 3) reduced cloning efficiency many generations after the exposure.

RESULTS

TK6 cells were exposed either to 55 MeV protons (LET= 1.46 keV/μm) at the 88 inch cyclotron at Lawrence Berkeley National Laboratory, or to 1 GeV/amu Fe ions (LET= 146 keV/μm) at the Alternating Gradient Synchrotron at Brookhaven National Laboratory. The cells were exposed to 63 cGy, 126 cGy, and 189 cGy of the given radiation - this corresponds to an average of 2, 4 or 6 Fe ion traversals per cell or 200, 400, or 600 proton traversals per cell. For each radiation type and each dose level we collected 20 individual surviving clones and these clones were expanded for initial characterization of the three parameters of instability delineated above at approximately 21 days post-irradiation (corresponding to 25-30 generations post-exposure). We have also isolated 10 control clones for analysis and in addition have performed parallel analyses on bulk cultures of unirradiated TK6 cells.

Fe clones: Karyotypic analysis has been performed on 30/65 clones from the Fe-exposed cultures and the parallel control clones 21 days after the exposure. The basic protocol involves G-banding of 10 metaphase spreads per clone. We classify our clones on the following criteria: karyotypic heterogeneity is defined by the observation of a structural abnormality in at least one metaphase out of ten. Other parameters that are noted are multiply rearranged chromosomes or dicentrics, 3 or more distinct subclonal populations, 3 or more distinct structural abnormalities in a single metaphase, and rearrangements involving a centromeric breakpoint. We have previously reported that aneuploidy alone is not significant. To date, two clones manifested substantial karyotypic instability (>3 distinct subpopulations within a given clone). Two other clones have unusual derivative or marker chromosomes that suggest multiple rearrangements.

Luria-Delbruck fluctuation analysis has been performed to determine the mutation rate for both normal growth and slow growth mutants at the *TK1* locus in all 60 of the Fe-exposed clones, the 5 parallel control clones, and in 3 separate determinations for bulk TK6 cells. The standard mutation rate is defined by the mean of the 5 unirradiated control clones and the 3 bulk TK6 determinations. The standard mutation rate for normal growth *TK1* mutants was 4.30×10^{-7} /cell/generation (range ± 2 standard deviations includes from $0.9.0 \times 10^{-7}$ /cell/generation), while the standard mutation rate for slow growth *TK1* mutants was 1.03×10^{-6} /cell/generation (range ± 2 standard deviations includes from $0.57-1.48 \times 10^{-6}$ /cell/generation). We have isolated one clone that is hypomutable irrespective of the growth rate of the mutants, 4 clones that have an elevated mutation rate for normal-growth mutants, and 9 clones that have an elevated mutation rate for slow-growth mutants.

Delayed cloning efficiency has also been checked on the 60 Fe-exposed clones, 5 parallel control clones, and in 3 separated determinations for bulk TK6 cells. The standard cloning efficiency was defined by the mean of the 5 unirradiated control clones and the 3 bulk TK6 determinations. The standard cloning efficiency was 0.658 and the range ± 2 standard deviations includes from 0.444 to 0.872. Three clones were markedly below the lower limit of the range, while two were marginally outside the range.

Proton clones: To date, 26 of 60 proton-exposed clones have been karyotyped 21 days post-irradiation. Of these, two had karyotypic instability with at least 3 distinct subpopulations. Luria-Delbruck fluctuation analysis of *TK1* mutation rates is ongoing in the proton-exposed clones. We have not seen markedly reduced cloning efficiencies in those clones we have analyzed thusfar.

CONCLUSIONS

We have seen manifestations of genomic instability in a small percentage (ranging from about 5-15% depending on the endpoint examined) of TK6 clones that survived either low fluence exposures to Fe ions or exposure to comparable doses of protons. To date we have not seen a clear correspondance between karyotypic instability, elevated mutation rates, and delayed cloning efficiencies evaluated 21 days post-irradiation, although some overlapping phenotypes were noted among the Fe-exposed clones. Additional karyotypic analysis is underway on the remaining Fe-exposed clones, and additional karyotypic and mutation rate analyses are underway for the remaining proton-exposed clones. Supported by NIH grant 73966 to A. Kronenberg.

CHROMOSOMAL ABERRATIONS IN HUMAN LYMPHOCYTES INDUCED BY 1 GEV PROTONS IN VITRO

E.Krasavin¹, R.Govorun¹, M.Repin¹, G.Tymoshenko¹, M.Lukashova², and S.Kozubek²

¹Joint Institute for Nuclear Research, Dubna, Moscow Region 141980, ²Institute of Biophysics, Brno, Czech Republic

INTRODUCTION

The program of Man space flights to Mars arises interest to the research in biological action of protons with relativistic energy. The information on relative biological efficiency (RBE) of protons with relativistic energy is controversial. There are data that in number of cases the RBE appreciably exceeds the ratio 1. In this aspect, research of cytogenetic damages in human blood lymphocytes was conducted within the frames of the agreement between the Joint Institute for Nuclear Research and the Radiation Biophysics Laboratory, NASA Johnson Space Center.

METHODS

Irradiation of human peripheral blood lymphocytes with 1 GeV protons was conducted at the synchrophasotron of the Joint Institute for Nuclear Research. Lymphocytes were isolated from whole-heparinized blood of healthy donors. Cytological preparations were made by standard procedure. The conventional cytogenetic method and the FISH technique (fluorescence *in situ* hybridization) were applied for the human chromosome analysis. The *in situ* hybridization was performed using Cambio's biotinylated chromosome 1 and Oncor digoxigenated chromosome 2 painting probed to visualize both chromosomes on the same slide.

RESULTS

The conventional method of the cytogenetic analysis revealed a linear dependence of the frequency of cells with chromosome aberrations on the irradiation dose. The non-linear character of the dependencies is observed for the total number of the chromosome aberrations and for the dicentrics. The translocation frequency of chromosomes 1 and 2 grows also non-linearly with the irradiation dose. The curves for the total number of chromosome 1 and 2 aberrations have analogous character. The frequency of translocations of these chromosomes reaches 50 % of the total number of their aberrations. The RBE co-efficients of 1 GeV protons are 0.8 – 1.0 at the unstable aberration yield criterion and 0.9 – 1.2 at the stable aberration formation criterion.

CONCLUSION

The relative biological efficiency of 1 GeV protons at the criterion of cytogenetic damage in human lymphocytes is observed in the range of 0.8 – 1.2.

MECHANISMS OF MUTAGENESIS IN SYNGENEIC HUMAN LYMPHOID CELLS EXPOSED TO 55 MEV PROTONS: DISSECTING MUTATIONAL MECHANISMS AT THE *TK1* LOCUS AS A FUNCTION OF *TP53* STATUS

A. Kronenberg¹, S. Gauny¹, C. Cherbonnel-Lasserre², W. Liu¹, C. Wiese¹, ¹Life Sciences Division, Lawrence Berkeley National Lab, Berkeley, CA 94720 and ²Commissariat à l'Energie Atomique, F-92265 Fontenay-aux-Roses Cedex, France

INTRODUCTION

The underlying genotype of cells can affect their susceptibility to mutation induction after exposures to the types of ionizing radiations found in the space radiation environment. We have demonstrated previously that syngeneic human lymphoblastoid cell lines differing in *TP53* status had widely varying susceptibilities to mutations induced by 55 MeV protons (LET~1.46 keV/μm throughout the sample volume). TK6 cells express normal p53 protein while WTK1 cells have two mutant *TP53* alleles (Xia, et al., Cancer Res. 55:12-15, 1995; Zhen, et al., Mutation Res. 346:85-92, 1995; Little, et al., J. Biol. Chem. 270:11033-11036, 1995). In the present report, we focus on the mechanisms of mutagenesis at the autosomal, heterozygous *TK1* locus, situated on chromosome 17q. We report that allelic recombination associated with loss of heterozygosity (LOH) was the dominant phenotype in the WTK1 cells while deletional LOH was the dominant phenotype in the TK6 cells.

RESULTS

WTK1 cells were substantially more resistant to cell killing by 55 MeV protons than TK6 cells and the shapes of the dose response curves were different -- there was a shoulder on the killing curve for WTK1 cells while for TK6 cells the dose response appeared to be exponential. Susceptibility to *TK1* mutation was linear as a function of dose in each cell line, but the magnitudes of induction were very different. The WTK1 cells with homozygous mutant *TP53* were much more susceptible to proton-induced mutation (slope for WTK1 cells = $134.0 \pm 14.0 \times 10^{-7}/\text{cGy}$, $r^2=0.803$, slope for TK6 cells = $2.11 \pm 0.11 \times 10^{-7}/\text{cGy}$, $r^2=0.950$).

We collected 252 *TK1* mutants arising after exposure to 190.5 cGy of 55 MeV protons. Southern analysis of these mutants in either genetic background demonstrated that the predominant types of *TK1* mutations involved LOH. The only type of change observed among WTK1 mutants that appeared on the dishes at early times post-irradiation was LOH (60/60 mutants), while fewer LOH mutants were seen among the early-arising TK6 clones (25/62 mutants) (χ^2 , 2 d.f.= 51.37, $p<0.001$). LOH was the predominant form of alteration observed at a later time post-irradiation irrespective of the genetic background of the cell at risk (60/71 mutants for TK6 cells, 60/60 mutants for WTK1 cells). Nonetheless, Southern analysis revealed more LOH among late-arising WTK1 clones (χ^2 , 1 d.f.= 9.01, $p<0.005$).

Gene dosage studies were performed using the *BCL-2* gene (located on chromosome 18q) as a loading control to ascertain the number of copies of the silent *TK1* allele remaining in the various mutants that had lost heterozygosity. Mutants that retained only one copy of the silent *TK1* allele were presumed to have arisen by deletion, while those with two copies of the silent *TK1* allele were presumed to have arisen through allelic recombination. Allelic recombination was a common mechanism of mutation in WTK1 cells (44/60 early arising LOH mutants, 32/60 late

arising LOH mutants), while deletion was the more common mechanism of mutation in TK6 cells (24/25 early arising LOH mutants, 48/60 late arising LOH mutants). In those *TK1* mutants with normal cell cycle times (early mutants), allelic recombination was much more common in the cells with mutant *TP53* (χ^2 , 1 d.f.= 31.95, $p<0.001$). For *TK1* mutants with protracted cell cycle times (late mutants), allelic recombination was also more frequent in the WTK1 genetic background (χ^2 , 1 d.f.= 14.96, $p<0.001$).

CONCLUSIONS

Protons are the principal type of charged particle radiation in the various space radiation environments (solar particle events, trapped radiation belts, and galactic cosmic radiation). We have shown that loss of function of the tumor suppressor protein p53 is associated with a ~65x increase in susceptibility to proton-induced mutation at an autosomal locus in human cells. These results are in keeping with similar studies in TK6 and WTK1 cells that showed increased susceptibility to x-ray-induced or alpha-particle-induced mutation in the WTK1 cells vs. TK6 cells (Amundson, et al., Mutation Res. 286:233-241, 1993; Amundson, Chen, and Okinaka, Int. J. Radiat. Biol. 70:219-26., 1996), and our own findings that the WTK1 cells were also more susceptible to Fe-ion induced mutation. The present study showed that the basic mechanism of proton-induced mutation was a function of the *TP53* status of the cell at risk, with deletion more common in cells with normal *TP53* and allelic recombination more common among cells with only mutant *TP53*. The same general pattern was reported by us in cells exposed to Fe ions (Kronenberg, et al., Proceedings of the 9th Annual Investigator's Workshop in Space Radiation Research, Loma Linda, CA , 1998, p. 32-33). We are presently testing the hypothesis that the increased susceptibility to recombination-mediated mutagenesis in WTK1 cells is associated with a failure to properly regulate the function of key proteins involved in homologous recombination. We note, however, that the difference in *TP53* status in WTK1 vs. TK6 cells is unlikely to represent the sole explanation for the increased mutability of WTK1 cells. Supported by NASA grant T-964W to A. Kronenberg.

KU-PROTEIN VISUALIZATION AFTER HEAVY ION EXPOSURE

N.F. Metting

Pacific Northwest National Laboratory, Richland, WA 99352

INTRODUCTION

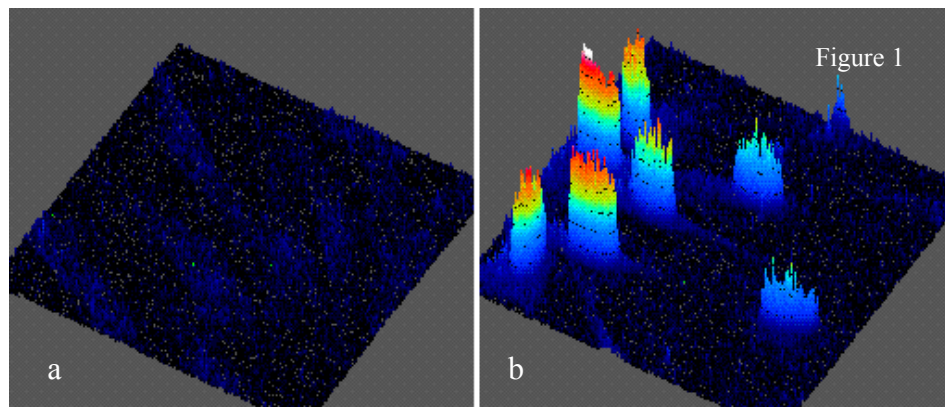
Ionizing radiation is good at making DNA double strand breaks, and high linear energy transfer (LET) radiations such as heavy ion particles are particularly efficient. For this reason, the proteins belonging to repair systems that deal with double strand breaks are of particular importance in the determination of long-term health risks from cosmic rays.

One such protein is Ku, a component in the non-homologous recombination repair system. The Ku protein is an abundant, heterodimeric DNA end-binding complex, composed of one 70 and one 86 kDa subunit. Ku protein binds to DNA ends, nicks, gaps, and regions of transition between single and double-stranded structure. These binding properties suggest an important role in DNA repair. The Ku antigen is important in this study because it is present in relatively large copy numbers and it is part of a double-strand-break repair system. More importantly, we consistently measure an apparent upregulation *in situ* that is *not* verified by whole-cell-lysate immunoblot measurements. This apparent upregulation is triggered by very low doses of radiation, thus showing a potentially useful high sensitivity. However, elucidation of the mechanism underlying this phenomenon is still to be done.

METHODS

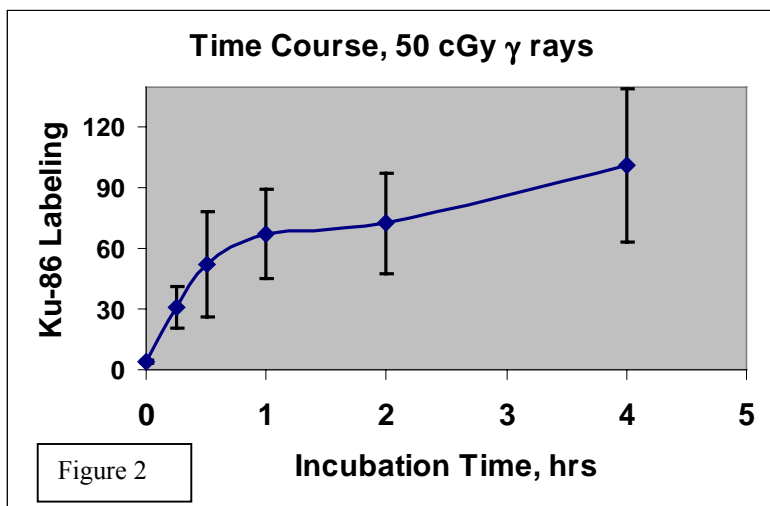
The *in situ* visualization immunoassay was used to look for the recruitment of a DNA repair protein, Ku-86, to the sites of particle traversal. Four types of human cells have been studied: the HeLa cervical carcinoma cell line, the NFF neonatal foreskin fibroblast cell strain, the HMEC normal mammary epithelial cell strain, and the HNEK skin epithelial keratinocyte strain. The doses of 1 GeV/amu Fe ions were calculated to give very low particle fluences to the cell nuclear cross-section, based on a track-averaged LET of 120 keV/mm and cell nuclear cross-sectional measurements. Three nominal fluences, plus the sham control, were used: 0, 1, 2, or 4 particles per cell nuclear area. Cobalt-60 gamma rays used in parallel experiments for a low LET comparison. After irradiation, cells were incubated for varying lengths of time, then fixed and stored at 4°C until probed for the

repair protein, Ku-86, by immunocytochemical methods. Results were visualized and quantified by flow cytometry or confocal laser scanning microscopy.



RESULTS

Ku-86 immuno-labeling. The DNA repair protein, Ku-86, was studied in γ -ray irradiated human neo-natal foreskin fibroblasts using immunocytochemistry. After irradiation, the cells were



incubated for various times before fixation, immunostaining, and quantification of cell nuclear staining by confocal microscopy. Figure 1a shows confocal data from control-unexposed cells immunostained with the Ku-86 antibody, and Figure 1b shows data from cells one hour after irradiation by 10 cGy. These data are plotted in three dimensions, with the intensity of Ku labeling on the Z axis. Each of these pictures represents a horizontal section, 0.19 μ m thick, through the cells in a plane parallel to the attachment surface. Notice that in the controls the Ku protein is seen more or less throughout the cell, and in relatively small amounts. The irradiated cells, in contrast, are highly labeled, and mainly in the cell nucleus.

A time course experiment of cells exposed to 50 cGy of gamma rays, Figure 2, showed a steep up-regulation of Ku-86 in cell nuclei. The amount of Ku labeling rose about 8-fold higher than unirradiated cells by 15 minutes, 17-fold higher in 1 hour, with a more gradual climb to a high of 25-fold at 4 hours. This may be interpreted as either a slowing down or a plateauing of the up-regulation after about 3 hr. In this figure, the error bars represent the standard deviation for at least 25 individual cells. In a similar experiment, cells were assayed by flow cytometry for both Ku-86 and DNA content, and protein up-regulation was found to occur in all phases of the cell cycle (data not shown).

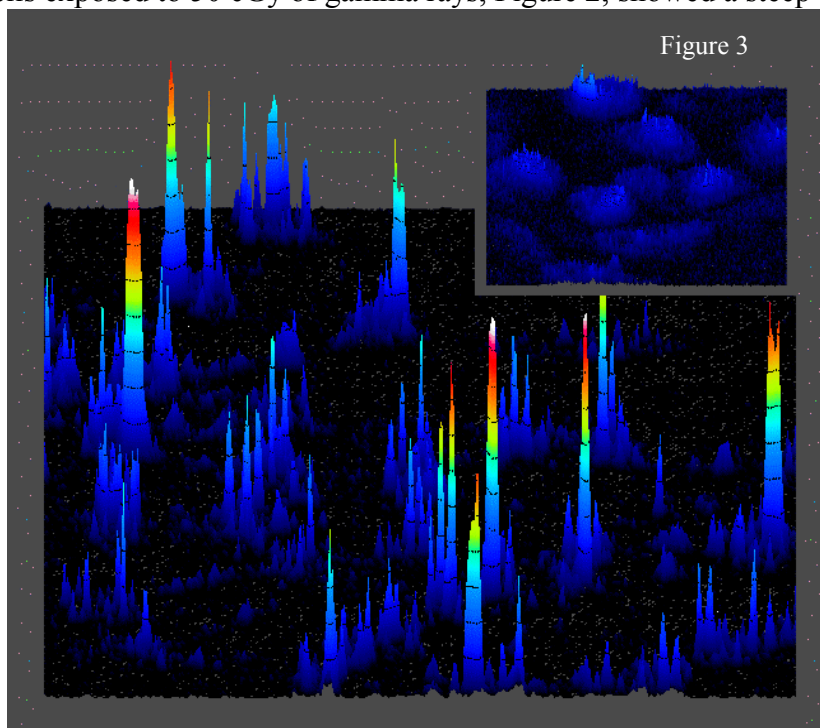


Figure 3 shows the DNA repair enzyme, Ku-86, relocated to the sites of damage induced by high energy iron ions traversing human HeLa cells. The 1 GeV/a.m.u. Fe ions approximate

cosmic ray particles that will be encountered on deep space missions. In this 3D picture, the protein staining intensity is plotted on the z axis, and each island group of peaks is a single cell. Cells were exposed to ~ 4 ions per cell nucleus, then incubated for three hrs. The inset picture shows control cells.

CONCLUSIONS

Analysis and comparison of these experiments is presently ongoing, but several tentative conclusions will be offered.

1. A differential response is shown for both DNA end-labeling and Ku-86 upregulation for different human cell types, and for different radiations.
2. The number of DNA end-labeling foci per irradiated HMEC cell is much higher than the calculated number of particles traversing the cell nucleus. These higher numbers probably reflect the sites of DNA synthesis, which in the unirradiated cells are masked by the more homogeneous distribution of endonuclease (repair) proteins. The recruitment of this activity to sites of both damage and normal synthetic activity is triggered within minutes of irradiation.
3. There is an up-regulation of Ku-86 protein in the nuclei of gamma-irradiated cells at low-but not higher doses that we are now studying for high LET irradiated cells. Preliminary data are not clear cut, and this may be due to the uncertainty in the number of particles traversing the cell, and the lower limit on dose imposed by the impossibility of delivering a fraction of a particle to the cell.

PLANS FOR FUTURE INVESTIGATIONS

Upcoming experiments are planned to help prove a new hypothesis that part of the apparent up-regulation of Ku protein is due to a protein conformational change that sensitively occurs in response to irradiation.

Supported by the National Aeronautics and Space Administration (NASA) Space Radiation Health Program under DOE contract DE-AC06-76RLO 1830.

DIFFERENTIAL PATTERN OF A PROTON- OR COBALT- INDUCED GENETIC FINGERPRINT: APPLICATION TO RADIATION-INDUCED CANCER CHEMOPREVENTION STRATEGIES

A.C. Miller, J Xu, T Whittaker, EJ Ainsworth, TM Seed. Radiation Casualty Management Team, Armed Forces Radiobiology Research Institute, Bethesda, MD 20889.

An accurate assessment of low dose-rate radiation risk requires a careful examination of the mechanism (s) of radiation carcinogenesis. Carcinogenesis is a multi-stage process that involves aberrant signal transduction and cell cycle pathways. These mechanisms involve specific molecular and genetic alterations, i.e., gene amplification, mutations, chromosomal rearrangements, that can not only be measured, but provide a novel means to assess carcinogenic risk factors and a strategy for chemo-intervention.

Oncogenes and tumor suppressor proteins, associated with control of the induction of neo-plastic cell growth, have received recent attention in environmental medicine since they may be useful tools for monitoring individuals exposed to carcinogenic chemicals. Their potential use as biomarkers is supported by human and animal studies demonstrating alterations in the expression of oncoproteins and tumor suppressor protein p53 in preneoplastic tissues. Recent *in vivo* studies have also demonstrated oncogene and tumor suppressor proteins alterations in preneoplastic tissues in animals exposed to radiation. Markers of genomic instability such as, microsatellite instability, have also been used in combination with oncogene mutation status for assessment of tumor prognosis. These data suggest that the use of a combination of genetic biomarkers may be the most efficacious approach to the development of markers of cancer risk following exposure to low dose radiation.

Molecular/genetic changes examined included *ras* oncogene expression, *ras* mutation status, tumor suppressor p53, cell cycle control gene cyclin D1 expression, *bcl-2* levels, and loss of chromosomal heterozygosity (LOH microsatellite stability). Markers were chosen based upon data from carcinogen-exposed humans. Using the well-characterized radiation carcinogenesis model (B6CF1 mouse), we examined the effects of cobalt (single dose 200 cGy, fractionated 8 x 25 cGy) or protons (single dose 200 cGy) on these molecular biomarkers and lung tumor development. Regardless of radiation quality or tumor status, 75-85% of all animals irradiated exhibited a time-dependent increase in *ras* oncogene expression/encoded protein content (249 days, 4- to 8- fold increase). Alterations in *ras* mutation status and tumor suppressor p53 content were observed only in proton- or cobalt (fractionated)- irradiated tissues, but not lung tissues from single dose irradiated animals. In addition, only proton-irradiated tissues exhibited alterations in *bcl-2* expression levels. Finally, only proton-irradiated animals that developed lung tumors demonstrated aberrations in all the biomarkers previously described plus a loss of chromosomal heterozygosity in two DNA markers measured in lung tissue adjacent to the tumor. Lung tissues from animals not exposed to radiation did not demonstrate similar gene/DNA alterations. Pharmacological intervention strategies were tested in both cobalt and proton irradiated mice using two prophylactic candidates that were previously shown to down-regulate the *ras* gene. Administration of buthionine-SR-sulfoximine (BSO) or amifostine (WR2721), prevented activation of *ras* in lung tissues of cobalt or proton- irradiated animals, respectively.

Furthermore, no alterations were measured in the other biomarkers examined in prophylactically-treated animals.

This study demonstrated that there are sequential molecular genetic changes following low dose radiation exposure that are radiation quality dependent; these findings suggest that specific altered oncogenes may be effective pharmacologic targets in cancer chemoprevention. A radiation-induced leukemia model is currently being initiated to further assess the radiation-induced genetic fingerprint and to better design a strategy to prevent or delay radiation-induced carcinogenesis.

MISREJOINING OF DNA DOUBLE-STRAND BREAKS INDUCED BY 900 MeV/u IRON IONS AND X-RAYS IN HUMAN FIBROBLASTS: IRON IONS ARE MORE EFFICIENT THAN X-RAYS AT LOWER DOSES.

B. Rydberg, B. Fouladi, and P. K. Cooper
Lawrence Berkeley National Laboratory, Berkeley, CA 94720.

INTRODUCTION

DNA double-strand breaks (dsbs) are probably the most important lesions produced by ionizing radiation. Among the dsbs, those that are either mis-rejoined or remain unrejoined are probably the most relevant for a variety of biological endpoints. With our assay to look at the integrity of large restriction fragments, we have previously published results showing that misrejoining of dsbs occurs with similar frequency for low and high LET radiation of various kinds after a dose of 80 Gy, including HZE Fe ions (1). In subsequent papers (2, 3) it was suggested on theoretical grounds that misrejoining might be dose dependent, and that the value at 80 Gy represents a saturation value. It was hypothesized that only dsbs in close proximity within the nucleus can mis-rejoin. To test this idea, we have studied misrejoining after various doses of X-rays and Fe ions.

METHODS

Fe ion irradiation was performed using the Alternating Gradient Synchrotron at Brookhaven National Laboratory. Irradiation with other particles (He, N) were performed at the 88 inch cyclotron at Lawrence Berkeley National Laboratory. X-rays were 150 kVp with 0.53 mm Cu and 1.02 mm Al filtration. Normal human fibroblasts at the G0 stage of the cell cycle and synchronized Chinese Hamster A_L cells harboring a single human chromosome 11 were irradiated with 10-160 Gy, incubated for various times at 37 °C, trypsinized, and embedded in agarose plugs. After lysis, the DNA was restricted with NotI or MluI and separated with pulsed field gel electrophoresis. Southern blots were probed for unique large restriction fragments. Comparison of the intact full size band with a smear of broken or mis-rejoined restriction fragments was determined on each lane to estimate dsb induction and joining of correct ends. A conventional FAR assay was used to estimate total rejoining, and the difference between total rejoining and correct rejoining was calculated as mis-rejoining. For details see (4).

RESULTS

We find a pronounced dose dependence for mis-rejoining of dsbs induced by X-rays and low LET He ions, with a diminishing percentage of dsbs undergoing misrejoining as the dose is lowered in the range of 80 - 10 Gy. In contrast, for Fe ions (150 keV/μm) and N ions (97 keV/μm) the frequency of misrejoining stayed at a high level down to the lowest dose tested of 20 Gy. Thus, Fe ions are more efficient than X-rays for mis-rejoining at lower doses. We also notice a larger fraction of unrejoined dsbs after 16 hr repair incubation for Fe ions and other high LET particles in comparison with X-rays.

CONCLUSION

Our new mis-rejoining data show that dsbs induced by high LET radiation, such as Fe HZE ions, are more likely than dsbs induced by X-rays to undergo misrejoining with wrong DNA ends at doses below 80 Gy. This result is consistent with the idea that two dsbs need to be close to each

other in order to mis-rejoin. At low doses of X-rays, randomly induced dsbs are not likely to be in close proximity. In contrast, a large proportion of dsbs induced by the Fe ions will be distributed along the track of the particle independent of dose, presumably in sufficient proximity for a mis-rejoining mechanism.

REFERENCES

1. M. Löbrich, P. K. Cooper and B. Rydberg, Joining of Correct and Incorrect DNA Ends at Double-Strand Breaks Produced by High-Linear Energy Transfer Radiation in Human Fibroblasts. *Radiation Research* 150, 619-626 (1998).
2. T. Radivoyevitch, D. G. Hoel, P. J. Hahnfeldt, B. Rydberg and R. K. Sachs, Recent data obtained by pulsed-field gel electrophoresis suggest two types of double-strand breaks. *Radiat Res* 149, 52-58 (1998).
3. T. Radivoyevitch, D. G. Hoel, A. M. Chen and R. K. Sachs, Misrejoining of double-strand breaks after X irradiation: Relating moderate to very high doses by a Markov model. *Radiat Res* 149, 59-67 (1998).
4. M. Löbrich, B. Rydberg and P. K. Cooper, DNA double-strand breaks induced by high-energy neon and iron ions in human fibroblasts. II. Probing individual notI fragments by hybridization. *Radiat Res* 139, 142-51 (1994).

CLUSTERED DNA DAMAGE IN HUMAN CELLS IRRADIATED WITH 1 GeV Fe^{+26*}

Betsy M. Sutherland¹, Paula V. Bennett¹, John C. Sutherland¹, John Trunk¹, Denise Monteleone¹, Olga Sidorkina² and Jacques Laval²,

¹Biology Department, Brookhaven National Laboratory, Upton NY 11973-5000,

²Institut Gustave Roussy, Villejuif, France

INTRODUCTION

Locally Multiply Damaged Sites, (LMDS) several DNA damages within a limited region of DNA, have been postulated to be difficult to repair, and thus potentially responsible for major portions of the biological damage inflicted by ionizing radiation. Studies with model systems containing damages on opposing strands within a few base pairs have indicated that some of clusters are indeed difficult to repair, and thus potentially lethal or mutagenic lesions. Their production by high LET particles has been modeled. However, whether they are actually induced in cells by ionizing radiation, and if so, their actual role in inducing biological damage, has not been evaluated, because there was no way to measure them in genomic DNA. Thus, our aim was to develop methods to quantify specific kinds of LMDS, which we term Clustered Damages, defined by four criteria: 1. two or more DNA lesions, 2. either a single strand break or a damage convertible to a single strand break by the nicking action of a lesion-recognizing enzyme, 3. on opposing strands, and 4. within about one DNA helical turn.

METHODS

In our method, to quantify Clustered Damages, DNA is isolated from irradiated cells, and treated with a lesion-recognizing enzyme that makes a nick at a lesion site. The DNA is then electrophoresed on non-denaturing agarose gels along with molecular length standards spanning the size of the experimental DNAs, and the frequency of damages is computed using number average molecular length analysis. The size of the DNA is reduced by the enzymatic cleavage ONLY when two lesions on opposing strands within about one helical turn. Thus the molecular signature for a Clustered Damage is the production of *de novo* double strand breaks upon treatment with a lesion-recognizing enzyme. We can measure four classes of such Clustered Damages: abasic site clusters [a damage cluster containing at least one abasic site, diagnosed by susceptibility to *Escheria coli* Nfo protein (Endonuclease IV, the kind gift of Dr. B. Demple, Harvard)], oxidized purine clusters (contain at least one oxidized purine cluster, diagnosed by susceptibility to *E. coli* Fpg protein), oxidized pyrimidine clusters [contain at least one oxidized pyrimidine, diagnosed by susceptibility to *E. coli* Nth protein (Endonuclease III)] protein], as well as double strand breaks.

RESULTS

Proof of Principle experiments using bacteriophage T7 DNA in solution irradiated by ¹³⁷Cs gamma rays indicated that all four classes of clustered damages are produced in the ratios 1 DSB: 2 oxidized purine clusters: 1.5 abasic clusters: ~0.5 oxidized pyrimidine cluster. Further, plots of these data on a logarithmic-logarithmic scale indicates that the dose-response lines for production of all four classes of clustered damages are straight lines with a slope of 1, thus indicating that a cluster is formed by a single radiation hit. This indicates that clustered damages would be expected to be formed even at low radiation doses.

We have asked whether human cells irradiated with low doses of Fe^{+26} ions would contain clustered damages. Oxidized pyrimidine clusters are produced in cells irradiated with doses as low as 10 rads of these ions, and that their frequencies are in the same range as double strand breaks. Such clusters may be responsible for a major portion of the biological damage inflicted by space radiation.

*Beam time graciously provided by the Space Radiation Health Program of the NASA Office of Life and Microgravity Sciences; research supported by the Office of Health and Biological Research of the US Department of Energy, and by CNRS and Electricite' de France, Contrat Radioprotection.

USE OF THE COMET ASSAY TO DETECT RADIATION DAMAGE OF SELECTED RADIATION SENSITIVE CELL POPULATIONS

D. Wilkinson, R.C. Wilkins, and J.R.N. McLean.

Radiation Protection Bureau, Environmental Health Directorate, Health Canada Ottawa, Ontario, Canada.

INTRODUCTION

Ionizing radiation induces cellular damage by directly or indirectly affecting genetic material. A damaged cell triggers a cellular response to either repair the detected damage or induce programmed cell death (apoptosis). The biological consequence of the acquired cellular damage is traditionally evaluated by the dicentric chromosome assay which is a tedious, expensive, cytogenetic assessment of irradiated cells. In the event that individuals became exposed to questionable quantities of ionizing radiation, a fast and easy screening assay would be needed to support the chromosome assay. The Comet Assay measuring the apoptotic fraction, developed in our laboratory, is currently being assessed for its potential as a biological dosimeter.

METHODS

The Comet Assay was used to measure the apoptotic fraction in peripheral blood lymphocytes. The apoptotic cells are easily distinguished from normal (undamaged or repaired) cells on the basis of their unique DNA distribution pattern following electrophoresis. Previous studies in our laboratory, using the Comet Assay to detect apoptosis in irradiated whole blood demonstrated a large spontaneous apoptotic fraction with significant inter and intra-donor variations, rendering it unsuitable as a biological dosimeter. To eliminate the background of spontaneously apoptosing cells and thus enhance the sensitivity of the assay, different white blood cell populations were isolated and tested to identify those most sensitive to radiation damage.

RESULTS

The CD4 and CD8 T-cell fractions were sensitive to radiation damage, with the CD8 T-cells being the most sensitive. The apoptotic fraction of 0.1 Gy irradiated CD8 T-cells was significantly higher than that observed for the unirradiated controls. This cell population also demonstrated an extremely low inter and intra-individual variation, suggesting that it may be an ideal cell type to be used as a biological dosimeter for ionizing radiation.

CONCLUSIONS

The Comet Assay measuring the apoptotic fraction has a good indicator of radiation induced biological damage under *in vitro* conditions. Future studies intend to test this assay as a biological dosimeter after *in vivo* exposure to ionizing radiation.

This report was carried out under a contract (AECB research project no. 98-237) with the Atomic Energy Control Board.

INDUCTION OF SYMMETRICAL AND ASYMMETRICAL CHROMOSOME ABERRATIONS IN MAMMALIAN CELLS BY FE-IONS, PROTONS AND PHOTONS: A SUBALPHA-ALPHA-OMEGA ANALYSIS

Jerry R. Williams¹, Haoming Zhou¹, John F. Dicello¹, Frank Cucinotta², and Yonggang Zhang¹.

Johns Hopkins Medical Institutions¹, Baltimore, Maryland 21287, and the NASA Johnson Space Center², Houston, Texas 77058.

INTRODUCTION

We are performing parallel experiments in animals (Sprague-Dawley rat) and in cells to determine the potency of three model space radiations (Fe-ions, protons and photons) to induce cancer in the rat and to induce cytogenetic damage in rat and human cells. Our goal is to identify descriptive parameters for both of these endpoints that will: i) provide a better mechanistic understanding of carcinogenic processes, and ii) provide data for extrapolation from biomarkers in cells to cancer in animals, from cancer in rats to cancer in humans and from laboratory exposures to expected exposures in space.

METHODS

We have examined the induction of symmetrical chromosome aberrations (chromosome type aberrations, e.g. dicentrics, rings) and asymmetrical chromosome aberrations (chromatid type aberrations, e.g. breaks and gaps) in several types of mammalian cells exposed to Fe-ions, photons and protons. Cell types included primary human lymphocytes, rat mammary epithelial cells exposed in vitro or in vivo, and human colorectal tumor cells varying in their status for p53 and p21. We measured symmetrical and asymmetrical aberrations per cell and per chromosome, number of cells with 0, 1, 2, 3 or greater than 3 aberrations per cell and ratio of symmetrical and asymmetrical aberrations.

We analyzed dose-response patterns using Poisson analysis, linear- quadratic analysis and subalpha-alpha-omega analysis. A Poisson distribution of chromosome damage suggest randomly induced lesions with a constant rate of induction over all dose ranges. Linear quadratic models would predict two components, one linear with dose and one with dose-squared. The subalpha-alpha-omega model suggests three different cellular response modes that reflect induced genetic expression at different doses and dose-rates.

RESULTS

1. Fe-ions induce more symmetrical and asymmetrical aberrations per unit dose than do photons. The dose-response patterns induced by Fe-ions, however, are significantly different than that for photons for both types of aberrations and thus the RBE paradigm may not be applied. Asymmetrical aberrations induced by Fe-ions show a maximum at approximately .01 Gy, with declining efficiency out to approximately 1.0 Gy. For symmetrical aberrations, 3 to 4 times higher photon doses are needed to induce the same level of aberrations induced by 0.10 to 1.0 Gy of Fe-ions.
2. Protons have an RBE of ~1.0 for symmetrical aberrations, compared to Cesium-137 gamma rays, for all doses and for all cell types. Data suggest that protons may be slightly more

efficient for induction of asymmetrical aberrations than Cs-137 photons at higher doses (2.5 Gy to 5.0 Gy).

3. The shape of the dose-response curve for either asymmetrical or symmetrical aberrations was relatively similar between cell types for each radiation, while the pattern for Fe-ions was significantly different from that for protons and photons..
4. The rate of induction of aberrations in rat mammary epithelial cells, irradiated in vivo and assayed in vitro, is significantly lower than in the same cells, or other cells, irradiated in vitro.
5. Cells that express wildtype p53 but have been rendered defective in CDKN1A (p21) by homologous recombination show high background levels of asymmetrical aberrations. Cells that express mutant p53 and have been rendered defective for p21 show elevated background levels of both symmetrical and asymmetrical aberrations.
6. Cells rendered defective in TP53 (p53) by homologous recombination show an unusual pattern of premature centromere separation after irradiation at higher doses of photons (2.5, 5.0 Gy).
7. Patterns of induction of aberrations, when compared to existing data for other endpoints, suggest that the subalpha-alpha-omega model may best describe underlying mechanisms that process radiation-induced chromosomal damage. At low doses of radiation, less than 0.5 Gy, a high-fidelity, intrinsic subalpha response is hypothesized to process radiation damage and to produce low levels of symmetrical aberrations but higher levels of asymmetrical aberrations. At doses above 0.5 Gy that can induce early response genes, we hypothesize that the alpha response dominates response and results in increasing symmetrical aberrations, an indicator of a more error-prone processing. At doses above 2.5 to 5.0 Gy, increased processing is through the combined alpha and omega responses.

CONCLUSIONS

Our data suggest that Fe-ions are more effective at inducing both symmetrical and asymmetrical lesions per unit dose than photons, however the shape of the dose response curves for Fe-ions and photons limit application of the RBE concept. While the rate of induction of symmetrical aberrations by protons was indistinguishable from photons, their induction of asymmetrical aberrations may be increased slightly at higher doses (>2.5 Gy). Thus, both Fe-ions and protons induced increased asymmetrical chromosomal damage, compared to photons. We hypothesize that this increase is a manifestation of post-replication processes acting on chromosomal damage that did not produce symmetrical aberrations during replication. Such damage is detectable and converted into chromosome breaks in late G2 phase or mitosis. The increased potency of both Fe-ions and protons for the induction of asymmetrical aberrations was surprising and represents an effect of these radiations heretofore not observed. The biological relevance of these lesions is unknown; however, elevated levels of asymmetrical aberrations have been associated with genetic instability and increased sensitivity to their induction by radiation has been associated with predisposition to breast cancer.

Our future studies will be directed toward seeking correlation between patterns for induction of chromosome aberrations and patterns of cancer induced by photons, protons and Fe-ions in animal models.

Supported by cooperative agreement NCC 9-58 from NASA with the National Space Biomedical Research Institute and by a grant from NIH, ES-07607.

Monday, June 14

Brookhaven National Laboratory

3:50 p.m. – 5:30 p.m.

Radiation Risk

Berkner Hall

NEW PERSPECTIVES ON LOW DOSE RISK ESTIMATION

S. B. Curtis

Fred Hutchinson Cancer Research Center, Seattle, Washington 98109-1024

Emerging ideas on the interplay of various biological mechanisms such as birth and death rates of cells (both normal and initiated) in the carcinogenic process may lead to a modification of our understanding about how dose and dose-rate affect the shape of the cancer dose-response curve. Here we present results of some recent work using the initiation-promotion-progression paradigm embedded in the two-stage clonal expansion model of Moolgavkar *et al.* for high LET radiation. Analysis of an updated epidemiological data set of the Colorado Plateau miners predicts that the probability of lung tumors depends strongly on *how long* the miners breathed the radon atmospheres. An “inverse dose-rate effect” or, more properly, a “protraction effect” is apparent at constant dose above 20 WLM for protraction intervals between 1 and 10 years. This effect is due to dose-rate dependence of the promotion step in the carcinogenic process. That is, even assuming the two (rate-limiting) mutation rates to be linear in increasing dose-rate, the probability of tumor is greater at a given dose for long protraction intervals (e.g., 48 years) than for short intervals (e.g., 1 year). Thus, the initial slope of the risk-response curve depends strongly on the protraction interval. For the high LET’s involved in the radon-decaying alpha particles, the effect is striking. The shapes of the dose-response curves are quite different, depending on the protraction interval. For doses up to 40 WLM, the dose-response curve is “concave downward” (sublinear) for short protraction intervals (1 year) and slightly “concave upward” (supralinear) for long protraction intervals (48 years).

There are several possible reasons for this behavior. One is that the dust and/or diesel fuel exhaust in the mines are promoters and that longer exposure to these pollutants causes the increased promotion. The effect, then, would not be due to the radiation at all. Another intriguing possibility, however, is that cell-killing of (or just proximity of irradiated) normal cells around the initiated cells by the alpha particles increases the promotional effect (i.e., proliferative characteristics) of the initiated population over time, thus increasing probability of tumor.

These and other considerations of the importance of tissue response in the carcinogenic process will be discussed in terms of their impact on radiation risks for long-term space flight.

MULTISTAGE MODELS AS AN APPROACH TO QUANTITATIVE CANCER RISK ASSESSMENT: COMPARISON OF THEORY AND EXPERIMENT

F. Burns, Z. Hiz, R. Shore, P. Zhao, S. Chen, A. Nadas and N. Roy

Department of Environmental Medicine, NYU Medical Center, 550 First Ave., New York, NY 10016

INTRODUCTION

In the multistage theory of carcinogenesis, cells progress to cancer through a series of mutations in cancer-relevant genes, and intermediate stages sometimes proliferate into benign neoplastic lesions. Although cancer induction by low LET radiation is subject to repair or recovery in the sense that multiple exposures produce fewer cancers than the same single dose, this recovery is not seen following exposure to high LET radiation. Cancer yields were fitted by a LET-dependent quadratic equation, and equation parameters were estimated by regression analysis for each type of radiation. The results are consistent with the interpretation that carcinoma induction can be explained by a pathway involving 2 radiation-induced mutations, while benign fibromas can be explained by only 1 radiation-induced mutation.

METHODS

Rat skin exhibits a variety of tumor types when exposed to ionizing radiation, including, squamous carcinomas, basal cell carcinomas, clear cell carcinomas, sarcomas and fibromas. Rat skin has been used extensively to study the dose-response and time-response characteristics of radiation-induced epithelial cancer and for investigating how alterations of specific oncogenes and tumor suppressor genes are associated with the absorption of the radiation and cause progression of a cell to cancer. Comparisons of radiation-induced cancer in experimental animals and humans are available for skin.

The multistage theory of carcinogenesis originally included up to 6 stages and was invoked to explain the steep increase of cancer in human populations as a function of age. Recent versions of this theory, especially the 2 stage version, have been postulated to explain aspects of experimental radiation and chemical carcinogenesis in animals emphasizing mutations and proliferative expansion of intermediate stages. A model is developed here to explain findings for rat skin carcinogenesis based on the following assumptions.

1. Each radiation-induced mutation involves 2 events that are either reparable and occur in separate radiation tracks or are irreparable and occur in a single radiation track. The identity of the reparable alteration is unknown, but is assumed to be premutagenic.
2. The minimum number of mutations required for cancer is 2, i.e. a cancer cell is created when a mutation occurs in 2 cancer genes, e.g., oncogenes, or in both alleles of tumor suppressor genes.
3. The 2 mutations needed for a cancer cell may occur by 2 separate routes:
 - a) Both mutations are the result of radiation action during or shortly after the irradiation.
 - b) One mutation is the result of radiation action, which leads to growth of a benign tumor, and a second mutation occurs in one of these benign tumor cells as a result of a random error in a naturally-occurring metabolic process.

The data suggest that rarely are both mutations produced by the radiation, so that b. becomes the most common route during which the naturally-occurring mutation may occur at any time. In addition clonal growth of benign tumor cells may occur, and the naturally-occurring mutation more than likely occurs in one of these cells. Next the cancer cell proliferates into a palpable cancer that is eventually scored and characterized in these experiments. Proliferative amplification of benign clones is difficult to observe and has only been shown definitively for mouse skin papillomas. The above assumptions coupled with the track nature of ionizing radiation lead to the dose-response relationship:

$$f(D) = CLD + BD^2 \quad (1)$$

$$f_d(D) = f(D) / D = CL + BD, \quad (1a)$$

where $f(D)$ is the cancer incidence at a given time, $f_d(D)$ is cancer incidence per unit dose, L is linear energy transfer, D is radiation dose and C and B are constants.

If the biological endpoint of interest requires only 1 alteration in proportion to dose, then by analogy a 'mono-action' model would lead to the following dose-response functions:

$$f(D) = (C_1L + C_2)D \quad (2)$$

$$f_d(D) = f(D)/D = C_1L + C_2. \quad (2a)$$

Equation 2a implies that $f_d(D)$ should be consistent with LET-dependent, horizontal straight lines when plotted against dose. Estimates of C_1 and C_2 may be estimated empirically from the vertical location of the lines at different LET values.

RESULTS

Equations 1a and 2a were tested against tumor yield data in rat skin exposed to ionizing radiation with different average LET values. Generally, rat skin exposed to ionizing radiation begins to develop epithelial and connective tissue tumors by about 10 weeks after exposure, and new tumors continue to appear at accelerating rates until about 80-100 weeks, after which the rate may decline. The consistency of this time pattern is the basis for constructing time-independent dose-response relationships based on an overall tumor yield function that is separable into a product of a function of dose and a function of time, i.e. is $Y(D,t) = f(D)g(t)$, where $Y(D,t)$ is the overall cancer yield in tumors per animal, D is the radiation dose and t is elapsed time since exposure. Separability implies that the dose-response function is time-invariant, but actual comparisons were based on the fitted temporal functions at 52 weeks as a convenient midlife reference point.

The dose-response implications of the model were tested by fitting Equation 1a to carcinoma data and Equation 1b to the fibroma data. Proportionality of the first term in Equation 1a and 1b with L , the linear energy transfer (LET), is an important, testable implication of the model. The results were a striking confirmation of the validity of Equation 1a fitted to the carcinoma yield per unit dose data. The argon ion slope, B , was 0.006 tumors/rat/Gy² and the y-intercept was 0.055 tumors/rat/Gy. The results for neon were parallel to the argon line but shifted downward to a y-intercept of 0.013 tumors/rat/Gy. However, the cancer yield for electron radiation was predicted incorrectly by the model. The predicted electron line should have a y-intercept indistinguishable from 0.0 tumors/rat/Gy and the same B value as argon and neon, however the electron data are lower and to the right of the predicted line indicating that B is about 45% smaller for electrons than predicted.

An analysis utilizing Equation 2a was performed for benign fibromas. Fibromas grow laterally and internally, rarely exceeding 3 or 4 mm in diameter and do not form palpable nodules above the skin surface. The neon ion data, for which the largest number of data points exist, show a close conformity to the expectations in Equation 2a, i.e. yield per unit dose is independent of dose. The y-intercept of the average argon response (obtained by fitting a horizontal line to the only 3 argon data points available) exhibits a ratio to neon intercept which is about to the ratio of LET values, as predicted by Equation 2a. Within the limitations of the data, C_2 seems to be negligible. In contrast to the results for carcinomas, electron-induced fibromas are more numerous than predicted from the LET ratios. Additionally the electron data exhibit a positive slope not predicted by the simple equation 2a.

DISCUSSION

Carcinoma and fibroma induction are interpreted in light of a model where radiation produces a mutation that advances a cell 1 stage in the progression to cancer. Almost certainly at least one more mutation is needed to produce a fully malignant cell, but this second mutation need not be produced by the radiation. These ideas generally encompass what is known as cancer progression or multistage carcinogenesis, where cancer-relevant mutations may occur because of action by an exogenous carcinogen, such as, ionizing radiation or as a result of naturally-occurring mutagenesis, associated with intracellular metabolic errors.

While the model fits the experimental results reasonably well, there are some discrepancies that will require additional experimentation and analysis. Nevertheless for the purposes of estimating risks at doses (or dose rates) where no experimental data are available or are ever likely to be available, such a model could be extremely useful. Additional data and further development of the model will likely improve its plausibility and possibly point to better ways to calibrate human cancer risks against animal models. (Work supported by NASA, DOE and NIH)

MUTAGENICITY AS AN INDICATOR FOR RADIATION RISK

J. Kiefer

Strahlenzentrum der Justus-Liebig-Universität, Giessen, Germany

Mutations play an important role in carcinogenesis. If transformed cells are to develop into an tumour they must retain their proliferative capacity, i. e. the number of surviving mutants is the decisive figure for risk assessment. An analysis of mutation induction by several types of radiations, including X-rays and charged particles shows that in all cases a linear relationship exists between mutant frequencies and the logarithm of surviving fraction. The slope of this curve which is termed “mutagenicity” indicates the mutagenic potential and may serve as a means of comparison between different agents. It is shown that mutagenicity is in a simple manner also related to the maximum number of surviving mutants and plays thus an important role in risk assessment. Our data for mutation induction with heavy charged particles are analysed in this way. The results indicate that mutagenicities increase up to a factor of about 6 compared to X-rays. There exists, however, no simple relationship with regard to LET, and ion energy appears to be more important. Highest values for mutagenicities are found with energies around 10 MeV/u.

MEASURING MUTATION IN COSMONAUTS *IN VIVO*: LACK OF EVIDENCE THAT THE SPACE ENVIRONMENT IS MUTAGENIC.

Barry W. Glickman, David J. Walsh, John Curry and Magomed Khaidakov
Centre for Environmental Health, Department of Biology, University of Victoria, Victoria, BC,
Canada V8W 3N5.

Exposure to ionizing radiation in space is one of the major health concerns of long-term space missions. The daily doses received on the low Earth orbit are relatively small, and vary from 0.01 to 1.0 mGy. However, the quality of radiation, as well as the protracted and fluctuating exposure, may significantly enhance the biological effects. In a previous study we analyzed mutation in 5 cosmonauts. (Khaidakov *et al.*, 1997) and reported that their *hprt* mutant frequencies were 2 to 5 times higher than in age-matched unexposed Western controls. To better address the issue, we have extended our sample collection to additional cosmonauts with the recent long-term flight experience and included Russian trainees for a more correct control. The mean mutant frequencies for cosmonauts and trainees were identical (17.2 ± 0.6 versus $17.6 \pm 4.7 \times 10^{-6}$) which is about 3-fold higher than age-matched Western controls but the same of reported for unexposed Russian (Curry *et al.*, 1997; 18.5 ± 8.9). Consistently high mutant frequencies observed suggest greater exposures to mutagens in the Moscow environs.

ESTIMATES OF GENETIC RISK IN OFFSPRING OF ASTRONAUT AND THE COUNSELING FOR ASTRONAUT

T. Suemitsu¹, T. Komiyama¹, T. Abe¹

¹ Medical Research & Operations Office, National Space Development Agency of Japan,
305-8505 Tsukuba, Japan

Radiation exposure limits are usually set chiefly by estimating the risk of attributable cancer mortality, although the contribution from genetic effects is also taken into consideration (ICRP60, NCRP98), e.g. ICRP60 roughly estimate that the probability of severe hereditary effects is one fifth of that of fatal cancer.

Studies of the offspring of atomic bomb survivors, do not identify the genetic effects of radiation (Table 1). On the other hand, various epidemiological studies on other objects, i.e. offsprings of childhood cancer survivors, reveal controversial results (Table 2). In addition, some studies show the induction of chromosomal damage in patients surviving testicular tumor following radiotherapy (Table.3) .

The discordance between those results might be due to biological, physical and epidemiological factors, and seems not to be settled in near future. Then, how should the risk in offspring of astronauts be estimated?

NCRP Report 115('93) gives the Table 11.1 revising the estimation by BEIR-V('90). It seems to be the worst scenario based on findings available at present. Supposing that astronauts would be exposed to around 1000mSv in their reproductive age, the greatest additional cases are 2 unbalanced translocations and 0.9 trisomy etc. per 1000 offsprings (Table 4.). These are not so high but never negligible, comparing with the risk level above which some genetic intervention is recommended on the ground e.g. prenatal screening of Down's syndrome. Although, there are various controversies as to genetic interventions, appropriate counseling would be inevitable.

This matter is to be included in astronaut's radiation health care program which NASDA is now developing. We are already making efforts to give full information to astronaut candidates.

Table 1. STUDIES OF THE OFFSPRING OF A-BOMB SURVIVORS

Effects	Results	References
germ line instability		Kodaira M et al ('95)
chromosome aberrations (translocation, trisomy)		Awa AA et al ('87)
Untoward Pregnancy Outcome*		Otake M et al ('90)

*: congenital malformations, still births and early mortality

Table 2. EPIDEMIOLOGICAL STUDIES ON GENETIC EFFECTS OF RADIATION

Author (Year)	Objects / Method	Results
[Offsprings of Childhood Cancer Survivors]		
Hawkins ('91)	comparison of offsprings of childhood cancer survivors treated / not with irradiation and / or alkilating agents	No Significance
Kalen et al ('98)	comparison of outcome of reproduction (malformation etc.) in women irradiated skin for skin hemangioma categorized by estimated ovarian dose	No Significance
Byrne et al ('98)	comparison of incidence of chromosomal anomaly, point mutation and malformation between offsprings of childhood cancer survivors and those of survivors' siblings	No Significance (Chromosomal anomaly ↑)
[Point Mutation after Chernobyl Accident]		
Dubrova et al ('96)	comparison of mutation rates at minisatellite loci of children born in Berarus and UK	↑ in Belarus
[Chromosomal Anomaly vs. Fallout]		
Bound et al ('95)	chronological surveillance of Down's syndrome born in north western part of UK	significant association between incidence of Down's syndrome and estimated ovarian dose

Table 3. INDUCTION OF CHROMOSOME ABERRATIONS IN SPERMATOZOA OF CANCER PATIENTS

Author (Year)	Diseases (#case)	Dose (Gonad) / Chemo-Tx	Term*	Numerica l	Structural
Martin et al ('86, '89)	seminoma etc. (13)	0.5 - 5 Gy / -	1 Mo- 5Yr	↑	↑
Jendery et al ('87)	? (1)	0.5 - 0.8 Gy / -	18- 20 Mo	→	→
Genesca et al ('90)	Wilms' tumor (2)	22, 40 Gy / D-Act	11Yr, 17Yr	→	↑
Brandiff et al ('94)	Hodgkin's disease (6)	0 - 4 Gy / MOPP	3 - 20Yr	↑	↑ [†]
	Hodgkin's disease (1)	0.5 Gy / Vb	38d	↑	
§	D-Act: D actinomycin, Vb: Vinblastin				
×	MOPP: nitrogen mustard + Vincristin + Procarbazine + Predonizolon				
†	from the end of treatment to the end of examination, no significance				

Table 4. ROUGH ESTIMATES OF GENETIC EFFECTS
RESULTING FROM PARENTAL EXPOSURE OF 1000mSv

Type of Disorder	Current Incidence per 1000 Live Born	Additional Cases in 1st Generation per 1000 Live Born
Autosomal Dominant (Severe)	2.5	0.5 - 2
X Linked	0.4	<0.1 - 0.8
Recessive	2.5	<0.1
Chromosomal	4.4	0.6 - 2.9
Unbalanced Translocation	0.6	0.5 - 2
Trisomy	3.8	0.1 - 0.9
Total	14.2	<1.9 - 8.6

calculated from NCRP115[Table 11.1], BEIR-V[Table 2.2]

Tuesday, June 15

Brookhaven National Laboratory

8:30 a.m. – 9:50 a.m.

Genomic Instability

Berkner Room

RADIATION INDUCED CHROMOSOMAL INSTABILITY: STUDIES OF RADIATION QUALITY AND TARGETED EFFECTS

M. Kadhim, D. Pocock, S. Lorimore, D. Stevens, M. Hill, E. Wright and D. Goodhead
MRC Radiation & Genome Stability Unit, Harwell, Didcot, Oxfordshire, OX11 0RD, UK

INTRODUCTION

There is now substantial evidence that the progeny of normal cells exposed to ionising radiation can exhibit delayed responses, including an ongoing raised incidence of denovo chromosome aberrations, gene mutations and enhanced death rate. These delayed responses may be explained as manifestation of transmissible genomic instability. The results from studies to date suggest that cell type, radiation quality (LET), and genetic characteristics (genetic predispositions) all influence the inducibility of the instability phenotype. These transmissible effects have been observed to occur at a higher frequency than would be expected in cell populations that have been exposed to doses where only a small fraction of the nuclei have been traversed by particle irradiation. However, the targets, and the underlying mechanism, for inducing instability are as yet not fully understood.

Previously, we have demonstrated that α -particles, but not 250 kV X-ray, efficiently induce transmissible chromosomal instability that is expressed in the clonal descendants of murine and human haemopoietic stem cells. This heritable effect occurred at a much higher frequency than would be expected from Poisson statistics of particle hits to surviving cell nuclei. Further investigation, carried out by our group, showed that, following α -particle irradiation, the instability phenotype occurred even in the progeny of grid-shielded non-irradiated stem cells from the same dish. This is apparently due to unexpected interactions between irradiated and non-irradiated cells. It has been referred to as a 'bystander mechanism'.

In order to further our understanding of the influence of radiation quality, and of targeting, on the induction of inducible chromosomal instability in the haemopoietic system, we carried out investigations into the corresponding effects of 1.5 keV aluminium K ultrasoft X-rays (Al-K X-rays) under two conditions. Firstly, cells were irradiated with 1.5 Gy Al-K X-rays (as the estimated isoeffective-killing dose to compare with the dose of α -particle used previously). The investigated clonal cells consisted predominantly of progeny from irradiated surviving cells. The entire irradiated population will have received an approximately uniform large number of low energy (0.5-1 keV) electrons, similar to intermediate-energy delta-rays from heavy-ion irradiations and a component of secondary electrons produced by 'hard' X-rays and γ -rays. The attenuation of the Al-K X-rays through the cell leads to a small reduction in the number of electrons tracks across the cell.

Secondly, cells were irradiated under a condition in which a shielding grid was interposed between the cells and the radiation source, such that the surviving population consisted predominantly of unirradiated stem cells. This is possible since Al-k X-rays interact almost exclusively via the photoelectric interaction. With the resultant electrons having a combined range of ~ 70 nm. In this case, indirect effects of irradiated on unirradiated cells should be observable. Such untargeted effects may have important implications for assessment of radiation risk from particulate, or other non-uniform, irradiations.

RESULTS

Chromosomal instability, as demonstrated by delayed non-clonal karyotypic abnormalities, was observed in the clonal descendants of the mouse haemopoietic stem cells after Al-K X-rays irradiation under both conditions. However, the reduction in the number of colonies exhibiting chromosomal instability as a result of the shielding, was not as great as would be expected for effects only in surviving irradiated cells. This provides direct evidence for the production of transmissible cell-to-cell effects between hit and non-hit cells, following irradiation with delta-ray like electrons.

CONCLUSION

The induction of transmissible chromosomal instability by Al-K X-rays has been demonstrated in the haemopoietic stem cells. The track structure or heterogeneous distribution of interactions seems to play an important, but as yet undefined, role in the radiation quality dependency. The targeting effects may be attributable to cell interaction and/or possible persistent increase in clastogenic activity from the surviving irradiated cells.

EMERGENCY OF PROGRESSIVE NEOPLASTIC CHANGES OF BREAST EPITHELIAL CELLS TREATED WITH ESTROGEN AND HIGH LET RADIATION.

G. Calaf, and T. K. Hei and E. J. Hall
College of Physicians and Surgeons of Columbia University. Center for
Radiological Research. New York, N. Y. 10032

INTRODUCTION

It is well accepted that cancer arises in a multistep fashion where environmental exposures are major etiological factors. The aim of this work was to establish an experimental breast cancer model in order to understand the mechanisms of neoplastic transformation induced by high LET radiation in the presence of estradiol 17- β (E).

METHODS

MCF10F (Cancer Res. 50: 60-75, 1990), an immortal cell line that arose spontaneously from a mortal human diploid mammary epithelial cells, has the morphological characteristics of normal breast epithelial cells. The cells do not exhibit anchorage independence, invasiveness and tumorigenicity in nude mice. We exposed MCF-10F cells to graded doses of either a) low doses of 150 keV/um 4He ions accelerated at the 4MV van de Graaf Accelerator of the Radiological Research Accelerator Facility of Columbia University; or b) 1 GeV/nucleon 56Fe ions accelerated at the Alternative Gradient Synchrotron at the Brookhaven National Laboratory and subsequently cultured in the presence or absence of E. The media used was DMEM/F-12 (1:1), supplemented with antibiotics, 0.5 ug/ml hydrocortisone, 10 ug/ml insulin, 5 % equine serum, 0.02 ug/ml epidermal growth factor.

RESULTS

MCF-10F cells treated with either a single 60 cGy dose or 60/60 cGy dose of a particles and 56Fe heavy ions, in the presence of E, induced altered morphology and cell growth; significantly increase in cell proliferation and telomerase activity in comparison to control or after removal of serum. Western blot analysis showed increased p53 protein expression levels with both type of radiations. A single 60 cGy dose or 60/60 cGy dose of a particles induced anchorage independent growth and invasive capabilities. Increased expression of BRCA 1, BRCA 2, RAD 51, cyclin D, p16, jun, fos, myc in the presence of E was observed by immunofluorescence studies performed with confocal microscopy; apoptotic genes, such as bcl2, p21, p27, BAX were down regulated.

CONCLUSION

Therefore, these studies showed that high LET radiation in the presence of estrogen induced a cascade of events indicative of transformation, including morphological phenotypic changes such as increased saturation density, loss of contact inhibition, decreased responsiveness to growth factors, invasive capabilities and telomerase activity and increased expression of markers indicative of the evolution process of carcinogenesis. (supported in part by NIH grants ES07890, ACS-88-006, and NASA-CA 73946).

INDUCTION OF GENOMIC INSTABILITY IN WTK1 HUMAN FIBROBLASTS

Helen Evans¹, Minf-Fen Horng¹, Marlene Ricanati¹, Rob Jordan², and Jeffrey L. Schwartz². Case Western Reserve University¹, Cleveland, OH 44106 and University of Washington², Seattle, WA 98195

INTRODUCTION

The objective of this research is to characterize the initial event(s) responsible for the induction of genomic instability by irradiation with HZE particles, with the hypothesis that the initial event consists of the inactivation of any one of the many genes necessary for the maintenance of genomic stability. If this hypothesis is correct, the characteristics of unstable clones should vary from one to another, and the characteristics will be defined by the initial inactivation. Our specific aims are to identify and characterize unstable clones among the survivors of a population of human lymphoblasts exposed to HZE radiation as well as to low LET radiation and unirradiated cells.

METHODS

WTK1 lymphoblasts were exposed to varied doses of Fe-56 radiation and Cs-137 gamma radiation. Survivors were cloned from among the irradiated cells as well as from unirradiated control clones. To date we have isolated and characterized 50 clones from the Fe-56 irradiated population, 25 from the Cs-137 irradiated population, and 50 from the control population.

RESULTS

Three clones from the Fe-56 population, two from the Cs-137 population, and one from the control population showed chromosomal instability, exhibiting a frequency of dicentric chromosomes and other aberrations, a high level of apoptosis, low plating efficiency, and slow growth that varied from the mean value for the control clones by two standard deviations. Two other clones from the Fe-56 population and one from the control population showed a significant increase in mutation rate at the thymidine kinase locus. but few other characteristics differing significantly from the mean value of the control clones. A number of clones exhibited cell cycle distribution abnormalities but showed very few additional alterations.

The chromosomally unstable cells had shorter telomeres than found in normal WTK1 cells. Because these cells are unstable, subclones of each vary among themselves. Perhaps because of this variation, the number of cells in the clonal population exhibiting chromosomal instability decreased during culture at 37°C either because of expansion of faster growing stable cells within the clonal population, or elimination of the unstable clones by apoptosis.

CONCLUSIONS

Our results to date show that radiation induces genomic instability as indicated either by a delayed increase in chromosomal aberrations or in mutant frequency. These studies suggest that there may be multiple targets for instability because not all unstable clones have the same characteristics. It is possible that the mechanism of the induction of genomic instability differs in each cell so affected.

THE XRCC2 AND XRCC3 DNA REPAIR GENES ARE REQUIRED FOR CHROMOSOMAL STABILITY

E. H. Goodwin¹, X. Cui¹, M. Brenneman¹, J. Meyne¹, M. Oshimura², and D. J. Chen¹

¹Los Alamos National Laboratory, Life Sciences Division, Mail Stop M888, Los Alamos, NM 87545, ²Department of Molecular and Cell Genetics, School of Life Sciences, Tottori University, Yonago, Tottori, 683-8503, Japan

INTRODUCTION

The *XRCC2* and *XRCC3* DNA repair genes are now considered members of the *RAD51* gene family, and are thought to play a role in homologous recombination. Mutation in either gene causes heightened sensitivity to ionizing radiation and particularly to the DNA cross-linking chemical mitomycin C (MMC). The influence of these genes on spontaneous and induced chromosomal instability was examined in human/hamster hybrid cell lines.

METHODS

The *irs1* and *irs1SF* hamster cell lines have lost *XRCC2* and *XRCC3* gene function, respectively. Microcell-mediated chromosome transfer was used to introduce complementing or non-complementing human chromosomes into each cell line. *irs1* cells received human chromosome 7 (which has the human *XRCC2* gene) or, as a control, human chromosome 4. *irs1SF* cells received human chromosome 14 (which has *XRCC3*) or human chromosome 7. Fluorescence *in situ* hybridization (FISH) with probes to the human chromosome and interstitial telomeric repeats was used to detect rearrangements occurring during the clonal expansion of cells that either received no prior treatment, or were exposed to MMC, γ -rays, or α -particles.

RESULTS

For each set of hybrid cell lines, clones carrying the complementing human chromosome recovered MMC resistance to near-wild-type levels, while control clones carrying non-complementing chromosomes remained sensitive to MMC. Cytogenetic analysis revealed that the human chromosome in complemented clones remained intact in almost all cells. However, the human chromosome in noncomplemented clones frequently underwent spontaneous chromosomal rearrangements including breaks, deletions, and translocations during clonal expansion. The influence of *XRCC3* on induced instability was examined in cells exposed to MMC or radiation doses that reduced survival by 50%. In noncomplemented cells, both MMC and γ -rays induced a statistically significant increase in chromosomal rearrangements in comparison to the already unstable untreated controls. However, complemented cells were not similarly affected. Alpha particles did not induce instability in these experiments.

CONCLUSION

Our results indicate that the *XRCC2* and *XRCC3* genes play essential roles in maintaining chromosome stability under normal cell culture conditions. *XRCC3* also diminishes induction of transmissible instability by the DNA damaging agents MMC and ionizing radiation. This may reflect roles in DNA repair, possibly via homologous recombination.

Tuesday, June 15

Brookhaven National Laboratory

9:50 a.m. – 10:50 a.m.

Posters III

Berkner Rooms A & C

PERSISTENT FE-ION-INDUCED SUPPRESSION OF CELLULAR PROTEIN BIOSYNTHESIS IN SURVIVING CELLS

Elizabeth K. Balcer-Kubiczek and George H. Harrison, Department of Radiation Oncology, Division of Radiation Research, University of Maryland School of Medicine, Baltimore, Maryland 21201

INTRODUCTION

It is well known that ionizing radiation has a profound effect on protein homeostasis but the underlying molecular mechanisms remain unknown. The central engine for protein biosynthesis is the ribosome. We report here that Fe-ion irradiation may persistently affect several ribosomal functions in survivors, including mRNA decoding and peptide chain assembly as well as ribosomal biogenesis, and import/export of ribosomal proteins from the nucleus to the cytoplasm.

MATERIALS AND METHODS

The cellular model used in the present study was MCF7 cell line. Changes in messenger RNA levels in irradiated versus control cells were detected by using our technology of differential hybridization to complementary DNA clones from a lambda g11 human MCF7 cell expression library. All RNA samples were collected from MCF7 cells 7 d after 2.5 Gy Fe-ions.

RESULTS

In MCF7-WT cells 7 d after irradiation with 2.5 Gy of 1 GeV Fe ions, 21 out of 2500 cDNAs were differentially expressed, i.e., the corresponding mRNAs were reduced by at least a factor of 2. Eleven of these were associated directly or indirectly with ribosomal ultrastructure or function.

Ribosomal Structure/Function	Identity of Associated Gene(s)
Transport of ribosomal proteins between the nucleus and cytoplasm	RAN/TC4
rRNA gene transcription and processing	fibrillarin, proliferating cell nucleolar antigen P40
Ribosomal biogenesis	rPS8, rpS11, rpL5, rpL23 RpL30, rpL34
Translation initiation	Initiation factor 4B

CONCLUSION

We have shown for the first time that one of the long-term effects of Fe-ion irradiation may be impaired protein synthesis due to a reduced rate of transcription of genes encoding structural ribosomal proteins and involved in ribosomal biogenesis. Fe-irradiation may specifically affect transport of transfer, ribosomal and messenger RNAs from the cell nucleus (a synthesis site) to the cytoplasm (a translation site). Since ribosomes are physically associated with the cytoskeleton as well as the telomeric regions of 5 specific chromosomes, these results may have additional important consequences in the response to microgravity and for genetic (chromosomal) instability.

PROTON-INDUCED APOPTOSIS IN CONFLUENT BUT NOT EXPONENTIAL HLE

E. A. Blakely, M. P. McNamara, P. Y. Chang, K. A. Bjornstad, and E. Chang
Life Sciences Division, Lawrence Berkeley National Laboratory, Berkeley, CA 94720

INTRODUCTION

One potential mechanism of radiation-induced cataractogenesis involves a pathway involving apoptosis. Li et al., 1995 (J Cell Biol 130:169) reported that apoptosis due to oxidative stress is associated with cataract, although there is evidence for confounding data from necrotic (Harocopos et al., 1988 IOVS 39:2696) or differentiating (Ishizaki et al., 1998 J Cell Biol 140:153) lens cells. Fiber cell differentiation in the chick lens may be associated with DNase II-sensitive apoptosis (Torriglia et al. 1995, JBC 270:28579), or with a combination of DNase I- and DNase II-sensitive apoptosis (Bassnett and Mataic, 1997 J Cell Biol 137:37), which is also reported in differentiating primate lens (Bassnett, 1997 IOVS 38:1678). We have examined proton radiation-induced apoptosis with DNase I/II TUNEL™ assays in normal and immortalized human lens epithelial (HLE) cell cultures.

METHODS

Normal human lens epithelial (HLE) cells are maintained on extracellular matrix (ECM) derived from bovine corneal endothelial cells and demonstrate molecular markers for differentiation. In addition, we are growing human lens cells immortalized by viral transformation (HLE-B3) that can be maintained without ECM *in vitro*, and do not demonstrate differentiation to the same degree as the normal cells on ECM. Comparisons have been made between exponentially growing and confluent cell cultures. Cell cultures of each type and cell density were irradiated with 0, 4, 8 or 12 Gy of 55 MeV/amu protons.

Two protocols were used on different areas of each unirradiated control and proton-irradiated sample to detect DNase I- and DNase II-sensitive apoptosis. Processing for TUNEL was done on the petri dish either immediately, or after 6 hrs. or 24 hrs. after irradiation. At the time of processing the cell cultures are permeabilized with ice cold 0.1% sodium citrate/0.1% Triton X-100 in PBS for 2 minutes. Cells are then treated with TUNEL (Boehringer-Mannheim) for 1 hour at 37°C. In the case of the detection of DNase-II-sensitive apoptosis this step is preceded by a digestion with Calf Intestinal Alkaline Phosphatase (Gibco BRL) for 1 hour at 50°C. The two DNase protocols are otherwise identical. Nuclei are counterstained with DAPI and 500 nuclei are scored to determine the percentage of TUNEL positivity.

RESULTS

Unirradiated normal control human lens epithelial cells show no DNase I-sensitive apoptosis, and little evidence of apoptosis by the DNase II-sensitive TUNEL assay during differentiation in culture. The immortalized HLE-B3 cells also show no DNase I-sensitive apoptosis and only a small percentage of DNase II apoptosis during growth in culture. Exponentially-growing, normal HLE and immortalized HLE-B3 cells are resistant to proton-radiation-induced DNase II-sensitive apoptosis. However, confluent differentiating HLE cells demonstrate a proton-dose-dependent linear increase in apoptosis within 6 hrs after exposure, while confluent immortalized HLE-B3 cells show a less significant proton-dependent increase in DNase II apoptosis compared to the normal cells.

CONCLUSION

The susceptibility of human lens epithelial cells to proton-induced apoptosis changes during fiber cell differentiation.

Supported by NASA Award #T-965W.

QUANTITATION AND STATISTICAL ANALYSIS OF PHYSIOLOGICAL RESPONSES TO 1 GeV/nuc Fe PARTICLE IRRADIATION USING DIGITAL FLUORESCENCE IMAGE DATA

D.E. Callahan, K.D. Benson, S. Costes, H. Chong, S.A. Ravani, C. Wang, and M.H. Barcellos-Hoff

Life Sciences Division, Lawrence Berkeley National Laboratory, Berkeley, CA 94720

INTRODUCTION

We have developed experimental protocols and analytical digital image analysis techniques for identifying, quantifying, and tracking the time-dependent or dose-dependent biological effects of different types of radiation on various types of tissue. As an initial example, the time-dependent response (3-96 h) of mouse liver to 1 GeV Fe particles will be presented. We will report on protocols for tissue sampling from multiple animals, digital image database management, algorithm development, and automated data reduction. We have also implemented protocols for surveying (and sharing with colleagues) large numbers of multi-channel images by use of a secure, Internet-browseable Image Library. This graduated system for image analysis and algorithm development allows large numbers of multi-channel, high-resolution images to be surveyed remotely (e.g., by a pathologist using an Internet Browser). This "collaboratory" approach (URL <http://www-itg.lbl.gov/DCEE>) helps identify sources of variability, eliminate inter- and intra-observer bias and allows close interaction between pathologists and image processing experts. This facilitates the development of novel image processing algorithms that can monitor and quantify subtle changes in complex tissue patterns.

Tissue is composed of an interdependent, three-dimensional system of different cell types embedded in a supportive, dynamic, insoluble protein matrix. The extracellular matrix also contains biologically potent, diffusible molecules (i.e., growth factors, proteases, chemokines) that are in a state of flux after radiation tissue damage. Microscopic observation of immunofluorescently stained cryosections from tissues of mice exposed to qualitatively different types of radiation indicate that changes in the amount and relative spatial distribution of specific tissue proteins can occur in a time-dependent, dose-dependent, and radiation quality-dependent manner (Ehrhart, et al., Rad. Res., 145:157-162, 1996).

In our studies, tissue responses to radiation can involve complex changes in the amount, accessibility, structure, and relative distribution of specific structural, signaling, or enzymatic tissue proteins. In addition, the same tissue can exhibit different responses in different tissue compartments. These changes can be tracked indirectly via immunohistochemistry using specific antibodies to proteins and secondary detection with fluorochrome labeled antibodies. Changes in the intensity or the distribution patterns of fluorescence signals allow us to monitor and quantify radiation-induced physiological responses in different types of tissue.

METHODS

Animal Irradiation, Collection of and Preparation of Specimens: Balb/c mice were irradiated whole body with 1 GeV Fe particles and four animals were sacrificed at each time point (3, 24, 48, and 96 h post-irradiation). One block of each tissue type of interest was recovered from each animal. Tissue specimens were immediately placed in tissue embedding medium, frozen, and

stored at -80 °F. Slices of tissue (5 μ thick) were obtained from tissue blocks by cryosectioning. Analysis of mouse liver is presented here. Two slices from each tissue block were obtained and processed in parallel. Changes in the extracellular matrix (ECM) of liver were monitored using antibodies to the basement membrane proteins laminin (LM) and collagen type IV (CoIV), and the interstitial protein fibronectin (FN). Cell nuclei were fluorescently labeled with DAPI.

Image Acquisition: Specimens were not identified according to treatment, and image fields were chosen on the basis of nuclei DAPI fluorescence (blue channel), not immunofluorescence (green channel). Three or four images were obtained for each tissue section in this random, blinded manner. Thus, 6-8 images were obtained for each animal, and 12-16 images were obtained at each time point (representing multiple images from duplicate tissue slices from two different animals). Fluorescence images (1024x1024 pixels, 6.8 μ square pixels) were obtained using a Zeiss Axiovert fluorescence microscope and 40x Plan-Neofluar objective (0.75 NA). Thus, each image represents an area of 30,300 μ^2 . Multichannel image acquisition was automated using custom software based on ScilImage (TNO Institute of Applied Physics, Delft, The Netherlands). A rotating optical filter wheel was used to selectively excite fluorochromes in sequence. Images of blue fluorescence (nuclei) were saved as a 12-bit monochrome image in channel 1 of a multislice image, and images of green fluorescence (immunofluorescence) were saved in channel 2. The ICS image format was used, where all important image acquisition parameters are kept in an associated text file. The digital camera (Xillix, Vancouver, Canada) contained a scientific-grade 12-bit charged coupled device (KAF-1400). This camera has a linear response suitable for quantitative imaging and a wide dynamic range (0-4096 gray scale). A fixed exposure time was chosen for each channel, so that all fluorescence intensities for a given experiment fell within the 12-bit linear range. Internal standardization was achieved by comparing only images stained with the same antibodies in the same experiment, captured with identical parameters.

Image Library: All images of a given experiment (\cong 100 multichannel images) were scaled to a common 8-bit scale (0-255 gray scale) on a channel by channel basis. This scale was established by obtaining a global, artifact-free minimum and maximum intensity value for each channel. These scaled images were then posted on the ImgLib as individual monochrome and combined, multichannel color images. The ICS image header text was also posted with each image. In addition, several large composite photos (\cong 70 images) with images arranged by treatment group were also added to the ImgLib (Thompson, M, et al. (<http://imglib.lbl.gov/ImgLib/> ImgLib.project)). Thus, subtle changes in the intensity and relative distribution of immunofluorescence could be rapidly observed by visual inspection.

Presentation, Quantitation, and Statistical Analysis of Tissue Response: Fluorescence intensity and distribution in tissue sections were quantified using image analysis as a function of time. We developed a semi-automated image analysis technique that we refer to as Fragmented Random Lines Analysis (FRLA). Three items serve as input for the FRLA of each experimental image (Figure 1). (1) A background corrected version of the immunofluorescence image, where the background is analytically obtained on an image by image basis (2) A binary image that is created using a threshold value that is analytically derived from the immunofluorescence image. (3) A set of 500-1000 random lines. Each random line is compared to the binary image on apixel-by-pixel basis; the fragments of each random line that intersect the binary image are obtained. Each line fragment is characterized by the distance (D) between its endpoints and the mean intensity (MI) of all the corresponding pixels in the immunofluorescence image. All the line fragment data (MI values, D values and MI, D data pairs) for all the images of a treatment group

are pooled and presented as histograms or 2D contour plots. Thus, differences between large numbers of pooled images, representing different treatment groups, can be represented in small figures that retain an easily understandable connection to visually apparent features of the original images. These features are fluorescence intensity and distribution of fluorescence intensity. Since large numbers (10^5) of line fragment data pairs are typically obtained, a random sample ($n=500$) of the pooled data arrays is taken for each treatment group. A 1D (for histograms), or 2D (for contour plots), two-sample K-S (Kolmogorov-Smirnov) statistical analysis is performed on the randomly sampled data.

RESULTS

Liver sections collected from animals 3 hr to 96 hr after 0.8 Gy (~ 3 particles / $10 \mu\text{m}^2$) whole body 1 GeV Fe-particle irradiation were immunostained with antibodies to FN, LM, and CoIV. The localization of these proteins became more distinctly sinusoidal and continuous following Fe-particle irradiation. No changes in perivascular collagen type I or III were noted.

FRLA analysis was conducted, which permits the evaluation of multiple animals and multiple images. Two sample K-S tests of FRLA data indicate that perisinusoidal FN, CoIV and LM immunoreactivity were significantly ($p<0.001$) increased as early as 3 hr post-irradiation. However, the time course indicated that maximal differences from sham were protein dependent: FN peaked at 3 hr, LM peaked at 24 hr, and CoIV peaked at 96 hrs, suggesting that the basis for the change in immunoreactivity were distinct.

CONCLUSIONS

FRLA (Figure 1) allows us to pool fluorescence image data taken from multiple tissue sections and from different animals. Thus, sources of variability such as normal tissue heterogeneity within a given animal, different physiological responses between animals, and differences in specimen preparation are all taken into account. Previous attempts to pool images in this manner (e.g., using metrics such as mean fluorescence intensity or total integrated intensity) did not resolve the subtle, but significant, responses seen at early time points (< 24 hr). For example, in data presented here, extracellular matrix remodeling following iron irradiation was seen to be statistically significant at time points as early as 3 hrs. FRLA and K-S statistical analysis allow us to reduce large numbers of images containing visually subtle, complex changes in fluorescence intensity and distribution to small, easily interpretable 1D histograms or 2D contour plots. This method of presentation clearly demonstrates the degree of scatter in the data and allows one to calculate the statistical significance of differences observed between treatment groups.

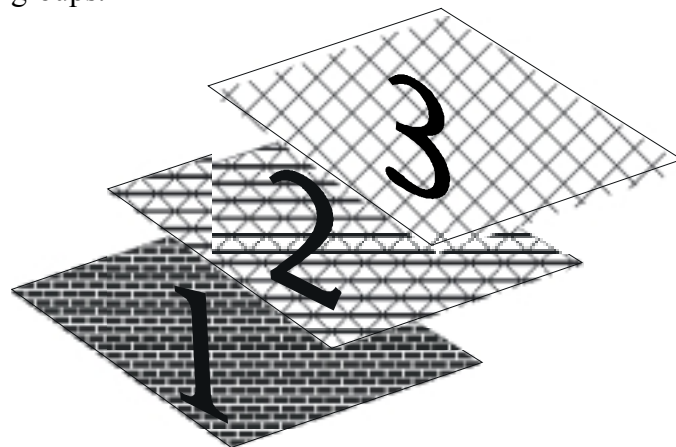


Figure 1: Three images serve as input for the FRLA. (1) The background-corrected, 12-bit gray-scale immunofluorescence image. (2) A thresholded, binary image of the immunofluorescence image (3) A set of random lines (represented here as a binary image)

FRTL-5 CELLS EXPOSED TO PHOTONS HAVE INCREASED PROTEIN KINASE C ISOENZYMES, REDUCED POLARITY AND A TRANSIENT CHANGE IN IMMUNO-DETECTABLE Cx32 GAP JUNCTION PROTEIN.

Lora M. Green^{1,2,3}, Deborah K. Murray¹, Ankur Bant², Da Thao Tran², Daila S. Gridley^{1,2} and Gregory A. Nelson¹.

Radiobiology Program, Loma Linda University Medical School¹; Loma Linda University Department of Microbiology & Molecular Genetics² and JL Pettis Memorial Veterans Medical Center, Loma Linda³.

INTRODUCTION

All cells, with the exception of the free-living cells of hematopoietic origin, are integrated to a greater or lesser extent by extracellular matrices, adhesion proteins (tight & adhesive junctions), gap junctions and cytoskeletal elements. It is this three-dimensional assembly that creates an organized, coordinately regulated tissue. The phenomenon of contact-effect in terms of radiation sensitivity is related to the state of cell assembly, whether they are existing as single cells, monolayers, spheroids or follicles. The clonogenic properties of cells are often discussed in the context of whether radiosensitivity &/or resistance is being affected by the status of cellular contact and modulation of adhesive properties required for such contact. The thyroid follicle is a polarized, contact-dependent entity that expresses multiple connexins that are distributed to different intracellular locations and are regulated differently. Thus, the thyroid provides an opportunity to investigate the contribution of “contact effects” at several levels, following irradiation.

The contact-dependent nature of gap junction formation necessitates that cells be in close proximity and as such, gap junctional competency is related to the integrity of the extracellular environment and influenced by changes in physical contact (adhesion protein expression). From our studies of inflammation based thyroid injury we found that the three normally expressed connexins (Cx, gap junction proteins) were reduced in amount (both protein and mRNA), but more importantly, they were not assembled in the plasma membrane at points of cell to cell contact. Further studies proved that increased protein kinase C (pKC) activity, due to increased amounts of several pKC isoenzymes, was directly responsible for the reduction of Cx43. Increased phosphorylation by this increase in pKC activity resulted in a modulation of cell-to-matrix, cell-to-cell and cell-to-cytoskeleton attachments, which indirectly caused the down-regulation of Cx32 and Cx26. This loss of coordinated assembly was also implicated in the loss of thyroid function (hypothyroidism).

The cellular response to inflammation that we have documented in thyroid epithelium is similar to that of cells exposed to radiation. Directly pertinent are reports of ionizing radiation causing an increase in pKC mRNA, and tissue remodeling in the mammary gland following irradiation. As a first approach to defining the changes that occur in thyroid epithelium we selected a thyroid cell line [Fisher Rat Thyroid cells (FRTL-5)] which is dependent on thyroid stimulating hormone for growth, forms well developed thyroid follicles *in vitro* and can conditionally produce thyroid hormones. Unlike normal rat thyroid cells, FRTL-5 cells express only Cx32, which we have previously shown to be expressed at the lateral surface connecting intra-follicular thyroid cells to each other. In this study we measure the level of seven pKC isoenzymes,

assessed polarity (F-actin assembly), and the levels of immuno-detectable Cx32 in FRTL-5 cells 2 hours and 6 hours following a single exposure to 3 Gray gamma rays.

MATERIALS/METHODS

FRTL-5 Cell Line — Fisher rat thyroid line (clone 5)(FRTL-5) were purchased and maintained according to American Type Culture Collection specification. The cultures were maintained free of antibiotics and routinely tested for mycoplasma. Cells are passaged by trypsinization and established in 35mm dishes that contained 25mm round glass cover slips, or in flasks. Cells were allowed to recover for a minimum of two days prior to radiation exposure.

Source of Radiation— The *gamma* radiation used in our experiments is from an El Dorado model 6 cobalt-60 irradiator. The dose was delivered as a single exposure of 3 Gy (0.63Gy/min).

Immunocytochemistry --The FRTL-5 cells established on glass cover slips were irradiated, harvested at appropriate times thereafter by fixation in -20°C ethanol. The cells were re-hydrated in PBS and immunoreagents added. For identifying the pKC isoenzymes we used *murine* monoclonal antibodies. The pKC antibodies were anti-pKC-alpha; anti-pKC-beta; anti-pKC-gamma; anti-pKC-delta; anti-pKC-epsilon; anti-pKC-iota and anti-pKC-lambda. Cx32 was labeled with mouse anti-Cx32. Fluorescein-conjugated, affinity purified secondary, antimouse IgG ($5\mu\text{g/ml}$) was added to the cover slips for 90 minutes at 25°C . Excess secondary antibody was removed by washing in PBST, cells were counter stained with $5\mu\text{g/ml}$ propidium iodide (10 min, $22-25^{\circ}\text{C}$), and mounted onto microscope slides for image analysis. F-actin localization was determined using FITC-phalloidin.

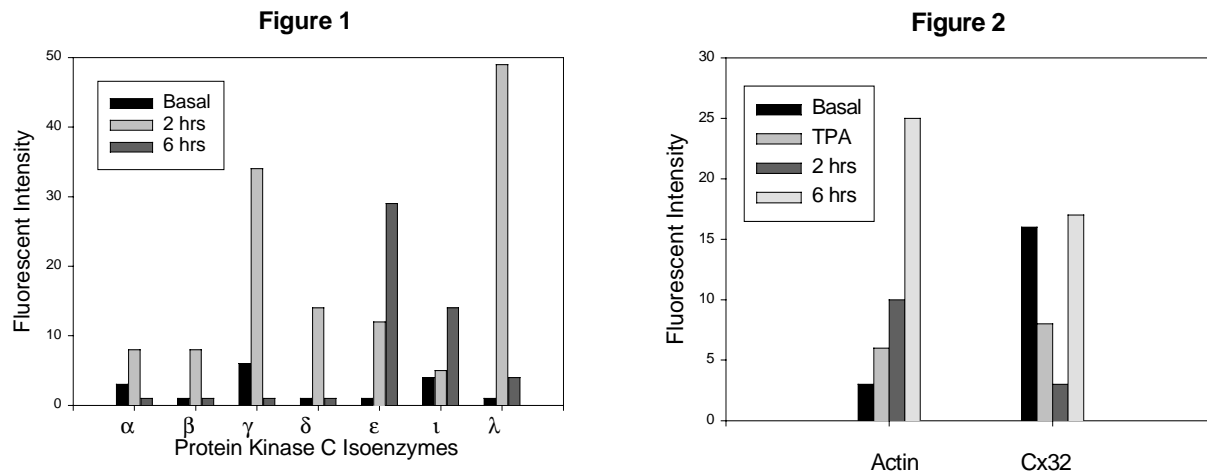
Laser Scanning Cytometry- The Laser Scanning Cytometer has an Olympus BX50 base and is configured with argon ion and helium-neon lasers for 4 color analysis. 4 photo-multiplier tubes support dichroic mirrors and optical interference filters, each detecting a specific fluorescent wavelength range. Cells for analysis are contoured by red fluorescence (PI) and gating parameters set for signal intensity (green-FITC) and cell size. Protocol settings and display parameters are optimized on a per cell-type basis using untreated and non-specific immunofluorescence stained slides. These programs are stored and utilized to scan the treated cells in a given experiment. The same parameters were used for all replicates to quantify relative changes with non-treated thyroid cells serving as the control (e.g. normal level).

RESULTS/DISCUSSION

Radiation Induced changes in pKC Isoenzyme Levels in FRTL-5 Cells Following Irradiation.

Well-established FRTL-5 thyroid cells were left untreated and identical sets exposed to gamma radiation. The basal pKC isoenzymes that we were able to measure by laser scanning cytometry were moderately low levels of pKC-gamma and pKC-iota. FRTL-5 cells that were gamma irradiated at a single dose of 3Gy were harvested 2 hours and 6 hours post irradiation. At two hours there were increases in the level of several isoenzymes, the most dramatic being pKC-gamma which was >3 fold and lambda which was >5 fold above basal levels. The profile of pKC isoenzyme levels changed at 6 hours post irradiation. All the levels were declining except for pKC-iota (2 fold over baseline) and pKC-epsilon which showed a three-fold increase over an almost undetectable basal level (**Figure 1**). Similarly treated sets of FRTL-5 cells are scheduled for exposure to protons and iron particles and sets have been harvested in appropriate buffers so that pKC activity assays and western blots can be performed to quantify these the changes we have measured. The results of these experiments suggest that changes in signal transduction occur fairly early following cells/tissue exposure to radiation. It is at this same time DNA

damage is being repaired and seems likely that pKC and other second messenger would be involved in this process. As we have seen in our inflammation studies there are a variety of changes that occur with regard to tissue integrity.



Radiation Induced changes in F-actin and Cx32 in FRTL-5 Cells Following Irradiation.

The loss of discrete organization of the actin filaments causes an increase in the fluorescent signal due to the cytosolic distribution of fluorescently labeled actin, when compared to the lower intensity of discretely organized actin in polarized thyroid cells. This loss of polarity in gamma irradiated FRTL-5 cells coincides with the increased activity of pKC. In that a similar effect (lower magnitude of change) can be demonstrated when TPA is used to activate pKC (**Figure 2**). Whether the increase at 6 hours reflects increased production of actin will be determined by western blot analysis.

In primary thyroid cells isolated from inflammatory sites, Cx32 is indirectly reduced by the sustained elevation in pKC activity, which causes alterations in cell-to-cell cohesion. In the FRTL-5 cells we see a transient reduction of Cx32 which after 6 hours returns to basal level. Whether there is a relationship between this modulation of Cx32 and the fluctuation of pKC isoenzymes remains to be determined.

In summary, radiation induced changes in organized tissues like the thyroid occurs at several levels. Of particular importance is the increases/up-regulation of kinase activity. The subsequent phosphorylation that results from this activity modulates cellular function and leads to the reduction of tissue integrity. It is important to understand changes in tissue integration for it is the context of the cellular environment that dictates its ultimate response.

PROTON VERSUS GAMMA RADIATION EFFECTS ON IMMUNOLOGICAL STATUS IN AN ANIMAL MODEL

D.S. Gridley^{1,2}, E.H. Kajioka², C. Gheorghe², J. Li², M.L. Andres¹, L.M. Green¹, G.A. Nelson¹, and J.M. Slater¹

Departments of ¹Radiation Medicine (Radiobiology Program) and ²Microbiology & Molecular Genetics, Loma Linda University School of Medicine and Medical Center, Loma Linda, CA 92354

INTRODUCTION

Deleterious consequences following exposure to radiation are of great concern when contemplating extended voyages in space. Profound immunodepression has been noted in astronauts, cosmonauts, nonhuman primates, and rodents during flight and/or after return to earth. Among the parameters that have been evaluated are responsiveness to mitogens and common recall antigens, natural killer (NK) cell cytotoxicity, leukocyte subset distribution, and cytokine production. The immune system is the body's defense against infectious agents, inanimate foreign materials, and neoplastic or otherwise altered cells. It is well known that the frequency of infections, cancer, and certain other diseases correlates with the degree of immunocompetence. It seems likely that the risk for problems due to impaired immune responses will increase as the duration of space flights increase. The underlying mechanisms responsible for the immunological changes associated with space travel, as well as the health-related significance of the changes, have not yet been clearly established. It has long been known that the lymphoid organs and immune system cells are highly radiosensitive. Changes in lymphocyte morphology and migration patterns have been noted at doses as low as 0.02 – 0.05 Gy. It has been suggested that the balance between certain lymphocyte populations may reflect or influence the degree of radiation-induced damage and could perhaps serve in biological dosimetry. The purpose of the present study was to evaluate acute immunological responses following whole-body irradiation and to directly compare the effects of protons and photons.

METHODS

Male C57BL/6 mice were purchased at 5-6 weeks of age and acclimatized for 2-3 wk before study initiation. The animals were lightly anesthetized and placed into a circular apparatus with triangular compartments. Protons or gamma rays were delivered in a single fraction of 3 Gy. A spread-out Bragg peak of proton radiation, 3.5 cm wide, was delivered at an energy of 149 MeV and a dose rate of 1 Gy/min. Gamma radiation was delivered using an Eldorado Model "G" gamma irradiation machine with a ⁶⁰cobalt (⁶⁰Co) source at a dose rate of 0.32 Gy/min. One day after irradiation, a 1% sheep red blood cell (sRBC) suspension was injected intraperitoneally into a portion of the animals at 200 µl/mouse. At 4, 10, 15, and 29 days post-irradiation, euthanasia was performed by rapid CO₂ asphyxiation. At each time of sacrifice, 5-6 mice were in each of the irradiated and nonirradiated sRBC-injected groups; ten additional animals (no irradiation, no sRBC) served as normal controls.

At the times of euthanasia, the animals and their spleens were weighed. The RSW was calculated as follows: $RSW = \text{spleen weight (g)} \times 10^4 / \text{body weight (g)}$. The spleens were then processed into single-celled suspensions, erythrocytes were lysed, and the remaining cells were counted using the trypan blue exclusion method. Peripheral blood was collected by cardiac

puncture in syringes containing heparin, erythrocytes were lysed using the Unopette Microcollection System and the remaining cells were counted.

In the spontaneous blastogenesis test, 50 μ l aliquots of whole blood were plated into 96-well microtiter plates; 200 μ l of RPMI 1640 medium and 50 μ l of ^3H -thymidine (1 μCi ^3H -TdR; specific activity = 46 Ci/mmol) were then added and the plates were incubated for 4 hr in 5% CO_2 at 37°C. The cells were harvested using a multiple sample harvester and the uptake of ^3H -TdR was quantitated in a beta-scintillation counter. The leukocyte counts and volume of blood (50 μ l) were used to convert disintegrations per minute (dpm) into dpm/ 10^6 leukocytes.

Immunophenotyping was carried out by direct labelling of peripheral blood cells with fluorescein isothiocyanate (FITC)- or R-phycoerythrin (PE)-conjugated monoclonal antibodies (MAb) and a FACSCaliburTM flow cytometer (Becton Dickinson). A 2-color immunophenotyping panel was set up for each sample as follows: a) cells only, b) IgG2a*PE/IgG2b*FITC - isotype controls, c) anti-IgG2a*FITC - isotype control, d) anti-CD3*PE/anti-CD19*FITC - mature T and B cells, e) anti-CD3e*PE/anti-NK1.1*FITC - NK cells, f) anti-CD3e*PE/anti-CD4*FITC - T helper/inducer (Th) cells, and g) anti-CD3e*PE/anti-CD8a*FITC - T cytotoxic (Tc) cells. Acquisition and analysis of at least 4,000 lymphocyte events/tube were performed utilizing CellQuestTM software, version 3.01 (Becton Dickinson). Lymphocyte purity was normalized to % lymphocyte total (Th + Tc + B + NK cells). The absolute numbers of each cell type were calculated as follows: leukocyte count/ml \times % lymphocyte total \times normalized % = absolute number of cells/ml.

To obtain anti-sRBC immunoglobulin titers, plasma samples were heat inactivated at 56°C for 30 min, a series of 2-fold dilutions was made, sRBC were added, and the mixture was incubated at 37°C for 1 hr. The cells were then serofuged for 30 sec and the amount of agglutination was observed with the aid of an agglutination viewer. The results were graded as follows: 4+ = one clump, clear background; 3+ = many large clumps, clear background; 2+ = many medium clumps, pink/clear background; 1+ = many small clumps, reddish background; and 0 = smooth suspension of cells.

Differences in quantifiable data were analyzed using Student's 2-tailed t-test and Microsoft Excel 1998 software. A p value of <0.05 indicated significant differences among groups.

RESULTS

The data showed significant depression ($p < 0.05$) in nearly all assays on days 4 and 10 after irradiation. However, spontaneous blastogenesis (^3H -thymidine uptake) of blood leukocytes, was significantly elevated at these times. Hematological reconstitution above control values was observed by day 15 for B cells (CD19+), but not for T cells (CD3+), T helpers (CD3+CD4+), T cytotoxic cells (CD3+CD8+), or natural killer cells (NK1.1+). There was a tendency for greater immunosuppression followed by a more rapid and somewhat higher rebound in proton irradiated mice, compared to the group receiving gamma radiation. Some of the data are presented in the tables below.

Table 1. Body weight, relative spleen weight, and leukocyte counts after irradiation

Group	Body weight (g)	RSW ^a	Leukocytes (10 ⁶ /ml)	
			spleen	blood
Normal control	23.3 +/- 0.3 ^b	17.0 +/- 0.6	24.7 +/- 3.6	6.2 +/- 0.4
<u>sRBC-injected</u>				
Day 4: sRBC control	23.6 +/- 0.7	19.7 +/- 1.6	13.6 +/- 3.1	6.5 +/- 0.9
Protons	21.2 +/- 0.7 ^c	10.2 +/- 0.2 ^e	2.6 +/- 0.7 ^e	0.7 +/- 0.2 ^e
⁶⁰ Cobalt	21.7 +/- 0.6	11.4 +/- 0.8 ^e	2.4 +/- 0.8 ^e	1.0 +/- 0.2 ^e
Day 10: sRBC control	23.7 +/- 0.3	24.6 +/- 2.9 ^f	38.2 +/- 6.9 ^g	8.3 +/- 1.1 ^h
Protons	22.0 +/- 0.6	19.9 +/- 1.4	7.4 +/- 1.2 ^e	1.5 +/- 0.3 ^e
⁶⁰ Cobalt	22.9 +/- 0.7	20.5 +/- 3.4	10.6 +/- 4.0 ^e	2.1 +/- 0.4 ^e
Day 15: sRBC control	22.6 +/- 0.1	19.3 +/- 0.9	19.5 +/- 2.1	4.0 +/- 0.5
Protons	22.9 +/- 0.1	21.5 +/- 1.1	19.0 +/- 2.5	5.7 +/- 0.6 ⁱ
⁶⁰ Cobalt	23.2 +/- 0.3	20.1 +/- 1.0	25.6 +/- 5.7	5.5 +/- 0.6 ^l
Day 29: sRBC control	25.4 +/- 0.7 ^d	20.2 +/- 1.2	20.3 +/- 4.5	6.3 +/- 0.9
Protons	24.5 +/- 0.7	18.2 +/- 0.6	14.8 +/- 2.8	6.2 +/- 0.7
⁶⁰ Cobalt	24.7 +/- 0.6	18.2 +/- 0.8	14.7 +/- 2.1	3.8 +/- 0.6 ^j

^aRelative spleen weight = spleen weight (g) x 10⁴/body weight (g). ^bMean +/- standard error of mean.

^cSignificantly lower than 'sRBC control' on day 4 (p<0.05). ^dSignificantly higher than 'Normal control' (p<0.025). ^eSignificantly lower than 'Normal control' and respective 'sRBC control' groups (p<0.01).

^fSignificantly higher than 'Normal control' (p<0.05). ^gSignificantly higher than all other groups except 'Normal control' and ⁶⁰Cobalt' on day 15 (p<0.05). ^hSignificantly higher than 'sRBC control' on day 15 (p<0.01). ⁱp<0.1 compared to 'sRBC control' on day 15. ^jp<0.1 compared to other two groups on day 29.

Table 2. Highest anti-sRBC immunoglobulin titers obtained in plasma from sRBC-injected mice

Group	Anti-sRBC immunoglobulin titer			
	Day: 4	10	15	29
sRBC control	2 ^a (1/6) ^b	16 (4/6)	4 (2/8)	8 (4/6)
Protons	0 (0/5)	2 (2/5)	0 (0/6)	8 (3/6)
Cobalt	0 (0/6)	0 (0/5)	0 (0/6)	8 (3/6)

^aTiter: reciprocal of the highest dilution at which there is still a detectable reaction.

^bNumber of mice with antibody titer/number of mice tested.

CONCLUSION

The data indicate that differences exist in the effects of proton and gamma radiation on cells of the immune system, that these differences are readily quantifiable after irradiation of the intact animal, and that the mechanisms needed to generate a primary response to antigen are greatly diminished *in vivo* by both forms of radiation under the conditions used.

INDUCTION AND REJOINING OF CHROMATID BREAKS FOLLOWING HIGH-LET RADIATION EXPOSURE

T. Kawata^{1,2}, E. Gotoh³, M. Durante⁴, Y. Furusawa⁵, H. Wu^{1,6}, T. Yang¹ and D. R. Morrison¹

¹NASA Johnson Space Center, Houston, Texas, USA; ²University of Keio, Tokyo, Japan;

³National Institute of Infectious Diseases, Tokyo, Japan; ⁴University of Naples, Naples, Italy;

⁵National Institute of Radiological Sciences, Chiba, Japan and ⁶Kelsey-Seybold Clinic, Houston, Texas, USA

INTRODUCTION

An earlier study of the induction and rejoining of chromatid breaks using a chemical-induced premature chromosome condensation technique (PCC) showed a fast and a slow repair processes in human cells exposed to gamma rays. In this study, we applied the PCC technique to analyze the frequency of chromatid breaks, and the kinetics of rejoining and mis-rejoining of breaks after high-LET irradiation in G2-phase human cells. The high-LET results were compared to those of gamma rays.

METHODS

Exponential growing human fibroblast cells AG1522 were irradiated with energetic carbon (290 MeV/u), silicon (490 MeV/u) and Fe (200 MeV/u) ions. Immediately following exposure, chromosomes were prematurely condensed by calyculin A then chromatid breaks and chromosome breaks (i.e. isochromatid breaks) in G2 cells were scored. Chromosomes were also collected using the PCC technique after several repair times ranging from 5 to 600 minutes at 37°C.

RESULTS

Calyculin A was able to induce premature chromosome condensation in cells immediately after irradiation. Kinetics of rejoining of chromatid breaks consisted of two exponential components having a rapid and a slow time constants. The number of chromatid breaks decreased rapidly in the first 10 minutes, and then continuously decreased at a slower rate. Chromatid and chromosome exchanges were formed very quickly. The frequency of residual breaks for heavy-ions was about three times that for gamma rays. Isochromatid breaks were observed in high-LET irradiated samples, and the single track effect appeared to be responsible for this type of breaks.

CONCLUSION

The chemical-induced PCC technique allows DNA double strand breaks to be analyzed easily, quickly and precisely. Using the technique, the difference in the relative frequency of different types of chromatid aberrations was detected between low and high-LET. The use of PCC should be considered to augment the quantitative assessment of high-LET radiation-induced DNA damage.

INVOLVEMENT OF MITOCHONDRIA TO CHANGE RADIATION SENSITIVITY IN HUMAN OSTEOSARCOMA CELLS

H.J. Majima¹, M. Suzuki¹, C. Yamaguchi¹, S. Kakinuma¹, H. Fuji¹, J.-P. Cao¹, D.C. Wallace², H.-C. Yen², K. Ando¹, K. Fujitaka¹, T. Nagano³ and T. Ozawa⁴

¹International Space Radiation Laboratory, and ²Center for Molecular Medicine, Emory University, Atlanta, GA, USA. ³Graduate School of Pharmaceutical Sciences, The University of Tokyo, Tokyo, Japan. ⁴Department of Bioregulation Research, National Institute of Radiological Sciences, Chiba, Japan.

INTRODUCTION

In 2000 years, the man-kind goes to space for long-term period, according to the plan of International Space Station, and Mars travel plan. In space field 1m Sv per day is estimated, which will be dose exposed through out a year on earth for a human being in average. Therefore, the studies to clarify the mechanism of cell death by X-ray and heavy irradiation and the any materials to protect the cells from the irradiation is in demand.

Aging renders the cells to cause damage in mitochondrial DNA, and neuro-degeneration accompanies with damage or mutation of mitochondrial DNA. Recent studies have suggested mitochondria regulates cell death, i.e., cytochrome c release from mitochondria and it renders activation of caspase which causes apoptosis. Bcl-2 protects cell death by inhibition of cytochrome c release. Mitochondrial membrane potential and pore formation regulates release of cytochrome c. Aging is known to give damage in mitochondrial DNA. And, neuro-degenerative diseases represent damage in mitochondrial DNA.

Mitochondrial DNA codes 13 components of electron transport chain. Lacking of mtDNA abrogates the electron transport system. We hypothesize that mitochondria deficient in functional electron transport system can result in increased production of superoxide and thus more oxidative stress.

X-irradiation causes cells death. There have been presented wide range of sensitivity to X-rays in mammalian cells, although the factors to decide the sensitivity to X-ray has not been completely discovered. The ATM and DNAPKcs assist damaged DNA from binding the breaking site. P53 gene let the cells to stop cell cycles when the DNA damage occurs. The most of studies to examine the cell death have been undergone in DNA damage. However recent studies also have shown set of signal transduction following the X-irradiation.

Here we demonstrates that mitochondrial DNA lacking cells, which is a model of mitochondrial damaged cells, is susceptible to X-irradiation and prevented by normal mitochondrial substitution. This study also suggests that mitochondria plays a key role to regulate cell death.

MATERIALS AND METHODS

Cell Lines: 143B of which mitochondrial DNA (+), Rho0 of which mitochondrial DNA (-) originated from human osteosarcoma cells were used in this study.

200kVp, 20mA, ~1 Gy/min of X-irradiation were given to the cells. Cell Survivals were determined by colony formation, and chromosomal aberrations also were observed after irradiation. DNA double strand breaks detection assay was performed by the CHEF pulse field gel electrophoresis method. Chromatin condensation was observed by Hoechst 33342 Staining, and mitochondrial ROS detection was observed by dihydrorhodamine 123. Nitric oxide was detected by DAF. Imaging studies employed a laser confocal unit (Yokogawa Electric Corp, CSU10, Tokyo, Japan) coupled to an inverted microscope (Olympus, Tokyo, Japan). The dye was excited at 488 nm and emission was filtered using a 515 nm barrier filter. The intensity of the laser beam and the sensitivity of the photodetector were held constant to allow quantitative comparisons of relative fluorescent intensity of the cells between experimental groups. Images of microscope fields were taken using a color chilled 3CCD camera (Hamamatsu Photonics, Hamamatsu, Japan). Cells were chosen for analysis on a random basis. Values for average staining intensity/cell were obtained using "IPLab" software programmed by the author (HJM).

RESULTS

Sensitivity to X-rays, clonogenicity, frequency of double strand breaks (DSB), chromosome aberration, free radical generation, apoptosis and oxidative damage markers, 8-OHdG were examined in 143B human osteosarcoma cell line (Rho+) and mtDNA-less (Rho0) cells derived from this cell line. No significant difference was observed between Rho+ and Rho0 cells without X-rays exposure for frequency of DSB and chromosome aberration. Clonogenicity assay showed greater sensitivity in Rho0 cells compared to Rho+ cells exposed to X-rays. More DSBs, and more chromosome aberrations in terms of gap, translocation, and deletion were observed in Rho0 cells. In addition, the extent of apoptosis was also greater in Rho0 cell with X-rays exposure.

CONCLUSION

Mitochondrial DNA(-) Cells (Rho0 Cells) are sensitive to X-rays.

Mitochondrial DNA(-) Cells (Rho0 Cells) produce more chromosomal aberrations.

Mitochondrial DNA(-) Cells (Rho0 Cells) produce more DNA double strand breaks.

X-ray irradiation causes mitochondrial ROS in both Rho+ and Rho0 Cells.

X-ray irradiation increases nitric oxide in both Rho+ and Rho0 Cells.

These results suggest that Rho0 cells lacking mtDNA has more oxidative stress and higher sensitivity to X-rays.

AMINOTHIOL INDUCED MODULATION OF P53 PROTEIN STRUCTURE

R.L. Wartens¹, D.K. Thai¹, J.C. Roberts¹, D.K. Gaffney¹ and A.E. Cress², ¹University of Utah Health Sciences Center and ²University of Arizona Cancer Center.

INTRODUCTION

The aminothiol WR1065 and the thiazolidine prodrug Ribose Cysteine (RibCys) are antimutagenic when added well after irradiation. This antimutagenesis when cells are exposed to aminothiols after irradiation must be due to some modification of the cell's response to DNA damage. In an attempt to better understand this modulation of the cellular response to radiation, we are investigating the intracellular changes in cells exposed to ionizing radiation and/or aminothiols.

METHODS AND RESULTS

Using immunofluorescence confocal microscopy, increasing amounts of the PAb421 p53 antibody epitope were detected in nuclei of γ -irradiated SK-N-SH neuroblastoma or HCT116 carcinoma cells, or in cells exposed to WR1065 or RibCys. Nuclear fluorescence increased to a 4-fold maximum by 1-2 hours after either 5 Gy irradiation or a 60-minute exposure to 4 mM aminothiols. Increased expression of the PAb421 epitope was observed in cells exposed to radiation doses as low as 0.5-1.0 cGy, or to WR-1065 concentrations as low as 100 μ M. Western analysis of irradiated or aminothiol-exposed cells using the PAb421 antibody indicated an increase in the PAb421 epitope between 0.5-2 hr after irradiation with little change the level of the epitope afterward. In contrast, Western analysis with the DO1 antibody indicated that p53 protein mass increased progressively for up to 6 hours after irradiation. In irradiated cells WAF1/p21 protein mass peaked by 3-4 hours and remained elevated for at least 6 hours. WAF1/p21 protein mass did not increase in aminothiol-exposed cells.

CONCLUSIONS

The results are consistent with γ -radiation or aminothiol exposure inducing a change in the PAb421 epitope between 0.5 and 2 hours after treatment. Either there is a change in the structure of p53 protein so that the PAb421 epitope becomes accessible, or there is an increase in expression level of this epitope, or both. The PAb421 antibody detects amino acids 372-381 (...KKGQSTSRHK...) in the carboxy terminus of the protein only when Ser 376 is dephosphorylated. Thus the results are consistent with Ser 376, phosphorylated in the unstressed cell, being dephosphorylated by a protein serine phosphatase beginning 0.5 hours after cell irradiation. Although Ser 376 remains unphosphorylated (i.e., continues to be detected by Western analysis) out to 6 hours post irradiation, the PAb421 epitope is detected by immunofluorescence microscopy only transiently. Thus amino acids 372-381 of the p53 protein must become masked beginning 2 hours after irradiation by association with some other nuclear protein.

Neither the signal for the induction, nor the consequence(s), of these stress-induced p53 protein changes is clear. Since they occur in response to both radiation and aminothiol treatment, we speculate that they are induced by intracellular redox changes.

Tuesday, June 15

Brookhaven National Laboratory

10:50 a.m. – 11:50 a.m.

Risk Mitigation

Berkner Hall

CONCEPTION OF COSMONAUTS' RADIATION SAFETY IN FLIGHT AS OPTIMIZATION OF RADIATION SAFETY SYSTEM ON THE BASIS OF ALARA PRINCIPLE

V.M. Petrov

State Scientific Center of the RF - Institute for Biomedical Problems, Moscow, Russia.

The ALARA principle should be the basis of cosmonauts' radiation safety. Let's believe that the benefit of space flight consist in the fulfillment of the flight program that is realized provided that cosmonauts' work-capacity is maintained on the required level. Assuming that required level depends on cosmonauts' adequate health one can conclude that radiation safety level is quantitatively connected with the required work capacity level. Therefore, the term "reasonably achieved" in the ALARA principle can be defined as the decrease of radiation dose up to values not resulting in health worsening lower than the acceptable level estimated from the relationship "safety - work-capacity" on the one hand, and duration of the corresponding changes in the work cyclogram caused by staying in radiation shelter, on the other hand. Hence, decrease of "benefit" will be proportional to time of staying in radiation shelter. The optimal level of radiation safety in every moment of the flight can be estimated, provided that the permissible portion of flight program non-realization and permissible health changes have been established.

COMPARISONS OF METHODS FOR ORGAN DOSE ESTIMATES: APPLICATIONS TO THE INTERNATIONAL SPACE STATION

Neal Zapp¹ and Francis A. Cucinotta²

¹Wyle Laboratories, Houston TX, 77058, U.S.A.,

²NASA Johnson Space Station, Houston TX, 77058, U.S.A.

Accurate determination of organ doses during spaceflight operations are needed for projecting possible flight rule violations in low earth orbit (LEO) and incrementing astronaut career exposures. Several methods for evaluating exposures to the blood forming organs (BFO) and other tissues exist and a systematic study of differences in these methods for space radiation exposures has not been made. These include the use of a 5 cm depth approximation, the use of the ICRP sphere, and evaluations using computerized anatomical man models. Also, in the past application of both tissue weighting factors or linear energy transfer (LET) dependent quality factors using the body external radiation environment or the actual organ exposures, respectively. We discuss inter-comparisons of these methods using the HZETRN/BRYNTRN code. We consider projected exposures to be incurred on the International Space Station (ISS) as a case study with individual contributions from trapped protons and galactic cosmic rays (GCR) discussed.

**SPACE ENVIRONMENT AND THE INTERNATIONAL SPACE STATION:
RECOMMENDATIONS TO REDUCE RADIATION RISK DURING
SOLAR MAXIMUM**

Dr. Ron Turner

ANSER, 1215 Jefferson Davis Hwy, Arlington, VA 22202

The National Academy of Sciences Space Studies Board, Committee on Solar and Space Physics has been examining the risk of the space environment to astronauts on the ISS, particularly during EVA on construction missions occurring during the peak of the solar cycle. This presentation is a status report on the progress of that study.

Tuesday, June 15

Brookhaven National Laboratory

11:50 a.m. – 12:30 p.m.

Project Review

Berkner Hall

ATMOSPHERIC IONIZING RADIATION (AIR) PROJECT REVIEW

R.C. Singleterry Jr¹, J.W. Wilson¹, A.H. Whitehead¹, P.E. Goldhagen², *et. al.*

¹NASA Langley Research Center, Mail Stop 188B, Hampton, VA 23681, ²U.S. Department of Energy Environmental Measurements Laboratory, 201 Varick St., New York, NY 10014

INTRODUCTION

The National Council on Radiation Protection and Measurement (NCRP) and the National Academy of Science (NAS) established that the uncertainty in the data and models associated with the high-altitude radiation environment could and should be reduced [1,2]. In response, the National Aeronautics and Space Administration (NASA) and the U.S. Department of Energy Environmental Measurements Laboratory (EML) created the Atmospheric Ionizing Radiation (AIR) Project under the auspices of the High Speed Research (HSR) Program Office at the Langley Research Center. NASA's HSR Program was developed to address the potential of a second-generation supersonic transport. A critical element focussed on the environmental issues, including the threat to crew and passengers posed by atmospheric radiation. Various international investigators were solicited to contribute instruments to fly on an ER-2 aircraft at altitudes similar to those proposed for the High Speed Civil Transport (HSCT). Table 1 contains a list of participating investigators, their institutions, and instruments with quantities measured. The flight series took place at solar minimum (radiation maximum) with northern, southern, and east/west flights. The investigators analyzed their data and presented preliminary results at the AIR Workshop in March, 1998. A review of these results follows.

REVIEW OF AIR WORKSHOP PAPERS

Approximately half of the preliminary workshop papers from the investigators have been completed and submitted for publication (references [3-7]). Tables 2 through 6 show results from the various detector systems (EML's preliminary neutron spectra and ionization chamber results [8] will be presented separately at this workshop by Paul Goldhagen). As shown in these data, all the reported instruments show approximately the same dose equivalents or dose equivalent rates for the same flight paths, within a factor of three. Some problems of intercomparability of data do exist because different analysis and reporting techniques were used. In this report, an effort was made to make the units as similar as possible; however, some problems like the choice of conversion factors from particle fluences to dose equivalent still exist. As the final reports, which will standardize their results, are gathered and published, these results should converge. Therefore, a comprehensive atmospheric computer model for the AIR Project, called the AIR Code, can be developed with some limitation according to the recommendations set forth by the NCRP and NAS.

STATUS OF HSR PROGRAM OFFICE AND THE AIR PROJECT

A number of factors contributed to the demise of the HSR Program and the associated industry support for the High-Speed Civil Transport development. While the program met all of its technical goals, the environmental barriers became more severe. At the same time the major industry partner, Boeing, could not continue to advocate and support a year 2006 HSCT in light of challenging production problems associated with their current line of subsonic transport. The program was scheduled for completion in 2001 with a possible extension, but will now be terminated at the end of Fiscal 1999. This premature closure directly impacts the AIR Project because the neutron analysis and incorporation of all the data into the AIR Code will take until

the end of the next fiscal year (FY00). Therefore, negotiations are in progress to fund the AIR project to completion. Resolution is not at hand at this time and completion of the AIR Project is in jeopardy.

PROJECT CONTINUATION

Assuming the AIR Project is funded to completion, the neutron data analysis, incorporation of the AIR data into the AIR Code, incorporation of the Japanese collaboration [9] model results into the AIR Code, and the final investigator's workshop are the primary tasks that need to be completed. This will take the Project to the end of FY00. The final product will be a code that will predict aircrew and passenger maximum exposure to normal flight with about a 20% uncertainty in the effective dose (the exact uncertainty will need to await the final analysis). This will allow regulatory bodies and the airline industry to establish radiation limits and economic analyses for vehicles of similar type to the HSCT. It will also result in an atmospheric environmental model for use in subsonic operations for which broad input has been derived from an international community.

REFERENCES

- [1] Anon.; *Radiation Exposure and High-Altitude Flight*, NCRP Commentary No. 12, NCRP, Bethesda, MD, 1996.
- [2] Anon.; *Radiation Hazards to Crews of Interplanetary Missions: Biological Issues and Research Strategies*, National Academy Press, Washington DC, 1996.
- [3] D.T. Barlett, L.G. Hager, R.J. Tanner; *The Determination Using Passive Dosimeters of Aircraft Crew Dose: Results for 1997 NASA ER-2 Flights*.
- [4] P.A. Chee; *TEPC Measurements of High Altitude Radiation*.
- [5] P. Tume, B.J. Lewis, L.G.I. Bennett, M. Pierre, T. Cousins, B.E. Hoffarth, T.A. Jones, and J.R. Brisson; *Assessment of High-Altitude Cosmic Radiation Exposure Using Tissue Equivalent Proposal Counters and Bubble Detectors*.
- [6] E. Normand; *Assessment of High Altitude Cosmic Radiation Exposure using a Simple Electronic Neutron Dosimeter, the PDM-303*.
- [7] H. Tai, P. Goldhagen, J. L. Shinn, J. W. Wilson, D. L. Maiden; *Atmospheric Ionizing Radiation (AIR) ER-2 Stratospheric Measurements Post-flight Analysis: The Argon Filled Ion Chamber*.
- [8] P.E. Goldhagen; *Overview of Aircraft Radiation Exposure and Recent ER-2 Measurements*, NCRP Proceedings No. 20, in press.
- [9] R.C. Singleterry Jr., J.W. Wilson, H. Tai, I.W. Jones; *Overview of the Atmospheric Ionizing Radiation Model and Validation Measurements*, 9th Annual Space Radiation Health Investigator's Workshop, Loma Linda, CA, June, 1998.

Table 1: Principal Investigators of Instruments on the ER-2 AIR Flights

Paul Goldhagen , U. S. Department of Energy Environmental Measurements Laboratory (EML) <ul style="list-style-type: none"> • Multisphere (Bonner Sphere) Neutron Spectrometer – <i>full range neutron spectrum</i> • Pressurized Argon Ionization Chamber – <i>total ionization, exposure rate, dose rate</i> • Scintillation Counters – <i>charged and neutral particle fluence rates and partial spectra</i>
Gautam Badhwar , NASA Johnson Space Center (JSC) <ul style="list-style-type: none"> • Particle Telescope – <i>charged particle fluences and spectra with species identification</i>
David Bartlett , National Radiation Protection Board (NRPB), United Kingdom <ul style="list-style-type: none"> • Track Etch Dosimeters – <i>dose equivalent</i>
Leslie G. I. Bennett , Royal Military College of Canada (RMC) <ul style="list-style-type: none"> • Superheated Drop/Bubble Detectors – <i>neutron dose equivalent</i>
Eugene Benton , University of San Francisco <ul style="list-style-type: none"> • Plastic Nuclear Track Detectors (PNTDs) – <i>fluence of target fragments</i>
Alexander Chee , The Boeing Company <ul style="list-style-type: none"> • Tissue-Equivalent Proportional Counter (TEPC) – <i>microdosimetric spectra, dose & dose-equivalent rates</i>
Thomas Cousins , Defence Research Establishment Ottawa (DREO), Canada <ul style="list-style-type: none"> • TEPC – <i>microdosimetric spectra, dose & dose equivalent rates</i> • Al₂O₃ Thermoluminescent Dosimeters (TLDs) – <i>non-neutron dose</i>
Francesco d'Errico , University of Pisa, Italy, and Yale University <ul style="list-style-type: none"> • Active Superheated Drop/Bubble Detector – <i>neutron dose equivalent</i>
Thomas Fogarty , Prairie View A&M University <ul style="list-style-type: none"> • Single-Event Upset Experiment – <i>single-event upsets in computer memories (not flown)</i>
Eugene Normand , The Boeing Company <ul style="list-style-type: none"> • PDM-303 Dosimeter – <i>high-LET dose equivalent</i>
Guenther Reitz , German Aerospace Research Establishment (DLR), Germany Rudolf Beaujean , University of Kiel, Germany <ul style="list-style-type: none"> • DOSTEL Particle Telescope – <i>HZE ion fluences and spectra</i> • PNTDs - <i>HZE ion fluences</i>

Table 2: NRPB's Track Etch Dosimeter Results

Flight Path	Neutron Dose Equivalent (μSv)	Non-neutron Dose Equivalent (μSv)	Total Dose Equivalent (μSv)
Northern Flight	104 ± 19	57 ± 2.3	161 ± 19
Southern Flight	19 ± 15	23 ± 1.7	42 ± 15
Easterly Flight	25 ± 10	15 ± 1.8	40 ± 10

Table 3: Boeing's (Dr. Chee) TEPC Results

Flight Path	Dose Equivalent Rate ($\mu\text{Sv/h}$)	Quality Factor
Ames (east/west)	12	2.2
Northern Flight (max)	30	2.5
Southern Flight (min)	4.8	1.75

Table 4: DREO's TEPC Results

Flight Path	Total Dose Equivalent (ICRP-60) for Neutrons (μSv)
Northern Flight	200
Southern Flight	75
Easterly Flight	115

Table 5: RMC's Bubble Detector Results

Flight Path	Total Dose Equivalent (ICRP-60) for Neutrons (μSv)	Dose Equivalent Rate for Neutrons ($\mu\text{Sv/h}$)
Northern Flight	59	7.4
Southern Flight	14	2.2
Easterly Flight	39	6.5

Table 6: Boeing's (Dr. Normand) PDM-303 Dosimeter Results

Flight Path	Raw PDM Reading (μSv)	Corrected PDM Dose Equivalent (μSv)
Northern Flight	570	114
Southern Flight	140	28
Easterly Flight	260	52

THE ATMOSPHERIC IONIZING RADIATION (AIR) PROJECT – PRELIMINARY RESULTS FOR NEUTRON SPECTRA AND IONIZATION RATE

P. Goldhagen¹, R. C. Singleterry Jr.², M. Reginatto¹, J. W. Wilson², H. Tai², W. Van Steveninck¹,
I. W. Jones², J. L. Shinn²

¹U.S. Department of Energy Environmental Measurements Laboratory, New York, NY 10014

²NASA Langley Research Center, Hampton, VA 23681

INTRODUCTION

Dose rates from galactic cosmic radiation at commercial aviation altitudes are such that crews working on present-day jet aircraft are a large occupationally exposed group with a relatively high average effective dose. Crews of future high-speed commercial aircraft flying at higher altitudes would be even more exposed. Present calculations of such exposures are uncertain because knowledge of important components of the radiation field, including neutrons, comes primarily from theoretical predictions. (The same is true for calculations of human exposures on the surface of Mars, which is at a similar atmospheric depth.) To help reduce these uncertainties for high-altitude flight, the NASA Langley Research Center (LaRC) and the U.S. Department of Energy Environmental Measurements Laboratory (EML) started the Atmospheric Ionizing Radiation (AIR) Project. The measurement part of the AIR Project is an international collaboration of 12 laboratories placing 14 instruments on multiple flights of a NASA ER-2 aircraft [1]. The AIR measurements will be used to benchmark and validate the LaRC AIR Model, a global computer model of the atmospheric cosmic radiation environment. An overview of the AIR Project will be presented separately at this Workshop by Robert Singleterry.

EML INSTRUMENTS AND RESULTS

The primary instruments for the AIR measurements are the EML multisphere neutron spectrometer and ionization chamber. These sensitive instruments record statistically significant readings each minute during flight, allowing correlation with altitude and latitude. Figure 1 shows graphs of the raw ionization chamber reading as a function of time after takeoff for the four 6½-hour ER-2 flights. Figure 2 shows a graph of the relative ionization chamber reading for the North 2 flight as a function of flight time along with the AIR Model prediction for the ionization rate in air. There is good agreement between the Model prediction and the relative measured values over a wide range of altitude and latitude. The EML multisphere neutron spectrometer uses heavy metal shells within the moderators of two of its 14 Bonner sphere detectors to enhance response at high energies (see Figure 3). A preliminary cosmic-ray neutron spectrum unfolded from measurements made on the North 2 flight is shown in Figure 4 along with a spectrum calculated by Armstrong *et al.* In addition to the large “evaporation” peak near 1 MeV, note the second peak near 100 MeV.

CONCLUSIONS

The current version of the AIR Model adequately predicts the measured relative ionization rate. We have measured full-range cosmic-ray neutron energy spectra at high altitudes. About half of the neutron dose equivalent is from neutrons with energies above 10 MeV. Nearby high-Z materials, such as iron, significantly increase secondary multiplicity and dose equivalent from high-energy neutrons and protons. Radiation exposures of astronauts on the surface of Mars will depend significantly on the atomic composition of Martian soil and the materials of their shelter. High-altitude radiation measurements such as those from the AIR project can be valuable in validating the radiation transport codes used to calculate exposures on the surface of Mars.

REFERENCE

1. Goldhagen, P. "Overview of Aircraft Radiation Exposure and Recent ER-2 Measurements," in NCRP Proceedings No. 20 *Cosmic Radiation Exposure of Airline Crews, Passengers and Astronauts* (National Council on Radiation Protection and Measurements, Bethesda, Maryland) in press.

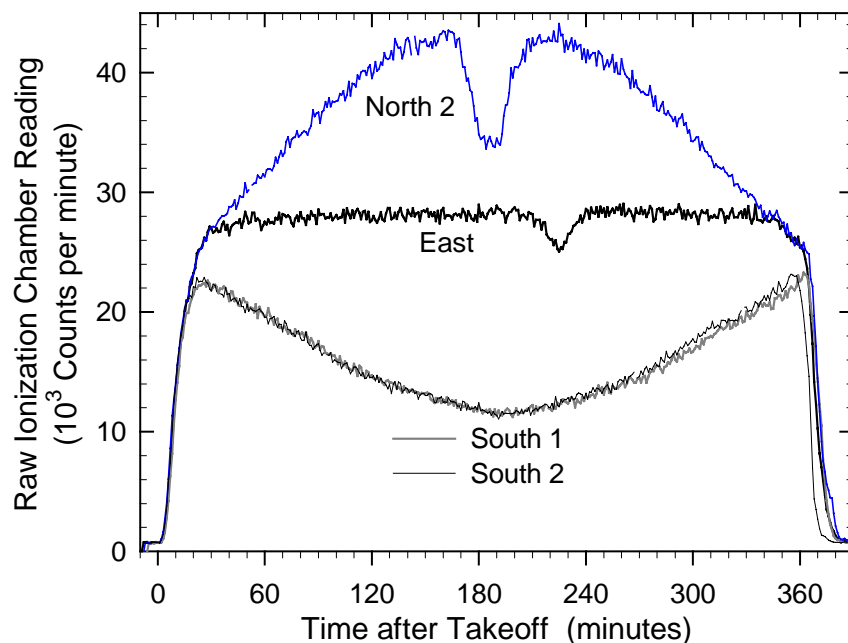


Figure 1. Ionization chamber reading as a function of time during the four 6.5-hour AIR ER-2 flights. The increase in ionization rate with latitude can be seen, as can the decrease during the altitude dips of the North 2 and East flights.

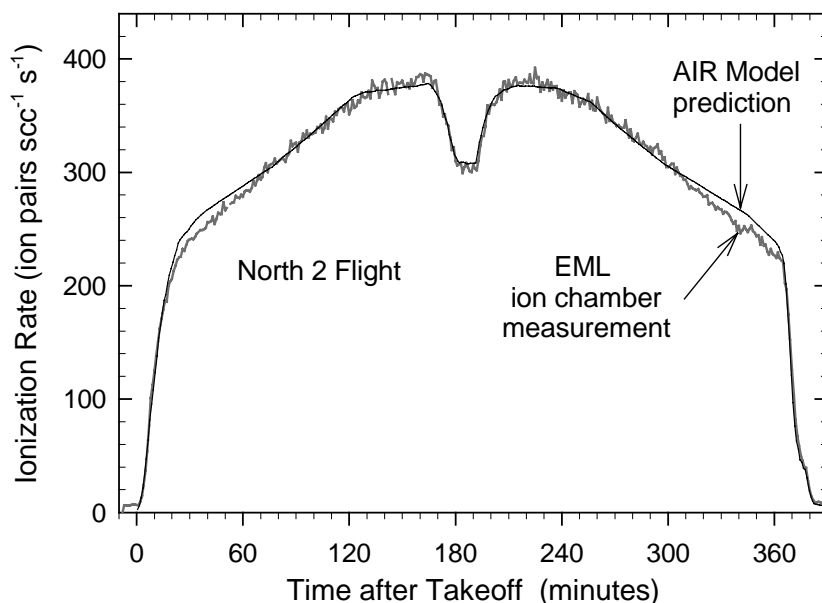


Figure 2. Comparison of the EML ionization chamber reading during the North 2 flight with the air ionization rate predicted by the LaRC AIR Model. The raw ionization chamber reading has been multiplied by a constant that gives good average agreement between the two curves for all the flights.

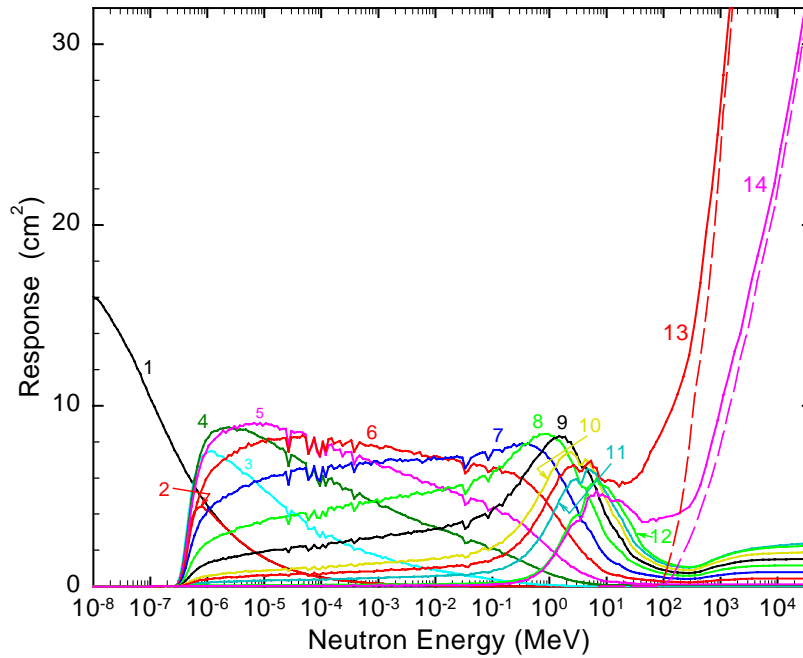


Figure 3. Preliminary calculated neutron response functions for each of the 14 detectors of the EML high-energy multisphere spectrometer (solid lines). The dashed lines show the proton response of the two detectors (number 13 and 14) with heavy metal (lead and steel) shells in their moderators.

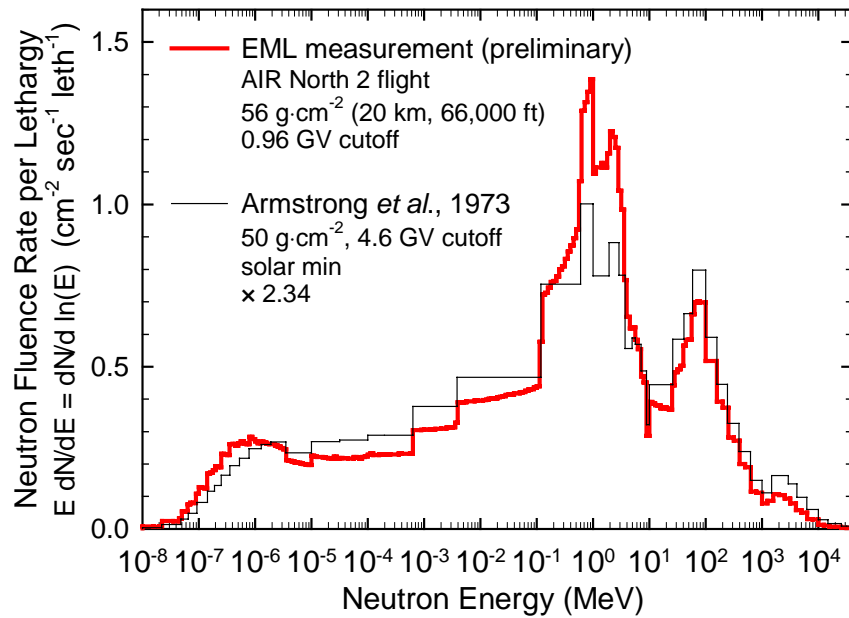


Figure 4. Preliminary cosmic-ray neutron spectrum measured on the North 2 flight and a calculated neutron spectrum from Armstrong *et al.* (1973). The Armstrong spectrum has been multiplied by 2.34 to compensate for the change in latitude and give the best fit to the EML data.

Tuesday, June 15

Brookhaven National Laboratory

1:30 p.m. – 2:30 p.m.

Posters IV

Berkner Rooms A & C

AN IMPROVED ALGORITHM FOR NEUTRON EXPOSURES

M. S. Cloudsley¹, J. H. Heinbockel¹, J. L. Shinn², R. C. Singleterry², R. K. Tripathi², J. W. Wilson²
¹ Old Dominion University, Norfolk, VA, ² NASA Langley Research Center, VA

INTRODUCTION

With the exception of mesons and their decay products the physical description of the radiation fields by the HZETRN code is now relatively complete. The evolution in code development is seen in figure 1 as computational procedures have been improved and new physical processes added over the last several years. The HZETRN code has been continually improved by testing with space and laboratory experiments and bench-marking for proton and neutron transport. Although exposure quantities, such as dose and dose equivalent, are well represented by the code, the low energy neutron spectra predicted by HZETRN are underestimated in the current version of the code. The reason for this underestimation is the presence of errors in the rescattering events which are so important in the slowing down process in low energy neutron transport. We describe a new algorithm for low energy neutron transport with improved low energy neutron spectra which includes rescattering events.

METHOD

We represent the secondary neutron production spectra in high energy particle collisions by Bertini's implementation of the two-step model including a direct reaction of two-body cascade particles and a second de-excitation process of evaporation particles. We represent the cascade particle transport by the HZETRN code and evaluate the evaporation processes as both a straight-ahead and isotropic distribution. The elastic collisional slowing down for the evaporation particles are represented in a multigroup treatment of the Boltzmann transport equation. Unlike the usual multigroup method used in reactor calculations where the neutron spectral properties are assumed in evaluation of the multigroup integrals we use the mean value theorem as a basis of evaluation. The mean values are chosen using a model calculation in which the Boltzmann equation is solved numerically and the material mean value points extracted to give agreement between the numerical and multigroup model problem solution. The multigroup method was coupled to the HZETRN code in both the straight-ahead and isotropic approximation to the evaporation source terms.

RESULTS

Referring to figure 2, the energy spectrum of neutrons generated within a 10 g/cm² depth in water was calculated for the Feb. 23, 1956 solar particle event using the original HZETRN code (dash), the HZETRN code without evaporation neutron contributions (dot-dash), the assumed straight-ahead source of neutrons in the multigroup method (solid), and the isotropic source distribution in the multigroup method (long dash). Also shown in the figure 2 are results from the LAHET Monte Carlo code for the same event. The LAHET code uses evaluated nuclear cross sections for the low energy neutron transport and the Bertini model for high energy interactions. In these HZETRN and multigroup calculations, the original cross sections of the old BRYNTRN code are used. One can see from the figure that the multigroup method greatly improves the neutron spectrum even in the straight-ahead approximation and even further

improves the neutron spectrum when the assumed isotropic source is used. The agreement is good at the higher energies and greatly improved at the low energies. It is expected that additional improvement will result if the low energy cross sections are updated. Toward this goal an improved nuclear database is now being constructed for which sample results are shown in figure 3. These cross sections are derived from the media-modifications of the nucleon-nucleon amplitudes and the quantum mechanically derived optical model.

CONCLUDING REMARKS

Estimates of exposures from galactic and solar cosmic rays continue to improve with more complete nuclear models and updated computational procedures. Exposure estimates for space travel behind aluminum shielding continue to increase in magnitude and indicate that to provide the necessary protection the vehicle will have to be heavier than originally thought or new materials and concepts will have to be developed. For example, only 2 g/cm^2 of aluminum was estimated by Letaw, compared with the latest estimates of 50 g/cm^2 for the soft spectrum of figure 1. This shielding requirement is impractical, and it is clear that new materials are needed which are more efficient in shielding against the hazards of galactic and solar cosmic rays. The improved estimates of the neutron exposures herein are not expected to change the results for Mars transit exposures but could be an important factor in that the backward propagating neutron component from the Martian regolith is expected to be intense on the Mars surface.

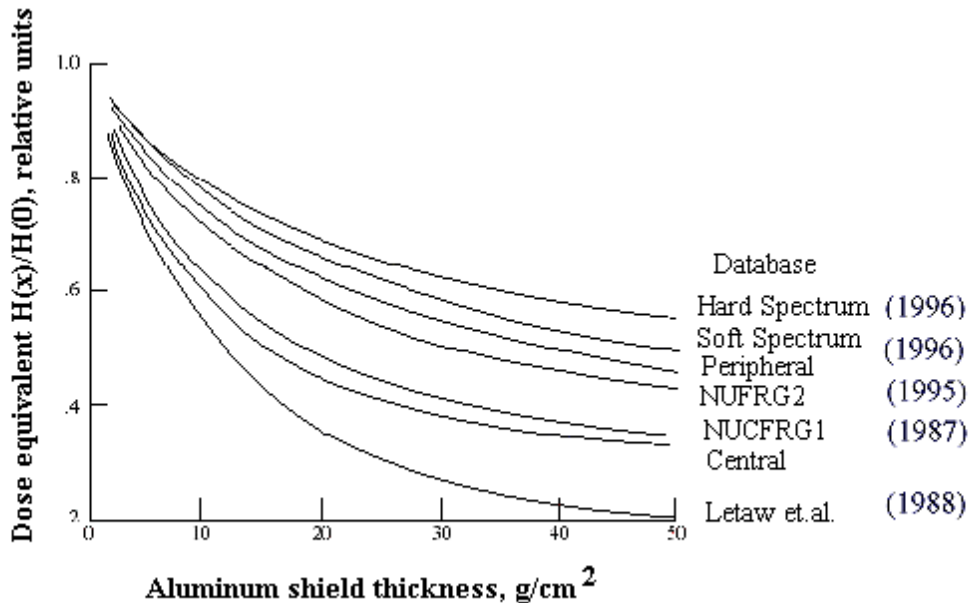


Figure 1. Shield attenuation for solar minimum galactic cosmic ray dose equivalent resulting from nuclear fragmentation models.

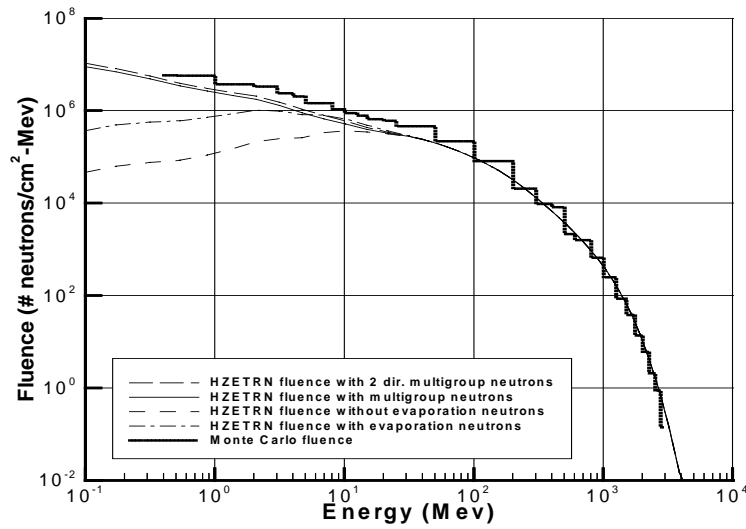


Figure 2. Energy spectra of neutron fluence at 10 g/cm^2 depth in water exposed to the February 23, 1956 solar particle event and calculated with the straight-ahead multigroup, two directional multigroup, and the HZETRN codes.

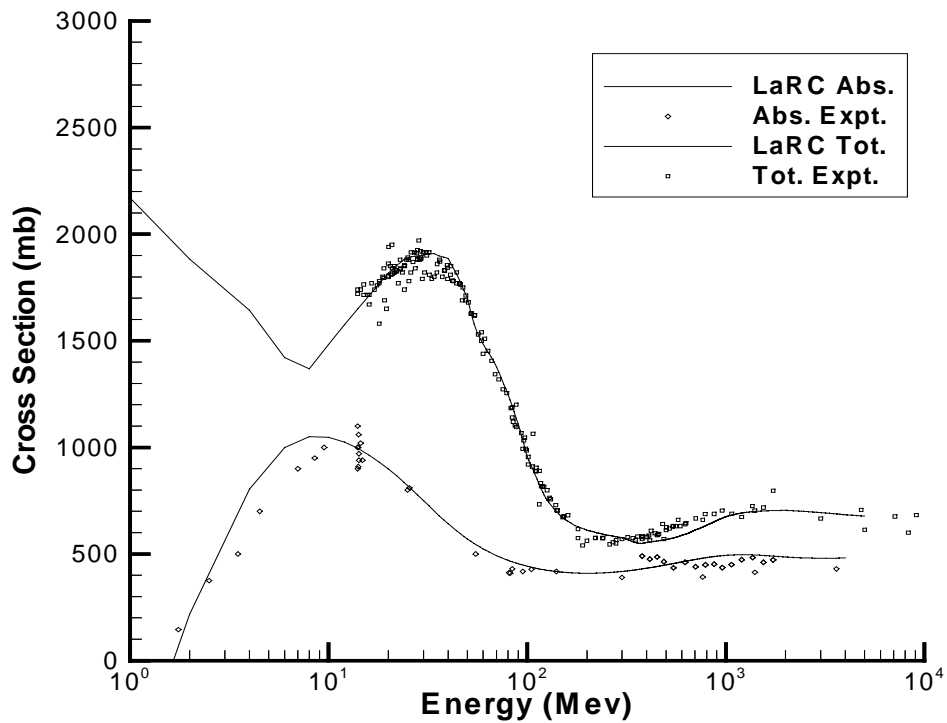


Figure 3. Aluminium cross sections as a function of neutron energy.

RECENT NEUTRON PRODUCTION MEASUREMENTS RELEVANT TO GCR TRANSPORT

L. Heilbronn¹, L. W. Townsend², R. S. Cary³, F. Deak⁴, K. Frankel¹, A. Galonsky⁵, K. Holabird⁶, A. Horvath⁴, A. Kiss⁴, J. Kruse⁵, R. M. Ronningen⁵, H. Schelin⁷, Z. Seres⁸, C. E. Stronach⁹, J. Wang⁵, P. Zecher⁵, and C. J. Zeitlin¹,

¹Lawrence Berkeley National Laboratory, Berkeley, CA; ²University of Tennessee, Knoxville, TN; ³Naval Surface Warfare Center, Dahlgren, VA; ⁴Eotvos University, Budapest, Hungary
⁵National Superconducting Cyclotron Laboratory, Michigan State University; ⁶Hughes Research, Los Angeles, CA; ⁷CEFET-PR Department of Physics, Curitiba-PR, Brazil; ⁸KFKI Research Institute, Budapest, Hungary; ⁹Virginia State University, Petersburg, VA

Neutrons are believed to contribute a significant fraction of the dose-equivalent in radiation environments encountered in the upper atmosphere, Earth orbit, and in deep space. A recent workshop [1] estimated that 30% to 60% of the dose equivalent on the International Space Station may come from neutrons, and a calculation [2] has estimated that close to 50% of the dose equivalent behind 50 gm/cm² of regolith shielding on a Martian base comes from neutrons. Because of the relatively short lifetime of the neutron, essentially all neutrons found in the environments mentioned above come from interactions of the primary GCR, SPE, and trapped radiation with shielding materials and human tissue. Neutron production cross section and thick-target yield measurements are needed to reduce uncertainties in model calculations which are applied to the problem of neutron production and transport in the upper atmosphere and in space. Thick-target yields from 155 MeV/nucleon ¹²C and ⁴He stopping in an aluminum target will be presented, along with comparisons to neutron yields from similar proton-induced interactions. Neutron production cross sections from 75 MeV/nucleon ¹²C + Al reactions will also be presented. Moving-source fits to the cross section data will be shown.

[1] "Predictions and Measurements of Secondary Neutrons in Space" Sept. 28-30, 1998, Houston, TX

[2] L. C. Simonsen, J. E. Nealy, L. W. Townsend, and J. W. Wilson, "Radiation Exposure for Manned Mars Surface Missions," Technical Paper 2979, National Aeronautics and Space Administration (1990).

SOLAR PARTICLE EVENT EXPOSURES AND LOCAL TISSUE ENVIRONMENTS IN FREE SPACE AND ON MARTIAN SURFACE

M. Y. Kim¹, J. L. Shinn², R. C. Singleterry², W. Atwell³, and J. W. Wilson²

¹College of William and Mary, ²NASA Langley Research Center, ³Boeing North American, Inc.

INTRODUCTION

Solar particle events (SPEs) are a concern to space missions outside Earth's geomagnetic field. The September 29, 1989 SPE is the largest ground-level event since February 23, 1956. It is an iron-rich event for which the spectra are well measured. Because ten times this event matches the ground level data of the February 1956 SPE, it is suggested that an event with ten-times the scaled spectra of the September 29, 1989 SPE be used as a worst case SPE for spacecraft design. For the worst case SPE, the input spectra were reconstructed using Nymmik's (1995) model for protons, the O and Fe ion spectra of Tylka *et al.* (1997) to evaluate the iron enhancement ratio, and the Solar Energetic Particle Baseline (SEPB) composition of McGuire *et al.* (1986) for the heavy ions. The necessary transport properties of the shielding materials and the astronaut's body tissues are evaluated using the HZETRN code. Three shield configurations (assumed to be aluminum) are considered: space suit taken as 0.3 g/cm², helmet/pressure vessel as 1 g/cm², and equipment room of 5 g/cm². A shelter is taken as 10 g/cm² on the Martian surface. The effect of shielding due to the Martian atmosphere is included. The astronaut geometry is taken from the computerized anatomical man (CAM) model.

FREE SPACE EXPOSURE

In free space, the hydrogen ions contribute to skin dose equivalent in a space suit over a wide energy range from 60 keV/amu to 45 MeV/amu as seen in Figure 1(a). Helium ions mainly contribute over the 0.3 to 10 MeV/amu range resulting from fragmentation of the aluminum shield nuclei. The Li to B ion group show significant contributions over the range 5 to 30 MeV/amu with heavier ions giving lesser contributions at higher energies (7 to 100 MeV/amu). The higher charge of the ion requires more energy to penetrate to the more protected sensitive tissues. The low-energy primary helium ions attenuate rapidly in shield materials. The helium ions from evaporation events in tissue nuclei dominate at larger shielded depths as seen in Figure 1(b). Note that the evaporation events in tissues cover a narrower energy range than those events in the aluminum shield. Heavier ions attenuate even more rapidly and contribute little to deep organ exposures. Protons and low energy helium ions are the main contributors in well-shielded areas as for the BFO in a space suit. The hydrogen and helium ions show similar broad energy contributions in the skin exposures with the helium result showing significant attenuation compared to the space suit exposures. The heavier ions are likewise reduced relative to the hydrogen contributions. Results for other body organs in various shield configurations are shown in Table 1. The total dose equivalent is significantly reduced in going from the space suit, to the pressure vessel, and to the equipment room. But, even a heavily shielded equipment room of a space vehicle does not provide sufficient shielding to satisfy the exposure limitation requirements of 25, 100, and 150 cSv for the BFO, ocular lens, and skin, respectively. This SPE may have dire consequences without a well-shielded region. A more heavily shielded region of a space vehicle is necessary to meet currently accepted limits.

MARTIAN SURFACE EXPOSURE

On the Martian surface, the contribution of heavier ions than helium is attenuated rapidly because of the shielding effect of Martian atmosphere and additional protection from the Martian surface. The evaporated helium ions and high-energy protons are dominant at the local sensitive tissues inside typical space suit and a lightly-shielded helmet shown in Figure 2. In these figures, the narrowing of the helium ion energy range is apparent. Dose equivalents of the organs in various shields are summarized in Table 2 for the worst case of SPE on Martian surface. For this SPE, shielding for the early response at skin and ocular lens is sufficient except at the BFO on the Martian surface. The 30-day exposure limits at the BFO are exceeded inside various shields except inside the shelter. According to the present estimates, the protection of the sensitive tissue of the BFO would be reached on Martian surface operations when adequate provision is made to seek the shelter in the case of this SPE.

CONCLUDING REMARKS

If the scaled September 29, 1989 event is a reasonable representation of the February 23, 1956 spectrum, then the design of adequate shielding for the Mars transfer will be an engineering challenge. In addition, careful attention also needs to be given to the evaluation of early radiation effects in micro-gravity and in the Martian gravity.

REFERENCES

- McGuire, R. E., T. T. von Rosenvinge, and F. B. McDonald, The Composition of Solar Energetic Particles, *Astrophys. J.*, 301, pp. 938-961 (1986).
 National Council on Radiation Protection and Measurements, in *Guidance on Radiation Received in Space Activities*, NCRP Report No. 98 (1989).
 Nymmik, R. A., Behavioural Features of Energy Spectra of Particles Fluences and Peak Fluxes in Solar Cosmic Rays, *Proc 24th Intern. Cosmic Ray Conf.*, 4, pp. 62-64 (1995).
 Tylka, A. J., W. F. Dietrich, and P. R. Boberg, High-Energy Solar Heavy Ions from IMP-8, *Proc. 25th Intern. Cosmic Ray Conf.*, 1, 101 (1997).

Table 1. Dose equivalent from the worst case SPE in free space (in cSv)

	Skin			Ocular lens			BFO		
Charge	Space suit	Pressure vessel	Equipment room	Space suit	Pressure vessel	Equipment room	Space suit	Pressure vessel	Equipment room
Z=1	17,380	5,540	577	6,680	3,180	501	378	314	168
Z=2	11,490	820	66	1,330	330	49	40	35	24
$3 \leq Z \leq 10$	530	50	2	90	20	2	1	1	< 1
$11 \leq Z \leq 20$	90	20	1	20	10	1	1	1	< 1
$21 \leq Z \leq 28$	20	10	2	10	10	1	1	1	< 1
Total	29,510	6,440	648	8,130	3,550	554	421	352	193
NCRP 30-day limit	150			100			25		

Table 2. Dose equivalent from the worst case SPE on Martian surface (in cSv)

	Skin	Ocular lens	BFO
Space suit	45	44	32
Helmet/Pressure vessel	44	42	31
Equipment room	38	37	28
Shelter	33	32	25

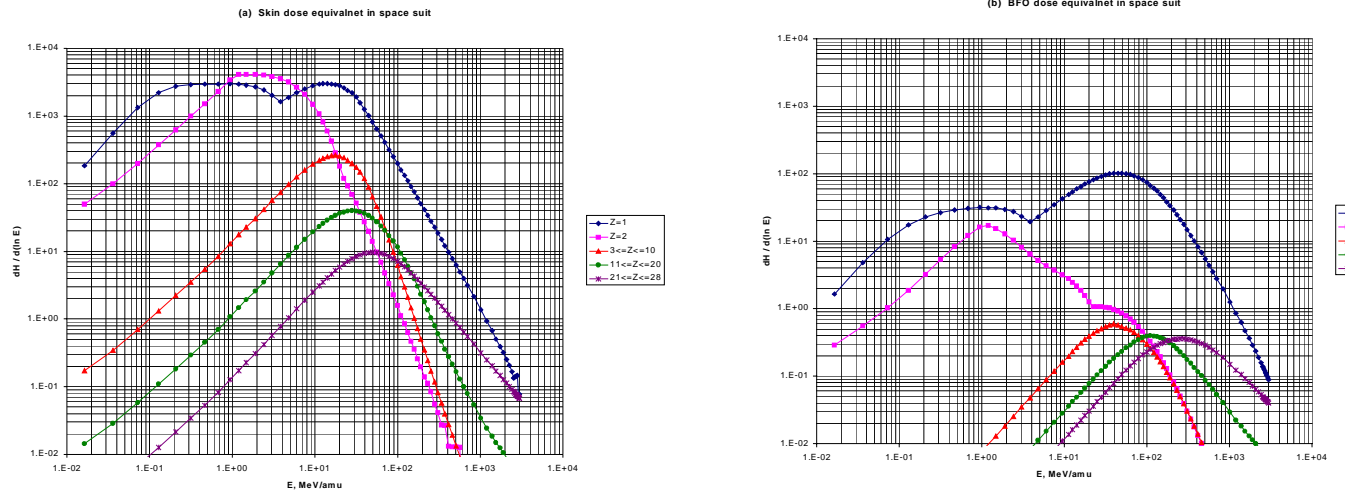


Figure 1. Dose equivalent from the worst case SPE exposure in free space.

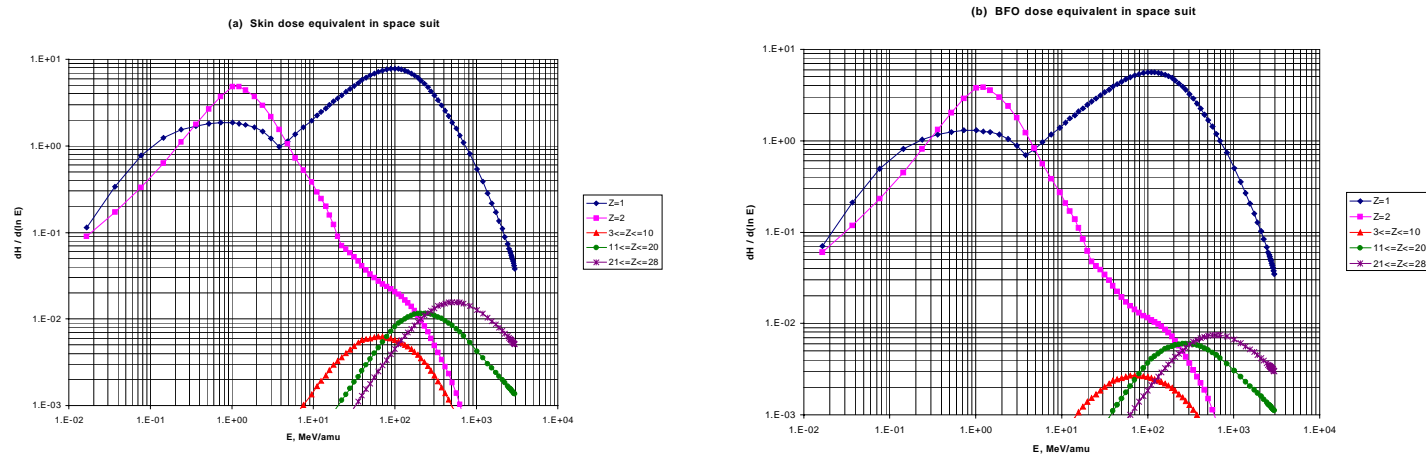


Figure 2. Dose equivalent from the worst case SPE exposure on Martian surface.

A COMPARISON OF DEPTH DEPENDENCE OF DOSE AND LINEAR ENERGY TRANSFER SPECTRA IN ALUMINUM AND POLYETHYLENE

Gautam D. Badhwar and Francis A. Cucinotta
NASA Johnson Space Center, Houston, Texas 77058-3696

A set of four tissue equivalent proportional counters (TEPCs), with their detector heads embedded at the centers of 0 (bare), 3, 7, and 9-inch-diameter aluminum spheres, were flown on the Shuttle flight STS-89 (inclination 51.65° , altitude ~ 400 km). Five such detectors, embedded at the centers of 0(bare), 3, 5, 8, and 12-inch-diameter polyethylene spheres were flown earlier on STS-81 (inclination 51.65° , altitude ~ 400 km). The data obtained from each of the TEPCs were separated into contributions from the trapped protons and galactic cosmic radiation (GCR). From the measured linear energy transfer (LET) spectra, the absorbed dose, and dose-equivalent rates were calculated. The results of dose-depth dependence for the two material were compared, and convincingly show the merits of using material rich in hydrogen to decrease the radiation exposure. The results were compared to radiation transport model HZETRN/NUCFRG2. The model predicts the observed GCR absorbed dose rate with a percentage root mean square error (rmse) of 12.5%, and dose equivalent rate with rmse of 8.2%. The maximum deviation is about 25%. Although these results for dose and dose equivalent rates are reasonable, there are systematic differences in the LET spectra with increasing shielding thickness, and shapes of the dose-depth curves, with fluxes at fixed LET differing by factor of ~ 3 . Similar comparison for trapped protons using the proton transport code BRYNTRN, and the AP-8 MIN trapped-proton model, show that the model breaks down with increasing shielding thickness also, and that there is a systematic bias, with the model under predicting dose and dose equivalents rates. These results point to the need for additional improvements in the radiation transport model. These results suggest that even now, with Space Station construction already started, one should consider using about 5 cm thick hydrogen rich material in the crew sleeping area, and certainly use hydrogen rich materials for Mars mission spacecrafts.

NUCLEAR FRAGMENTATION OF LIGHT IONS

J. Miller¹, A. Fukumura², L. Heilbronn¹, T. Murakami² and C. J. Zeitlin¹

¹Lawrence Berkeley National Laboratory, Berkeley, California

²National Institute of Radiological Sciences, Chiba, Japan

Data on the fragmentation of light ions are needed to extend the nuclear fragmentation data base used by heavy ion transport models and to study the behavior of light nuclei, which are prominent in both the primary galactic cosmic radiation and in the secondary radiation produced by the interactions of primary ions in matter. We have measured fragment production near the beam axis for carbon, neon, oxygen and silicon ions at energies between 290 and 600 MeV/nucleon. Targets included polyethylene, graphite, aluminum, copper, lead, tin and tantalum. Charged fragments are identified by their energy loss in a stack of silicon detectors augmented by plastic scintillators and a thick sodium iodide detector. From the data we have extracted partial and total charge changing cross sections and the angle dependence of fragment yields and absorbed dose between 0 and 10 degrees. With the exception of protons, the absorbed dose is dominated at each fragment charge by the fragments produced along the beam axis, indicating that at least in this case it is reasonable to assume that the bulk of the dose, even after fragmentation, will be concentrated in the forward direction. The measured total charge changing cross sections for several projectile-target systems have been compared to calculations using the NUCFRG2 fragmentation model [1], and agreement between the measurements and the model is generally good. However, even small uncertainties in model predictions may translate into large increases in mission costs, if the resulting uncertainty in biological effect dictates increased shielding.

[1] J.W. Wilson, J.L. Shinn, L.W. Townsend, R.K. Tripathi, F.F. Badavi and S.Y. Chun, NUCFRG2: A semiempirical nuclear fragmentation model. *Nucl. Instr. and Meth. B* 94 95, (1994).

CURRENT STATUS AND NEW DEVELOPMENTS IN THE USE OF THREE-DIMENSIONAL COMPUTER OPTICAL MEMORIES FOR RADIATION DOSIMETRY*

M. Moscovitch^(a), G. W. Phillips^(b), A. K. Readshaw^(a), G. O. Brown^(a), R. G. Weiss^(a), N. A. Guardala^(c), J. L. Price^(c), S. C. Mueller^(a), D. Emfietzoglou^(a), J. Mobley^(d), J.S.Bogard^(d), and T. Vo-Dinh^(d)

^aGeorgetown University, Washington, DC 20007; ^bUS Naval Research Laboratory, Washington, DC 20375; ^cNaval Surface Warfare Center, West Bethesda, MD 20817; ^dOak Ridge National Laboratory, Oak Ridge, TN 37831

The exotic radiation environments that are present during space flight pose a unique personnel dosimetry problem. These radiation fields contain a variety of high energy high atomic number particles (HZE) having a broad energy spectrum. Since the biological effects of HZE particles depend on both the particle type and the energy spectrum, providing adequate dosimetry to crew members requires the measurement of both these variables.

Three-dimensional optical random access memories (3-D ORAM) have been proposed for use as a radiation dosimeter and spectrometer for neutrons or heavy-charged-particles⁽¹⁻³⁾. 3-D ORAM make use of bistable photosensitive materials for storage of large volumes of computer data. A typical 3-D ORAM element is composed of a photochromic molecule such as spiropyrans (SP) embedded in a poly (methyl methacrylate) (PMMA) matrix. The SP molecule can exist as two distinct geometrical forms (i) spiropyran and (ii) merocyanine. Information is stored or read at the intersection of two laser beams using two-photon absorption to convert the SP molecule from one isomeric form to the other. Theoretical calculations show that neutrons and heavy charged particle radiation is capable of altering the information stored on 3-D ORAM, enabling it to function as a radiation dosimeter^(4,5). We have recently conducted the first experimental study to determine the effects of ionizing radiation on 3-D ORAM materials^(6,7). The results show that the properties of these materials are promising for space dosimetry since the energy and the dose can both be determined from the radiation response of the 3-D ORAM element. Initial design of a 3-D ORAM reader is currently underway at Oak Ridge National Laboratory⁽⁸⁾.

REFERENCES

1. Moscovitch M., U. S. Patent No. 5,319,210 (1994).
2. Moscovitch M., *Health Phys.* **66**, S13 (1994).
3. Moscovitch M., U.S. Patent No. 5,498,876 (1996).
4. Moscovitch M. and Emfietzoglou E., *J. Appl. Phys.* **81**, 58-69 (1997).
5. Emfietzoglou E and Moscovitch M., *Phys Med. Biol.*, **44**, 207-221(1999).
6. Phillips G.W., Readshaw A. K., Brown G.O., Weiss R.G., Guardala N.A., Price J.L., Mueller C.M. and Moscovitch M., *Appl. Radiat. Isot.*, **50**, 875-881(1999).
7. Readshaw A.K., Phillips G.W., Brown G.O., Weiss R.G., Guardala N.A., Price J.L., Mueller C.M. and Moscovitch M., *Radiat. Protect. Dosim.* (1999 in press).
8. Mobley J., Bogard J.S., Moscovitch M. and Vo-Dinh T., *SPIE*, Vol. **3534** (1999 in press).

*This work was supported by: NASA (MM, DE and AKR), The US Department of Energy NN-20 program (MM, GWP, NAG, JLP, JM, JSB and TVD), the US Department of Energy Health Physics Faculty Research Award Program (MM and DE), the National Science Foundation(RGW and GOB), Georgetown University President Rev. Leo O'Donovan (MM, SCM and AKR), the Naval Research Laboratory Advanced Graduate Research Program (GWP).

ESTIMATES OF CREW DOSE RATES FOR THE AUGUST 1972 SOLAR PARTICLE EVENT: A HIGH DOSE RATE EVENT

J. L. Parsons and L. W. Townsend

Department of Nuclear Engineering, The University of Tennessee, Knoxville, Tennessee 37996-2300

INTRODUCTION

Risks to crews of future interplanetary missions from exposures to large solar particle events (SPE) are a function of the total dose and the dose rate received during the events. Previous estimates of absorbed doses from the large events of August 1972 and October 1989 indicate that values in excess of 10 Gy are possible for crew members only protected by a spacesuit or thinly-shielded spacecraft. Current thinking, based upon an earlier analysis of the October 1989 event, is that dose rates from SPEs are expected to be low, even when the total absorbed dose is large. Recent estimates of dose rates from events that occurred between 1986 and 1993 suggest that dose rates from large SPEs are “low-dose rate” events, as defined by various advisory bodies (NCRP, ICRP, UNSCEAR). In this work, we present an analysis of the organ dose rates for the large SPE of August 1972. The calculations of absorbed doses and dose rates are made using the BRYNTRN space radiation transport computer code and the CAM model.

METHODS

The hourly proton fluence values for the August 1972 event are parameterized using an exponential rigidity function. These incident, energetic proton spectra and their reaction products (protons, neutrons, ^2H , ^3H , ^3He and ^4He) are transported through the aluminum shield material (1, 2 and 5 g/cm²) and then through an additional 100 cm of water (assumed to be equivalent to soft tissue) using the BRYNTRN computer code. The calculated absorbed doses versus depth, at each time, are then folded with the CAM model body organ self-shielding distributions to yield dose estimates for each organ. Using these computational tools and methods, profiles of organ doses versus time are generated for the skin, ocular lens and bone marrow behind each thickness of aluminum shielding considered herein (1, 2 and 5 g/cm²). Although the profiles vary in magnitude for each organ and shield thickness, they are all well-represented by a Weibull functional form

$$D(t) = D_{\infty} \{1 - \exp[-(\alpha t)^{\gamma}]\}$$

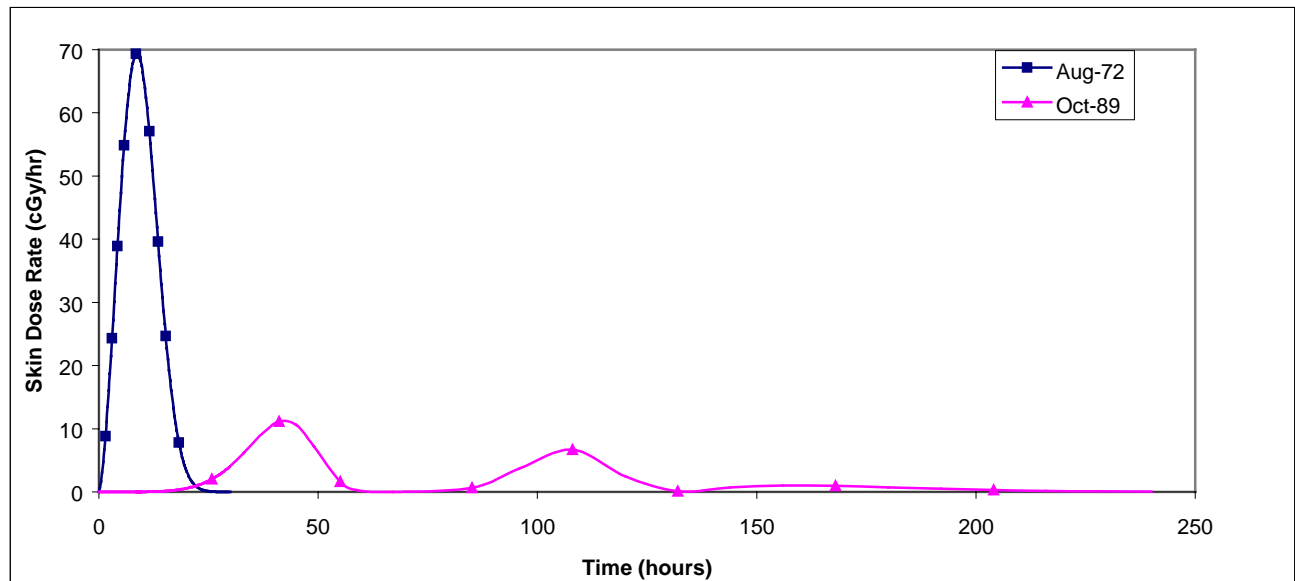
where $D(t)$ represents the organ dose at time t (time since protons began arriving), D_{∞} is the organ total absorbed dose for the event, and γ and α are fitting parameters. Once the organ dose-time profiles are parameterized they are differentiated in time to yield smoothed, continuous dose rate curves of the form

$$R(t) = D_{\infty} \alpha^{\gamma} \gamma t^{\gamma-1} \exp[-(\alpha t)^{\gamma}]$$

RESULTS

Organ absorbed dose rates behind 1, 2 and 5 g/cm² aluminum shielding are estimated. The shielding thickness (areal density) of 1 g/cm² is representative of the protection provided by a typical spacesuit and 5 g/cm² is typical of shielding provided by a manned spacecraft. Values for

2 g/cm² of aluminum shielding are estimated to facilitate comparison between our predicted dose rates and those estimated previously for the October 1989 SPE. The figure displays the skin dose rate estimates for 2 g/cm² shielding for the August 1972 and October 1989 SPEs. Note that the 1972 dose rates are much larger. Results for the skin, ocular lens and bone marrow dose rates will be available at presentation.



CONCLUSION

The organ dose rates for the August 1972 solar particle event are much higher than those estimated for any of the events that occurred in 1986-1993. The August 1972 dose rates are not low dose rates as defined by UNSCEAR, ICRP or NCRP.

OBSERVING SOLAR PARTICLE EVENTS

Dr. Ron Turner

ANSER, 1215 Jefferson Davis Hwy, Arlington, VA 22202

NASA Grant NAG5-3888

The natural radiation from steady, low-flux galactic cosmic rays (GCR) and infrequent, high-flux solar particle events (SPEs) may pose a serious health risk to humans on the International Space Station and during missions to Mars or the Moon. The flux of protons with energy greater than ten MeV may increase over background by four to five orders of magnitude for a period of several hours to a few days during these events. The frequency of large events varies with the solar cycle. There may be ten to twenty significant events within a ten-year period. Of these, none to four may be large enough to pose substantial risk to an astronaut.

The total radiation dose to an inadequately shielded astronaut (in a thin-skinned spacecraft or engaged in extravehicular activity, or space walks, for example) may be large enough to cause acute effects such as radiation sickness or nausea. Even under modest shielding, the radiation dose from an SPE may contribute to cataract induction and an increased risk of cancer later in the astronaut's life. For further discussion of the radiation hazards, see the National Research Council Space Studies Board report, *Radiation Hazards to Crews of Interplanetary Missions* (1996).

The first two reports of this series covered the underlying physics of SPEs (Turner, 1996) and the methods used today to forecast SPEs (Turner, 1997). This report describes the various components of a system, or architecture, that may be employed to produce the data needed for SPE and SPE-precursor observations. The fourth and final installment of the series will discuss various ways to combine these elements to support a comprehensive SPE risk mitigation strategy for a return to the Moon or for future human missions to Mars.

This report is divided into the following areas (see Figure 1.1): solar monitoring (what is going on at the Sun to observe activity that may lead to an SPE); heliospheric monitoring (what is the state of the solar wind, interplanetary magnetic field, and fluctuations in the nominal solar wind to be able to predict the propagation of accelerated protons from the source to the astronauts); and energetic particle monitoring (what is the solar proton and ion flux in the region near the astronauts). In each section, representative instruments are described, including the role they may play, their heritage, strengths, and limitations. Finally, there is a section on communications and data fusion concerns which discusses what means are available to get the right data to the right place in a useful format.

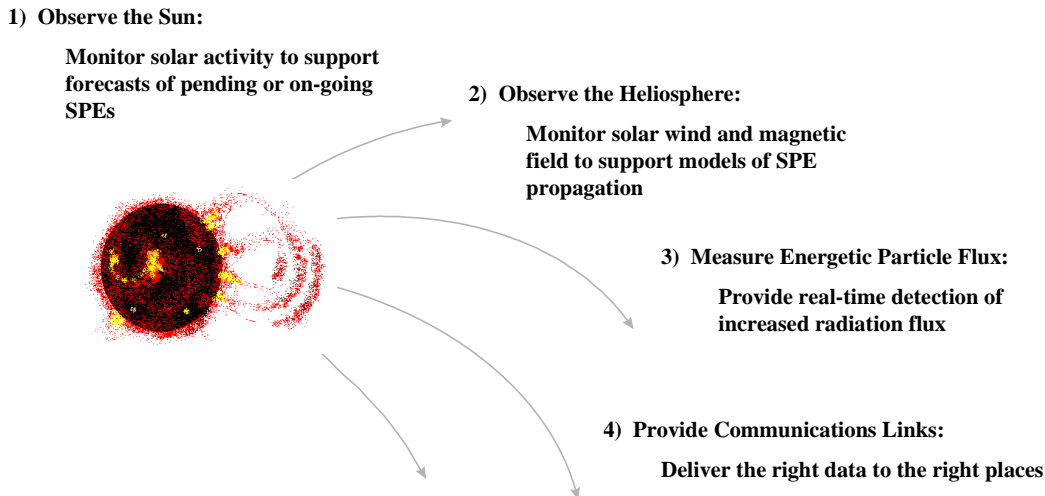


Figure 1.1. Functions to be performed by an SPE Risk Mitigation Architecture

Solar monitoring is required to place the forecasts and observations of SPEs into a context of ongoing and potential solar activity. Near-real time observations of solar active regions and emerging Coronal Mass Ejections (CMEs) may provide data useful to project the progress of an SPE over a period of hours to days. Additional progress in understanding the physics of CMEs may lead to a multiday forecast of the probability of an SPE. A variety of instruments are needed to support these tasks, from solar surface imagers (observing the Sun in visible, ultraviolet, X-ray, and radio wavelengths) to near-Sun solar coronagraphs. There is an extensive suite of research spacecraft and ground-based facilities providing experience and proof of concept from which we will be able to select the appropriate operational instruments for an SPE risk mitigation architecture.

Heliospheric observations provide information necessary to model or monitor the propagation of solar energetic particles from the source to the astronauts. Density fluctuations from solar emissions and from boundaries between slow and fast solar wind streams affect the shape of the interplanetary magnetic field, along which the energetic particles move. They also affect the strength, structure, and motion of CMEs and the associated shocks that accelerate the energetic particles. The data that may be necessary for SPE propagation models include information on the general state of the solar wind plasma, the interplanetary magnetic field, and local disturbances moving through the inner heliosphere. Both *in situ* and remote sensing methods may contribute to the characterization of the heliosphere. The *in situ* instruments are typically small, low-cost sensors with long heritage. Remote sensing techniques include scattered zodiacal light observations of interplanetary mass density fluctuations and recently implemented observations of interplanetary radio signals that may provide a measure of CME shock speed.

Direct measurements of *in situ* solar energetic particles will continue to provide the most important contributions to an SPE risk management strategy. Measurements at the astronauts' location will be able to confirm that a solar particle event is underway and to provide information about the flux, rate-of-change of flux, and total fluence of the event. In addition, instruments may be needed to measure the relative contribution to the total flux from particles with different energies, from ten MeV through several hundred MeV. Finally, it may be necessary to identify

the flux of high energy, high mass ions that make up an on-going SPE. Additional energetic particle measurements at locations significantly away from the astronauts may also contribute to forecasting the evolution of an on-going event. A variety of instruments are available to provide these measurements, including particle telescopes, solid state detectors, and proportional counters.

The natural radiation measured outside a spacecraft generates a shower of secondary particles as it is slowed (and possibly stopped) by shielding surrounding an astronaut. The total radiation exposure to the astronaut is a combination of this secondary radiation and the surviving natural radiation. The complexity of shielding, uncertainties in the flux, and the need to know the crew exposure as well as possible may require real time dose and dose rate measurements to substantiate or replace the modeled dose estimates and projections based on measures and forecasts of the external environment. Options including the traditional “film-badges,” tissue-equivalent proportional counters, solid state detectors, and possible biodosimetry techniques are briefly discussed.

The communication infrastructure is an important factor to consider in the construction of a total SPE warning system for two main reasons: cost and timeliness. Some of the elements of an SPE architecture may be located far from Earth. Trade-offs are needed to allocate the costs of potentially high data rate transmissions between the sender and the receiver. On a Mars mission, the communication to the astronauts will take up to 20 minutes to arrive from Earth. Since the highest energy particles move with speeds close to the speed of light, techniques are needed to ensure that warnings and support are provided in a timely fashion.

Tuesday, June 15

Brookhaven National Laboratory

2:30 p.m. – 3:10 p.m.

Program Reviews

Berkner Hall

PROGRESS IN HEAVY ION RESEARCHES WITH HIMAC

Kazunobu Fujitaka

Space Radiation Laboratory, National Institute of Radiological Sciences, Japan

Heavy ion research programs in Japan have progressed since the start of HIMAC operation in 1993. Since then about 500 cancer patients have been treated with carbon ions, and similar facilities are planned to be built in three local prefectures in future.

As was introduced in 9th Workshop in Loma Linda University, HIMAC is potentially a good cosmic ray simulator for researches on radiation effects on materials, detectors and organisms. It can provide ions from hydrogen to xenon of which energy spans 100-800 MeV/u covering significant energy region for human body.

Recent achievements by HIMAC beam include the development of a neutron monitor for the use in space. As dose control of astronauts will be done by effective dose (or effective dose equivalent), we need to know individual dose due to single radiation component as the Sv/Gy conversion factor depends on particle characteristics. However, neutron measurements in space are not easy because space is a mixed field of neutrons and protons. One of the devices to overcome this is a phoswich detector composed of two scintillators of different light-decay nature. The detector has been tested with carbon beam of 100 MeV/u from HIMAC, and it demonstrated that the detector could distinguish the two components satisfactorily while it failed when applied to 290 MeV/u beam. Data will be shown at the meeting.

Another test being conducted with HIMAC is the long term irradiation of biological samples at low dose rate. The method is tricky as that an incubator is placed at a point which is out of beam-axis so that the samples are irradiated at low dose rate, nearly 1 mSv/day, which approximates cosmic ray dose rate. The incubator accommodates cultivated human cells, and mutation rates and survival rates are examined once a week for hundreds days. However, ion composition and energy are not reasonably approximated because the main beam is composed of carbon ions of 290 MeV/u in daytime in weekdays for patient treatment, while it is composed of other ion species of different energy and/or dose rates in remainder time. Such is not exact, but smart way to simulate space radiation roughly without interrupting hospital uses. Analyses of these experiments are in progress.

LOMA LINDA UNIVERSITY RADIOBIOLOGY PROGRAM STATUS REPORT

G.A. Nelson, J.O. Archambeau, L.M. Green, D.S. Gridley, M.M. Moyers & J.M. Slater

The Loma Linda University Radiobiology Program continued to grow and develop along several paths. Infrastructure improvements added to the capability to simulate space radiation environments and to carry out high precision biological and physical investigations with proton beams. LLU staff development and research projects are maturing and joint ventures with visiting scientists have begun in earnest. A collaborative research initiative aimed at several National Research Council high priority goals has been launched and proton services have been provided for biological & physical investigations as well as space flight hardware performance validation.

Infrastructure Development

The NASA beamline continues to be upgraded to provide irradiation conditions more closely matched to space flight environments. Beam spot sizes have been increased to 52 cm with accompanying reductions in dose rate to permit longer term exposures at dose rates in the ≤ 1 cGy/min range for biological research. Low fluence beam monitors and automated control system improvements are directing growth towards the capability for chronic low dose rate irradiation schedules with improved environmental control of biological specimens including rodents. Microdosimetric and nanodosimetric characterizations of proton beam dose composition are also being conducted.

Improvements to supporting laboratories are underway to enhance animal care, gamma radiation controls, hematology and cell biological analysis. Additional microflow caging systems boost the housing available in the animal care facility and a low dose rate gamma source complements a clinical ^{60}Co irradiator. An automated veterinary blood analyzer is available and a full time flow cytometrist is now on staff who can provide service to outside users for analysis of cells in suspension or in microscope slide format.

Service to Extramural Community

Beam services have been provided to several outside user groups. The NSBRI rat tumorigenesis project has had the most challenging proton beam requirements while University of California at Riverside and San Diego scientists were the newest users. The most notable space flight hardware to be tested was the Human Research Facility Ultrasound unit scheduled for International Space Station. Numerous inquiries were received to arrange future beam time support for studies awaiting funding under the annual Life Sciences Division NRA

Education Activities

Seminars on several topics related to charged particle radiobiology were delivered to the LLU community and were incorporated into the training of radiation medicine residents. Andrew Grosovsky (U.C. Riverside) and Munira Kadhim (MRC Harwell) discussed genomic instability. Gail Woloschak (Argonne National Laboratory) reported on radiation-induced gene expression while Jamie Milligan (U.C. San Diego) discussed clustered damage to DNA and Bernard Rabin (U. Maryland) presented studies on behavioral consequences of radiation exposure.

The summer and fall of 1999 will see the first extended research activities by outside visitors when Robert Pearlstein of Duke University and Munira Kadhim of MRC Harwell utilize the visitors' laboratory to conduct proton studies on transgenic mice showing accelerated aging of the central nervous system and genomic instability in hematopoietic stem cells respectively.

The LLU radiation medicine resident program has recently been extended from a three year to a four year program which includes 1 year of laboratory experience. Beginning in the summer of 1999 two LLU residents will begin their research projects along with resident S. Gordon from U.C.L.A. One Ph.D. student (J. Li), one M.D./Ph.D. student (D. Kim) and two M.S. students (D. Tran & E. Kajioka) are currently working towards degrees from LLU while two M.D. / Ph.D. students are doing laboratory rotations. Postdoctoral fellow N. Moire will complete her one year program this summer while fellow M. Pecaut began a two-year research project in January.

Individual Scientific Projects

Radiobiological studies using protons are being conducted on several topics by LLU staff and students. Individual project topics include induced gene expression in *C. elegans* and rat thyroid cells, immune system responses to radiation in mice, combined treatment of experimental tumors with recombinant TNF-alpha and radiation, remodeling & functional changes in rat thyroid and retinal tissues and the role of cell communication in controlling cellular responses to radiation. Results from two of these areas of investigation will be presented in other abstracts from this meeting.

Mouse Proton Irradiation Project

NASA advisory committees have identified charged particle-induced tumorigenesis and adverse changes to central nervous system and immune system as high priority issues for the Space Radiation Health Program. The NSBRI radiation project is addressing the tumorigenesis issue and the feasibility of radioprotectants with the Sprague-Dawley rat model. LLU has initiated a complementary project using a mouse model to address charged particle-induced tumorigenesis, immune function and behavioral alterations in an integrated investigation. Together these studies should provide critical data on charged particle radiation carcinogenesis and interspecies extrapolation on an accelerated schedule. The draft mouse study design was reviewed by a NASA-organized advisory panel that also critiqued the NSBRI project. Recommendations have been incorporated into the mouse project which is being led by LLU with collaborative investigations by extramural scientists. The integrated study design and objectives will be presented along with preliminary results from pilot investigations.

Wednesday, June 16

Brookhaven National Laboratory

8:30 a.m. – 9:30 a.m.

Tracy Chiu-hsu Yang Lecture

Dr. John Little

Harvard University

**“Cellular Mechanisms of Response
to High LET Radiation”**

Berkner Hall

Wednesday, June 16

Brookhaven National Laboratory

9:45 a.m. – 10:45 a.m.

CNS

Berkner Hall

GCR TRANSPORT IN THE BRAIN: ASSESSMENT OF SELF-SHIELDING, COLUMNAR DAMAGE, AND NUCLEAR REACTIONS ON CELL INACTIVATION RATES

M.R. Shavers^{1,*}, W. Atwell², F. A. Cucinotta³,

¹Baylor College of Medicine, One Baylor Plaza Houston, TX 77030-3498; ²Boeing North American, 555 Gemini Houston 77058; ³NASA Johnson Space Center, Houston, TX 77058

Radiation shield design is driven by the need to limit radiation risks while optimizing risk reduction with launch mass/expense penalties. Both limitation and optimization objectives require the development of accurate and complete means for evaluating the effectiveness of various shield materials (Wilson *et al.* 1995) and body-self shielding. For galactic cosmic rays (GCR), biophysical response models indicate that track structure effects lead to substantially different assessments of shielding effectiveness relative to assessments based on LET-dependent quality factors. Methods for assessing risk to the central nervous system (CNS) from heavy ions are poorly understood at this time (NRC, 1996). High-energy and charge (HZE) ion can produce tissue events resulting in damage to clusters of cells in a columnar fashion, especially for stopping heavy ions (Todd *et al.*, 1973). Grahn (1973) and Todd (1986) have discussed a microlesion concept or model of stochastic tissue events in analyzing damage from HZE's. Some tissues, including the CNS, maybe sensitive to microlesion's or stochastic tissue events in a manner not illuminated by either conventional dosimetry or fluence-based risk factors. HZE ions may also produce important lateral damage to adjacent cells (Cucinotta *et al.*, 1998a).

Fluences of high-energy proton and alpha particles in the GCR are many times higher than HZE ions. Behind spacecraft and body self-shielding, the ratio of protons, alpha particles, and neutrons to HZE ions increases several-fold from free-space values. Models of GCR damage behind shielding have placed large concern on the role of target fragments (Cucinotta *et al.* 1991; Wilson *et al.* 1991; Dicello, 1992; Shavers 1996). The self-shielding of the brain reduces the number of heavy ions reaching the interior regions by a large amount and the remaining light particle environment (protons, neutrons, deuterons, and alpha particles) may be the greatest concern. Tracks of high-energy proton produce nuclear reactions in tissue which can deposit doses of more than 1 Gy within 5-10 cell layers. Information on rates of cell killing from GCR, including patterns of cell killing from single particle tracks, can provide useful information on expected differences between proton and HZE tracks, and clinical experiences with photon irradiation. To model effects on cells in the brain, it is important that transport models accurately describe changes in the GCR due to interactions in the cranium and proximate tissues.

We describe calculations of the attenuated GCR particle fluxes at three dose-points in the brain and associated patterns of cell killing using biophysical models. The effects of the brain self-shielding and bone-tissue interface of the skull in modulating the GCR environment are considered. For each brain dose-point, the mass distribution in the surrounding 4π solid angle is characterized using the CAM model to trace 512 rays (Billings and Yucker 1973). The CAM model describes the self-shielding by converting the tissue distribution to mass-equivalent aluminum (Atwell 1994), and nominal values of spacecraft shielding is considered. Particle transport is performed with the proton, neutron, and heavy-ion transport code HZETRN (Wilson 1991) with the nuclear fragmentation model QMSFRG (Cucinotta *et al.* 1998b). The distribution

of cells killed along the path of individual GCR ions is modeled using *in vitro* cell inactivation data for cells with varying sensitivity. Monte Carlo simulations of arrays of inactivated cells (Cucinotta et al., 1999) are considered for protons and heavy ions and used to describe the absolute number of cell killing events of various magnitude in the brain from the GCR. Included are simulations of positions of inactivated cells from stopping heavy ions and nuclear stars produced by high-energy ions most importantly, protons and neutrons.

***Supported by NASA Grant HEDS-032 from Code UG to F.A. Cucinotta**

REFERENCES

- Atwell, W. Anatomical models for space radiation applications: An overview. *Adv. Space Res.* 14(10): 415-422; 1994.
- Billings, M. P.; Yucker, W. R. Summary final report. The computerized anatomical man (CAM) model. Huntington Beach, CA: McDonnell Douglas Astronautics Com.-West; Report MDC-G4655; 1973.
- Cucinotta, F. A.; Katz, R.; Wilson, J. W.; Townsend, L. W.; Shinn, J.; Hajnal, F. Biological effectiveness of high-energy protons: Target fragmentation. *Radiat. Res.* 127:130-137; 1991.
- Cucinotta, F.A.; Nikjoo, H.; and Goodhead, D. T. The effects of delta-rays on the number of particle-track traversals per cell in laboratory and space exposures. *Radiat. Res.* 150: 115-119; 1998a.
- Cucinotta F. A.; Wilson, J. W.; Shinn, J. L.; and Tripathi, R. K.: Assessment and requirements of nuclear reaction data bases for GCR transport in the atmosphere and structures. *Adv. in Space. Res.*, Vol. 21 (12): 1753-1762, 1998b.
- Cucinotta, F. A.; Nikjoo, H.; Goodhead, D. T. Applications of amorphous track models in radiation biology. *Radiat. & Env. Biophys.* (In press); 1999.
- Dicello, J.F. HZE cosmic rays in space: Is it possible that they are not the major radiation hazard? *Radiat. Prot. Dosim.* 44: 253-257; 1992.
- Grahn, D., Ed. HZE particle effects in manned space flight. *Natl. Acad. Sci. Washington, DC*; 1973.
- National Research Council, Radiation Hazards to Crews on Interplanetary Missions. National Academy Press, Washington D.C., 1996.
- Shavers, M. R.; Poston, J. W.; Cucinotta, F. A.; Wilson, J. W. Dose equivalent near the bone-soft tissue interface from nuclear fragments produced by high-energy protons. *Health Phys.* 70:473-483; 1996.
- Todd, P. The evolving microlesion concept. *Adv. Space Res.* 6(11):187-189; 1986.
- Todd P.; Schroy C.B.; Schimmerling W., Vosburgh K.G., Cellular effects of heavy charged particles. *Proceedings of the Open Meeting of the Working Group on Space Biology of the Fifteenth Plenary Meeting of COSPAR.* (ed. PHA Sneath) Akademie-Verlag, Berlin, 261-270; 1973.
- Wilson, J.W.; Townsend, L.W.; Schimmerling, W.; Khandelwal, G. S.; Kahn, F.; Nealy, J. E.; Cucinotta, F. A.; Simonsen, L. C.; Shinn, J. L.; Norbury, J. W. Transport methods and interactions for space radiations. Washington, DC: U.S. Government Printing Office; NASA TP-1257; 1991.
- Wilson, J.W.; et al., Issues in protection from galactic cosmic rays. *Radiat. Environ. Biophys.* 34:217-222; 1995.

INDUCTION OF APOPTOSIS IN RETINAL EXPLANTS EXPOSED TO LOW- AND HIGH-LET RADIATION

M. E. Vazquez¹, M. Saito², K. Nojima², Y. Furusawa² and A. Pelzer
Brookhaven National Laboratory, Medical Department, New York 11973.
National Institute of Radiological Sciences, Chiba, Japan

INTRODUCTION

The possibility of radiation injury to nervous system functional integrity looms as a problem critical to understanding the hazards of extended manned forays into space. Several *in vivo* studies suggest that chronic brain exposure to space conditions and HZE particles might produce effects similar to aging, functional decrements and neurodegeneration. However, the basic mechanism(s) of heavy ion radiation effects remains to be elucidated. Even less known are the effects of charged particles at the cellular and molecular level in neurons.

Neuron death is an important phenomenon in the developing and mature nervous system. Programmed cell death plays a key role in the forming the neural architecture and the neural network organization of the developing nervous system. In the mature nervous system, neuron death is closely related to the various neurodegenerative diseases, such as Alzheimer's and Parkinson's diseases, as well as neuron ageing. This neuron death is frequently associated with apoptosis, a process characterized by cell shrinkage, chromatin condensation and internucleosomal DNA cleavage. Apoptotic neuron death occurs under many conditions, such as development, neurotrophic factor deprivation, exposure to β -amyloid, transient ischaemia, exposure to free radicals and low-LET radiation. However, little is known about high-LET radiation-induced apoptosis in neural cells.

In this study, we examined the time course and dose-response of radiation-induced apoptosis in retinal explants following a single dose of x-rays or carbon ions. These studies intend to expand previous experiments in order to examine the cellular alterations associated with the heavy ion neurotoxicity, and how changes in LET modulate the biological response. The specific objectives were:

- a) To determine the dose-response curves and time course for neurotoxic effects induced by primary ion beams and x-rays in retinal explants.
- b) To determine the relationship between the global retinal explant cell vitality, apoptosis and neurite outgrowth, as a function of dose, LET and time post treatment.

To achieve these objectives, we used an *in vitro* model that have been previously shown to be sensitive to exposure to radiation, and which may provide a neurobiological basis for defining the risks of exposure to heavy particles on central nervous system functional integrity.

METHODS

In order to study the neural effects of heavy ions, an *in vitro* model in which neuronal regeneration occurs under controlled conditions were employed. Retinal explants taken from E6 chick donor embryos were exposed to 135 and 290 MeV/n carbon ion beams at HIMAC, and x-rays at NIRS. The LET spectra used ranged from ~ 7 to 24 keV/ μ m. Explants in a monolayer configuration were irradiated with doses from 10 to 500 cGy at the plateau position of the Bragg curve for carbon ions, and from 100 - 500 cGy for x-rays. The dose rate employed ranged from 50 to 100 cGy/min for heavy ions and 349 cGy/min for x-rays.

After exposure, explants were re-cultured on hydrated collagen lattices, covered with an enriched medium and incubated at 37°C and 5% CO₂ for 3 days. Daily, samples were imaged for morphometry and/or processed following specific protocols for the assessment of cellular toxicity and apoptosis determination.

Microscopic detection of apoptosis

Dissociated cells from retinal explants were seeded in slide chambers (LabTek) at different times post-irradiation and further cultured for 2 hours at 37°C, 5% CO₂, fixed and stained. Apoptotic cells were recognized by condensed nuclear chromatin, fragmented nuclei, and the appearance of apoptotic bodies. The morphological changes were visualized by Hoeschst 33258 (Molecular Probes). For quantification, of apoptosis, the cells were viewed under a fluorescence microscope (Zeiss) and at least 300 cells were scored.

Neurotoxicity methods.

Regenerative neurite outgrowth from retinal ganglion cells within explants were used to evaluate the neurotoxicity of heavy ion particles, since neurite outgrowth is considered a neuronal marker of functional integrity. At 24 h intervals, samples were imaged or fixed and stained following specific protocols for morphometry. The morphometric analysis were carried out employing an inverted microscope using phase contrast optics interfaced with an image analyzer system. The following parameters were measured: maximum neurite length, neurite outgrowth area and explant area.

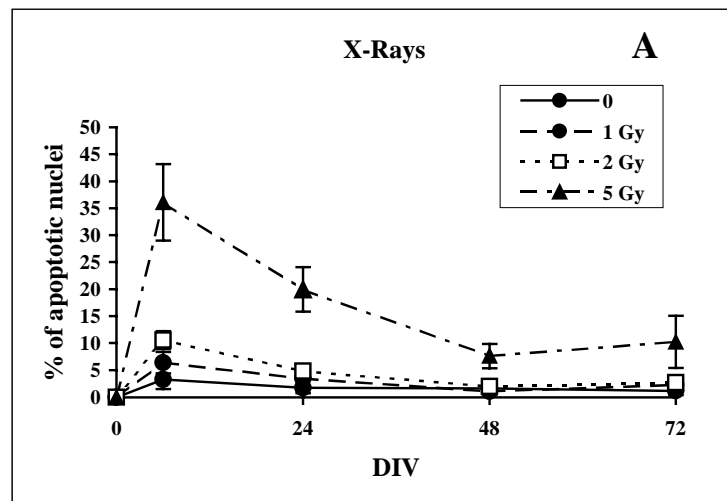
Cellular cytotoxicity

Cells obtained from dissociated explants were stained with propidium iodine and analyzed by FACScan to determine radiation-induced cell damage. Samples were taken at 24 hrs. interval and data were be analyzed as a function of time post-treatment, dose and LET

RESULTS

The results indicate that in the control group, the percentage of apoptotic cells was very stable, about 5% during culture, but in the irradiated groups, both x-rays and carbon ions, the percentage of apoptotic cells increase with time after irradiation in a dose-dependent manner (Figure 1).

The percentage of apoptotic cells in the cultures exposed to x-rays became statistically significantly higher than the controls at 6 hours after exposure solely at the 200 (10%) and 500 (36%) cGy dose level. At later times, the induction of apoptotic cells decreases reaching control values at about 48 h after exposure with 200 cGy. Explants irradiated with 500 cGy of x-rays, showed a decrease of the effect after 6 h post treatment, but values remained higher than the



controls until the end of the culture period.

Figure 1. Time course of apoptosis in retinal explants in culture after single doses of x-rays (200 kV, 19 mA).

Explants exposed to 290 MeV/n carbon ions, showed a similar dose-response pattern, namely a maximum increase of apoptotic nuclei at 6 hours post-exposure only at the 200 (26%) and 500 (29%) cGy dose level; then it decreased with time and returned to the control level at about 48 h after irradiation (Figure 2B). In contrast, samples exposed to 135 MeV/n carbon ions, did not show significant differences with the controls at all the doses and times examined (Figure 2C).

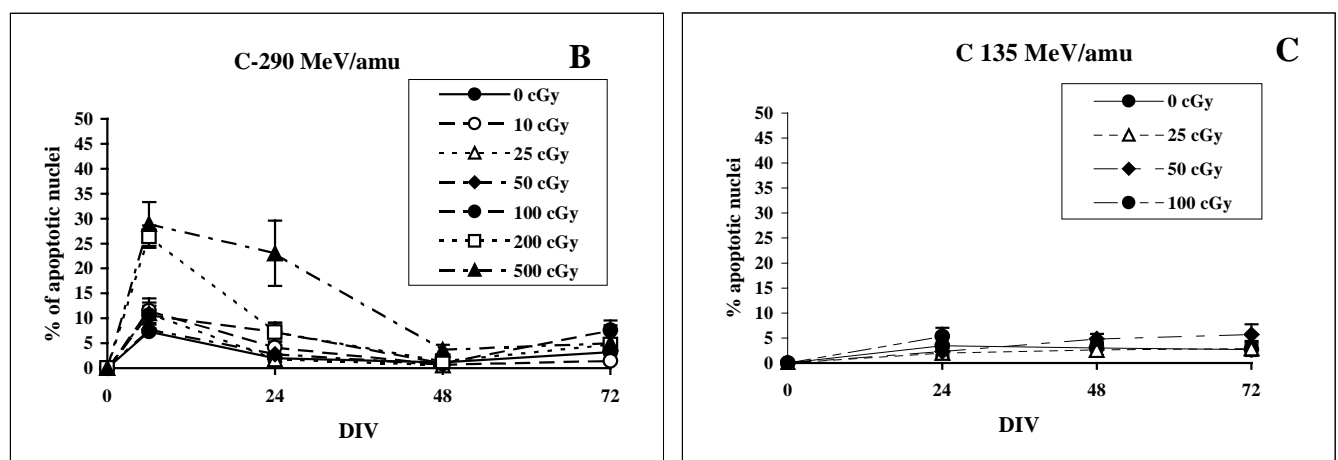


Figure 2. Time course of apoptosis in retinal explants in culture exposed to single doses of carbon ions B) 290 MeV/n (LET: 13 keV/ μ m) and C) 135 MeV/n (LET: 24 keV/ μ m).

Preliminary analysis of the data suggests a dose and time dependent increase of cell damage after exposure to heavy ions and x-rays determined by flow-cytometry. In addition, the morphometric analysis of neurite outgrowth from exposed explants, shown to be a less sensitive parameter than apoptosis induction and cell damage.

CONCLUSION

We conclude that low- and high-LET radiation induces apoptosis in retinal explants, and that the development of apoptosis follows a specific time course. Over the LET range examined, the induction of apoptotic cells by x-rays and heavy ions increased sharply at early times with doses in excess of 100 Gy.

THE NEUROBEHAVIORAL AND NEUROCHEMICAL CONSEQUENCES OF 1 GeV/n Fe PARTICLE EXPOSURE

M. E. Vazquez, S.J. Gatley, M. A. Cosenza, and B. E. Pyatt
Brookhaven National Laboratory, Medical Department, New York 11973

INTRODUCTION

Locomotor activity is heavily influenced by the nigrostriatal dopamine system, whose deterioration in humans leads to Parkinson's Disease. A limited amount of work has been conducted concerning the effects of HZE radiation on this system. High-energy ^{56}Fe particles have been shown to be the more behaviorally toxic than other radiation types. Rabin *et. al.* (1991) found that after exposure of rats to low doses (0.1-0.2 Gy) of 600 MeV/n ^{56}Fe particles, the taste aversion produced by injection of amphetamine (a dopamine enhancing drug) is eliminated. Four months after exposure to 1 GeV/n particles, the ability of amphetamine to produce a taste aversion had recovered, possibly indicating an up-regulation of dopamine receptors.

Although HZE particles appear to affect taste aversion, this may not be due to their high-LET character, since an increase in LET did not correspond to increases in behavioral toxicity. There is other evidence that radiation affects the dopaminergic system. A significant reduction of the oxotremorine enhancement of K⁺-evoked dopamine release occurs in striatal slices between 3-180 days after irradiation. In addition, the concentrations of different dopamine metabolites are higher in striatum from control animals than they are in irradiated animals at several time-points following exposure to high-energy iron particles.

HZE radiation also affects motor performance. Experiments where rats are trained on an accelerated, a shock-avoidance motor performance test, show that different radiation qualities vary in terms of their efficiencies to disrupt performance of the task. More striking, control rats are able to suspend themselves on a wire for longer periods of time than can rats irradiated with energetic iron particles. In the present on-going study, we have measured the effects of ^{56}Fe particle HZE radiation on cocaine-stimulated locomotor activity in rats at times up to 8 mo after irradiation. We also have also obtained brain tissue samples on sacrifice to measure neurochemical markers of the dopamine system. Our hypothesis was that the nigrostriatal dopaminergic system would be adversely affected by HZE radiation, and that this would be exposed in the form of an attenuated response to cocaine, and in a reduction in the level of dopamine receptors and transporters in the striatum.

METHODS

Animals: Male Sprague-Dawley rats were housed in Institutional Animal Facility of Brookhaven National Laboratory, Upton, NY. Temperature was maintained at $22^{\circ}\text{C} \pm 2^{\circ}\text{C}$ and humidity was maintained at $50\% \pm 10\%$. Rats were given commercial laboratory rodent chow and water *ad libitum*. The animal rooms were maintained on a 12-hour reverse light-dark cycle with lights on at either 8 PM or midnight and lights off at 8 AM or noon.

Radiation Exposure: Subjects were whole-body irradiated at Brookhaven National Laboratory's Alternating Gradient Synchrotron (AGS) with 1000 MeV/n ^{56}Fe particles. Animals were exposed to 0.8 and 1.5 Gy of Fe ions at a dose rate of 1 Gy/min. Control animals were

obtained from the same supplier and were matched by weight (250-300g, Taconic, Germantown, NY).

Monitoring Locomotor Activity: Rats were weighed before each experiment and then placed singly in clear acrylic boxes (16" x 16" x 16") equipped with arrays of photocells placed at the bottom (i.e. sensitive to lateral movements) and at a height of 4 inches (sensitive to rearing). Activity (beam interruptions per minute) was recorded for one hour (exploratory activity) prior to injection and for an additional two hours after I/P injection of cocaine hydrochloride (10 mg/kg) or 0.9% saline vehicle. The experiment was conducted at approximately monthly intervals for 8 months, and vehicle experiments were conducted one week after cocaine experiments. Data for each group (0 Gy, 0.8 Gy, and 1.5 Gy) in terms of exploratory activity, response to saline, and response to cocaine were analyzed and compared using Microsoft Excel.

Neurochemical studies: After 8 month post-treatment, animals were sacrificed and brains were removed and dissected along the midline. The right side of each brain was frozen in isopentane and stored at -70° for later autoradiographic receptor studies. Uptake of [^3H]dopamine was measured in freshly prepared synaptosomes isolated from the left striatum.

RESULTS

The weights of animals in the 0.8 Gy irradiation group did not differ from the control group. However, the weights of animals in the 1.5 Gy group were lower than those of control animals at all the time points.

No group differences were seen in terms of exploratory locomotor activity at any time-points, and no group differences were observed after cocaine or saline injection for the first month. In the second month, however, unirradiated rats showed a higher peak of activity after the saline injection than did either group of irradiated animals. Furthermore, the high-dose group (1.5 Gy) had a lower average peak activity than did the control or low-dose irradiation groups (0.8 Gy) when they were injected with the cocaine solution. Subsequent locomotor activity testing showed no group differences up to 8 month post-treatment.

No differences were observed in our ex vivo measure of striatal dopamine uptake, between control, low dose and high dose groups.

A high incident of tumors was detected in the irradiated animals with the highest incidence at the 0.8 Gy dose group. The histological analysis of these tumors is proceeding.

CONCLUSIONS

Our studies so far allow us to exclude dramatic changes in dopamine transport or in spontaneous or cocaine stimulated locomotor activity up to 8 months after irradiation of rats with 1 GeV ^{56}Fe particles at doses of 0.8 Gy or 1.5 Gy. This was unexpected given the assumption that a significant fraction of the animals' brain cells would be "hit" by iron particles. The behavioral response to cocaine did appear to be attenuated in the animals that received the higher dose at 2 months post irradiation. However, at later time-points this effect disappeared, suggesting that the brain systems involved have sufficient functional redundancy to allow recovery from moderate radiation induced lesions. Neuroreceptor measurements on brain tissue from these animals may help our understanding of neurological effects of HZE radiation. Further behavioral and neurochemical studies are required.

Wednesday, June 16

Brookhaven National Laboratory

11:15 a.m. – 11:55 a.m.

Gene Expression

Berkner Hall

EVIDENCE FOR THE PRESENCE OF FACTORS MODULATING RADIATION-INDUCED G2 DELAYS

Nge Cheong, Ya Wang and George Iliakis

Department of Radiation Oncology, Kimmel Cancer Center of Jefferson Medical College, Philadelphia, PA 19107

INTRODUCTION

It is well established that exposure of human cells to ionizing radiation leads to growth delays mediated by arrests in the progression of cells through different phases of the cell cycle. Among these cell cycle arrests those exerted in G1 and G2 phases are the most pronounced. It is believed that they serve as checkpoints where the integrity of the genome is assessed before allowing further progression through the cycle. Manipulation of these checkpoints is expected to modify the response of cells to ionizing radiation. Here, we present evidence that certain cell lines produce and excrete low molecular substances that increase the duration of the G2-delay.

METHODS

For experiments, two cell lines of rat origin with widely differing radiosensitivity to killing by X-rays were used. Cell survival was measured by colony forming assays. Repair of radiation-induced DNA double strand breaks was measured using asymmetric field inversion gel electrophoresis (AFIGE), a pulsed field gel electrophoresis method. The distribution of cells through the cycle was measured by flow cytometry.

RESULTS

The experiments show that the radioresistant A1-5 cells produce a substance that significantly increases the duration of the G2-delay in cells exposed to ionizing radiation. This substance is termed G2-Arrest Modulating Activity (GAMA) and can be removed from the cells by a medium change. Fractionation experiments indicate that GAMA is a low molecular weight peptide, with moderate stability to heat exposure. Arrest of cells in G2 by GAMA is not associated with an increase in apoptosis. The effect of GAMA on radiation-induced G2 arrest can be eliminated either by caffeine or staurosporine. The fact that GAMA is produced by a very radioresistant cell line suggests a correlation between its excretion, its effect on G2 arrest, and the observed radioresistance to killing.

CONCLUSIONS

The results suggest that certain types of cells produce substances that increase their resistance to DNA damaging agents by up-regulating checkpoint responses. Identification and characterization of such substances may lead to the development of novel radioprotectors.

CONFOCAL IMAGE ANALYSIS OF LAMININ IN BASEMENT MEMBRANES FOLLOWING WHOLE BODY IRON PARTICLE (1 GeV/nuc) IRRADIATION

S. Costes and M.H. Barcellos-Hoff, Life Sciences Division, Lawrence Berkeley National Laboratory, Berkeley, CA 94720

This study was motivated by the previous observations on mammary glands showing irregularities in laminin immunoreactivity one hour after whole body irradiation with 1 GeV/nucleon iron particles for a dose of 0.8 Gy (Ehrhart, et al., Rad. Res., 145:157-162, 1996). These alterations were evident for 9 days and resolved by 14 days, but were not observed if collagen IV was stained instead of laminin, or following irradiation with Co⁶⁰ (5 Gy). The rapidity of such a change suggested that the effect might be due to a physical event specific to HZE, rather than a biological event. If this hypothesis is correct, the effect should be dose dependent and non-organ specific. A quantitative approach was taken in order to test our hypothesis.

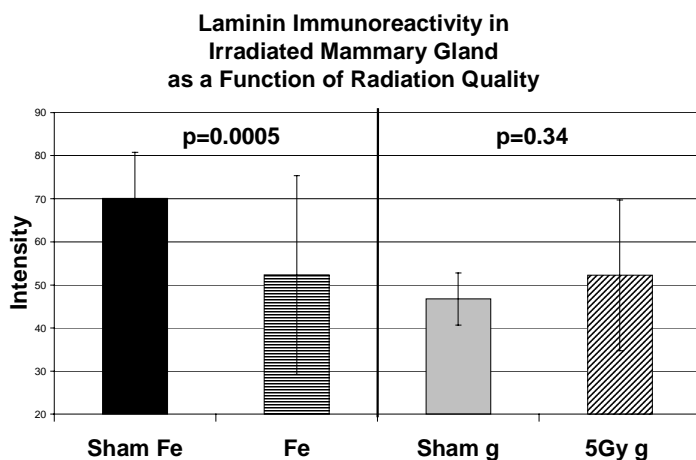
As reported last year at this meeting, we tested the dose dependence and organ specificity using skin acquired from animals irradiated with 1 GeV iron particles at the AGS at Brookhaven National Laboratory in October 1996 and May 1998. Laminin was immunolocalized in mice irradiated with whole body doses 3, 10, 40, 80, 160 and 500 cGy and a reference dose of 5 Gy cobalt-60. Since skin is a sheet, it is easy to sample and has a rather flat basement membrane, whereas the basement membranes form tubes around mammary gland ducts create geometrical artifacts when they are projected on sections. Therefore, we used confocal laser microscopy for more precise imaging of the basement membrane. This allowed evaluation of thicker specimen (20 micron thick instead of 5). Thus, three-dimensional images made of a stack of 40 slices of size 250 micron x 250 micron x 0.5 micron were taken for each section. An algorithm was written in order to segment the basement membrane from the collected three-dimensional image, which was tested for different image patterns such as: average intensity, contrast and sharpness of the membrane staining.

The analysis of skin collected soon (1-3 hour) after irradiation following 6 doses, 3 animals per dose point, 2 sections per animal, and 3 three-dimensional images per section corresponds to 4320 slices of 0.5 microns thickness. Laminin-stained basement membranes were evaluated for contrast, sharpness and average intensity for each dose group. No effect was evident using these parameters dose dependence was observed. This experiment was repeated three times. Since laminin immunoreactivity does not appear altered in skin, these data do not support the hypothesis that the laminin alteration observed in mammary gland is a physical event and lends credence to a biological effect.

However, there were a number of problems that complicate the interpretation of these data: First, due to artifacts that laser confocal microscopy brings in acquiring data, compiling the optical slices for analysis may have obscured certain changes. Therefore, we decided to gather only one slice per region of interest in the specimen, this slice being at mid-depth of the specimen. Second, different laminin antibodies are available. We therefore compared the original laminin protein antibody (tLM) to two new antibodies, one against the whole protein (sLM) and one against a laminin $\alpha 1$ chain fragment (E3). Third, we developed new segmentation techniques to

extract the membrane in the images. The average intensity and standard deviation of the membrane, and of the periphery of the membrane were computed. In addition, the histograms of the membrane and its periphery were also computed.

These modifications were used to reevaluate and quantitatively analyze laminin immunoreactivity in mammary gland. The result of this second approach is very interesting. We observed the effect that was initially described in Fe-particle irradiated mammary gland, but not in gamma-irradiated tissue (Figure). We have also found that the effect is antibody dependent. It



is most pronounced using the original tLM antibody raised against the whole laminin protein, less distinct with sLM, and was not evident with E3 antibodies. Again, no response was observed with any antibody after Co⁶⁰ irradiation. Using image analysis, the effect was localized to the membrane periphery rather than the intensity of the membrane itself. However, we noted that the degree of the effect is also animal dependent, suggesting that it is mediated by systemic or genetic factors. Taken together the data point toward a fast biological response specific to HZE irradiation that may change laminin conformation, stability and/or access in the basement membrane. We are currently reevaluating the data from irradiated skin using the new image segmentation and analysis for comparison with the current mammary gland analysis.

Our studies show that HZE-irradiation elicits distinct microenvironment changes when compared to sparsely ionizing radiation. Laminin is an important mediator of epithelial integrity and serves as a barrier to invasive growth. A hallmark of cancer is the ability to destroy and traverse the basement membrane. Radiation induced changes in basement membrane integrity might thus promote neoplastic progression.